The oxidation of *n*-octane by iridium and cobalt PNP complexes

By

Dunesha Naicker

Submitted in fulfillment of the academic requirements for the degree of
Master of Science in the
School of Chemistry,
University of KwaZulu-Natal,
Durban,
South Africa

December 2011

As the candidate's supervisor I have approved this dissertation for submission.

Signed:_____Date:_____

Prof. Holger B. Friedrich (Supervisor)

Abstract

Paraffin activation has practical implications in the replacement of current petrochemical feedstocks (olefins), by utilizing economical and easily accessible alkanes, which may result in more efficient strategies for fine chemical synthesis and the proficient use of energy. However, the chemical inertness of paraffins limits their conversion to more valuable products. Several pincer chelate complexes are utilized in stoichiometric and catalytic C–H activation. These pincer ligands have attained much interest in that they are part of a system, which displays high stability, activity and variability. In this study four aminodiphosphine (PNP) pincer ligands were successfully synthesized and characterized by NMR, IR and HRMS. To investigate the steric effects on the metal center, four different functional groups on the nitrogen atom were used, a cyclic ring (cyclohexyl (**3.1**)) branched chain (*iso*-propyl (**3.2**)); straight chain (pentyl (**3.3**)); and aromatic ring (benzyl (**3.4**)). The ligands were successfully complexed to the transition metals iridium and cobalt and characterized by elemental analyses, IR, HRMS and thermogravimetric measurements. The thermal behaviour of the ligands showed that ligands **3.1**-**3.3** displayed similar decomposition patterns. Similar fragmentation patterns were observed for the iridium and cobalt complexes containing ligands **3.1** and **3.3**.

The complexes were tested in the oxidation of *n*-octane in two solvent systems, DCM and MeCN with H_2O_2 and *t*-BuOOH as the oxidants. The optimum substrate to oxidant ratio was found to be 1:5. No conversion was observed with H_2O_2. The conversion in DCM for the iridium catalysts was much higher than that of the cobalt catalyst. However, higher conversion was obtained in MeCN for the cobalt catalysts. No conversion was observed for the iridium catalyst in MeCN. The selectivity to ketones was much higher than to the alcohols, with only the C(1) position being most selective to the alcohols.

The *in situ*, single pot testing of *n*-octane using a ruthenium precursor and ligand **3.1**-**3.4** undertaken in DCM showed no conversion, whilst in MeCN a conversion of 17% was observed. The selectivity was similar to that obtained by the cobalt catalysts in MeCN. All testing showed that the catalyst containing ligand **3.1** was the most active giving the highest conversions in different solvent systems, which is attributed to the bite angle effect.

Preface

The experimental work described in this dissertation was carried out in the School of Chemistry, University of KwaZulu-Natal, Westville Campus, Durban, from January 2010 to November 2011, under the supervision of Prof. H. B. Friedrich.

These studies represent original work by the author and have not otherwise been submitted in any form or degree or diploma to any tertiary institution. Where use has been made of the work of others it is duly acknowledged in the text.

_____

Dunesha Naicker

B. Sc (Honours) (UKZN-Westville Campus)

Declaration - Plagiarism

I, _____ declare that

1. The research reported in this thesis, except where otherwise indicated is my original research.
2. This thesis has not been submitted for any degree or examination at any other university.
3. This thesis does not contain other persons' data, pictures, graphs or other information, unless specifically acknowledged as being sourced from other person.
4. This thesis does not contain other persons' writing, unless specifically acknowledged as being sourced from other researchers. Where other written sources have been quoted, then:
    a. Their words have been re-written but the general information attributed to them has been referenced.
    b. Where their exact words have been used, then their writing has been placed in italics and inside quotation marks, and referenced.
5. This thesis does not contain text, graphics or tables copied and pasted from the Internet, unless specifically acknowledged, and the source being detailed in the thesis and in the References sections.

Signed: _____

Conference Contributions

Part of the work discussed in this dissertation has been presented as a poster presentation at the following conferences:

CATSA Conference 2010, Bloemfontein, poster presentation, *Synthesis and characterization of PNP pincer complexes*, D. Naicker and H.B. Friedrich

SACI Conference 2011, Johannesburg, poster presentation, *Synthesis and characterization of PNP pincer complexes*, D. Naicker and H.B. Friedrich.

SACI Symposium 2011, University of KwaZulu-Natal (Westvillle, Durban), poster presentation, *Synthesis and characterization of PNP pincer complexes*, D. Naicker and H.B. Friedrich.

CATSA Conference 2011, Johannesburg, poster presentation, *C-H activation of n-octane by cobalt and iridium PNP pincer complexes*, D. Naicker and H.B. Friedrich

Acknowledgments

I thank God for His richest blessings, grace and for being my light in times of despair, "*for without your grace, nothing is possible*".

My sincere thanks to my supervisor, Prof. Holger B. Friedrich for his exceptional guidance and supervision.

I gratefully acknowledge SASOL and THRIP for their financial support. A special thanks to my mentor, Dr Gerrit Julius, for his encouragement and input.

In addition, I thank the following people: Mr Dilip Jagjivan for his assistance with the NMR, Ms. Jayambal Govender and Ms. Charmaine Magwaza for their efficient handling of the financial matters, Ms Anita Naidoo for help with instrumentation analysis, Mr Gregory Moodley for ensuring the availability of chemicals and solvents.

I thank Ms. Thashini Chetty for her aid with the thermal gravimetric analysis. My sincere and deepest gratitude to Dr Pramod Pansuriya, for his generosity and assistance with the synthesis and characterization. I thank Mr Stuart Miller for his willingness to share some valuable techniques. Furthermore, I take this opportunity to thank the members of the Catalysis Research Group for their valuable input during the group meetings.

I sincerely thank Mr Mohamed Fadlalla for his help, encouragement, friendship and willingness to share ideas. Thanks to my exceptional friends, Ms. Merilyn Manikam, Ms. Sharmini Pillay, Ms. Karisha Narraidu, Mr Michael Pillay, Dr Hitesh Parekh, Ms. Ashona Singh, Ms. Lynette Komarsamy, Ms. Veresha Dukhi, Mr Ebrahim Kadwa, Ms. Thobekile Makatini and Mr Leven Chetty for their unwavering friendship and support.

My heartfelt and endless gratitude to my parents, Mr and Mrs Naicker, for their understanding and effortless support and to my wonderful sisters, Ms. Perushni Naicker and Ms. Sushmita Naicker, for their love, care and patience.

List of Figures

Fig. 1.1: Diagram of the active site of MMO derived from *Methylococcus capsulatus* (Bath). 7
Fig. 1.2: Structure of coenzyme B_{12}. 8
Fig. 1.3: Acid–catalyzed cracking of paraffins. 11
Fig. 1.4: The termolecular transition state of metalloradical alkane activation. 19
Fig. 2.1: Schematic structure of the pincer ligand showing the donor atoms (X) and central anionic atom (Y). 25
Fig. 2.2: Structure of the iridium pincer complex used by Jensen and co-workers. 30
Fig. 2.3: Dual coordination modes of the cobalt pincer complexes. 33
Fig. 2.4: Structure of the PNP pincer complex with the different R functional groups. 36
Fig. 4.1: Assignment of the protons of ligands **3.1**–**3.4**. 58
Fig. 5.1: Conversion observed for the optimization of substrate to oxidant ratio for both the catalyst ([($^{Ph}PN_{cyclohexyl}P^{Ph}$)Ir COE][$BF_4$] (**3.6**)) and the blank. 94
Fig. 5.2: Conversion observed for the iridium catalysts (**3.6-3.9**) at substrate to oxidant ratio of 1:5. 95
Fig. 5.3: Selectivity of the iridium catalysts (**3.6-3.9**) to the products of oxidation. 94
Fig. 5.4: Selectivity of the iridium catalysts (**3.6-3.9**) to C(1) products. 96
Fig. 5.5: Selectivity of the iridium catalysts (**3.6-3.9**) to C(2) products. 97
Fig. 5.6: Selectivity of the iridium catalysts (**3.6-3.9**) to C(3) products. 97
Fig. 5.7: Selectivity of the iridium catalysts (**3.6-3.9**) to C(4) products. 98
Fig. 5.8: Conversion observed for the cobalt catalysts (**3.10-3.13**) at substrate to oxidant ratio of 1:5. 99
Fig. 5.9: Selectivity of the cobalt catalysts (**3.10-3.13**) to the products of oxidation. 100
Fig. 5.10: Regioselectivity of the cobalt catalyst **3.10** to the products of oxidation. 100
Fig. 5.11: Regioselectivity of the cobalt catalyst **3.13** to the products of oxidation. 101
Fig. 5.12: Conversion observed for the optimization of substrate to oxidant ratio for both the catalyst ([($^{Ph}PN_{cyclohexyl}P^{Ph}$)$CoCl_2$](**3.10**)) and the blank. 102

Fig. 5.13: Conversion observed for the cobalt catalysts (**3.10**-**3.13**) at substrate to oxidant ratio of 1:5. 103
Fig. 5.14: Selectivity of the cobalt catalysts (**3.10**-**3.13**) to the products of oxidation. 104
Fig. 5.15: Selectivity of the cobalt catalysts (**3.10**-**3.13**) to C(1) products. 104
Fig. 5.16: Selectivity of the cobalt catalysts (**3.10**-**3.13**) to C(2) products. 105
Fig. 5.17: Selectivity of the cobalt catalysts (**3.10**-**3.13**) to C(3) products. 105
Fig. 5.18: Selectivity of the cobalt catalysts (**3.10**-**3.13**) to C(4) products. 106
Fig. 5.19: Conversion observed using the ligands (**3.1**-**3.4**) at substrate to oxidant ratio of 1:5. 107
Fig. 5.20: Selectivity of the ruthenium precursor with ligands (**3.1**-**3.4**) to the products of oxidation. 108
Fig. 5.21: Selectivity of the ruthenium precursor with ligands (**3.1**-**3.4**) to C(1) products. 109
Fig. 5.22: Selectivity of the ruthenium precursor with ligands (**3.1**-**3.4**) to C(2) products. 109
Fig. 5.23: Selectivity of the ruthenium precursor with ligands (**3.1**-**3.4**) to C(3) and C(4) products. 110

List of Tables

Table 4.1: Peak shifts of the proton at carbon (1) of ligands **3.1–3.3**. 58

Table 4.2: ^{31}P NMR shifts of the ligands **3.1**-**3.4**. 60

Table 4.3: Comparison of IR data of COE and $[IrCl(COE)_2]_2$, (**3.5**). 62

Table 4.4: Comparison of IR data of the ligand ($^{Ph}PN_{cyclohexyl}P^{Ph}$) (**3.1**) and the respective [($^{Ph}PN_{cyclohexyl}P^{Ph}$)IrCOE][$BF_4$] (**3.6**). 65

Table 4.5: Comparison of IR data of the ligand ($^{Ph}PN_{pentyl}P^{Ph}$) (**3.2**) and the respective complex [($^{Ph}PN_{pentyl}P^{Ph}$)IrCOE][BF_4] (**3.7**). 65

Table 4.6: Comparison of IR data of the ligand ($^{Ph}PN_{iso\text{-}propyl}P^{Ph}$) (**3.3**) and the respective complex [($^{Ph}PN_{iso\text{-}propyl}P^{Ph}$)IrCOE][$BF_4$] (**3.8**). 66

Table 4.7: Comparison of IR data of the ligand ($^{Ph}PN_{benzyl}P^{Ph}$) (**3.4**) and the respective complex [($^{Ph}PN_{benzyl}P^{Ph}$)IrCOE][BF_4] (**3.9**). 66

Table 4.8: Comparison of IR data of the ligand ($^{Ph}PN_{cyclohexyl}P^{Ph}$) (**3.1**) and the respective complex [($^{Ph}PN_{cyclohexyl}P^{Ph}$)$CoCl_2$] (**3.10**). 68

Table 4.9: Comparison of IR data of the ligand ($^{Ph}PN_{pentyl}P^{Ph}$) (**3.2**) and the respective complex [($^{Ph}PN_{pentyl}P^{Ph}$)$CoCl_2$] (**3.11**). 69

Table 4.10: Comparison of IR data of the ligand ($^{Ph}PN_{iso\text{-}propyl}P^{Ph}$) (**3.3**) and the respective complex [($^{Ph}PN_{iso\text{-}propyl}P^{Ph}$)$CoCl_2$] (**3.12**). 70

Table 4.11: Comparison of IR data of the ligand ($^{Ph}PN_{benzyl}P^{Ph}$) (**3.4**) and the respective complex [($^{Ph}PN_{benzyl}P^{Ph}$)$CoCl_2$] (**3.13**). 70

Table 4.12: Thermoanalytical data (TGA, DSC) for the PNP ligands (**3.1- 3.4**). 72

Table 4.13: Thermoanalytical data (TGA, DSC) for the PNP-Iridium complexes (**3.6- 3.9**). 76

Table 4.14: Thermoanalytical data (TGA, DSC) for the PNP-Cobalt complexes (**3.10- 3.12**). 83

Table 5.1: Industrial applications of oxidative functionalization of hydrocarbons. 88

Table 5.2: Column specification and GC parameters. 91

Table 5.3 : Selectivity parameters in the oxidation of *n*-octane by iridium catalyst (**3.6-3.9**). 98

Table 5.4: Selectivity parameters in the oxidation of *n*-octane by cobalt catalysts (**3.10-3.13**). 101

Table 5.5: Selectivity parameters in the oxidation of *n*-octane by cobalt catalysts (**3.10**-**3.13**). 106

Table 5.6 : Selectivity parameters in the *in situ* oxidation of *n*-octane by ruthenium precursor with ligands (**3.1**-**3.4**). 110

List of Schemes

Scheme 1.1: The relationship between bond strength, selectivity and reactivity. 3
Scheme 1.2: The difference between activation by transition metals (A) and that occurring via radical or electrophilic routes (B). 4
Scheme 1.3: Oxidation of alkanes by cytochrome P450. 6
Scheme 1.4: The mechanism of coenzyme B_{12} in its 1,2 hydrogen transfer. 9
Scheme 1.5: The catalytic cycle for alkane activation by Pt(II) species 15
Scheme 1.6: Reactivity of Pt(II) ligands on the rate of H-D exchange. 16
Scheme 1.7: The mechanism of transfer dehydrogenation by an iridium pincer complex. 17
Scheme 2.1: Binding of SO_2 on pincer complexes of NCN with the formation of five-coordinte adducts. 26
Scheme 2.2: Self assembly of SCS pincer complexes containing palladium. 28
Scheme 2.3: Functionalized palladium SCS pincer complexes for substrate discrimination. 29
Scheme 2.4: Mechanism of alkane dehydrogenation of linear alkanes proposed by Jensen. 30
Scheme 2.5: C–H activation of benzene by iridium PNP pincer complex. 32
Scheme 4.1: Synthetic procedure for ligands **3.1**-**3.4**. 57
Scheme 4.2: Synthesis of the iridium complexes **3.6**–**3.9**. 63
Scheme 4.3: Synthesis of the cobalt complexes **3.9**–**3.13**. 67
Scheme 4.4: Proposed decomposition pathway for ligands **3.1**–**3.3**. 71
Scheme 4.5: Proposed decomposition pathway for ligands **3.4**. 74
Scheme 4.6: Proposed decomposition of the iridium complex **3.6** and **3.8**. 78
Scheme 4.7: Proposed decomposition of the iridium complex **3.7**. 79
Scheme 4.8: Proposed decomposition of the iridium complex **3.9**. 80
Scheme 4.9: Proposed decomposition of complex **3.10** and **3.12**. 81
Scheme 4.10: Proposed decomposition of complex **3.11**. 82

Abbreviations

ATR = Attenuated total reflection
asym. = Asymmetric
COA = Cyclooctane
COE = Cyclooctene
d = Doublet
DCM = Dichloromethane
DFT = Density functional theory
DSC = Differential scanning calorimetry
eqn = Equation
ESI = Electron spray ionization
Et_3N = Triethylamine
EtOH = Ethanol
FID =Flame ionization detector
FT-IR = Fourier Transform-Infrared
g = Gram
GC = Gas Chromatography
HOMO = Highest Occupied Molecular Orbital
HRMS = High resolution mass spectroscopy
Hz = Hertz
J = Coupling constant
Kcal/mol = Kilocalories per mole
L = Ligand
l = Liter
LUMO = Lowest Occupied Molecular Orbital
M = Metal
m = Multiplet
m = Medium
MeCN = Acetonitrile
MeOH = Methanol
min = Minute
ml = Milliliter (10^{-3} liter)

mmol = Millimolar
MMO = Methane monooxygenase
mol = Moles
Mp = Melting point
mV = Millivolts
MW = Molecular weight
N = Nitrogen
NMR = Nuclear magnetic resonance
ODH = Oxidative Dehydrogenation
P = Phosphorous
Ph = Phenyl
PNP = Aminodiphosphine
ppm = Parts per million
por = Porphyrin
qui = Quintet
rt = Room temperature
s = Strong
sym. = Symmetric
t = Triplet
TBA = *tert*- butyl ethylene
t-BuOOH = *Tert*-butyl hydroperoxide
THF = Tetrahydrofuran
TGA = Thermal gravimetric analysis
w = weak
XRD = X-ray diffraction
µl =Microliter (10^{-6} liter)

Contents

Title i

Abstract ii

Preface iii

Declaration iv

Conference contributions v

Acknowledgments vi

List of figures vii

List of tables ix

List of schemes xi

Abbreviations xii

Content xiv

Chapter One 1

Introduction 1

1.1 Paraffin C–H bond activation 1

1.1.1 Factors that affect the activation of paraffins 2

1.1.2 Enzymatic paraffin activation 4

1.1.2.1 C–H activation by Cytochrome P450 5

1.1.2.2 C–H activation of methane by methane monooxygenase 6

1.1.2.3 C–H activation by coenzyme B_{12} 8

1.1.3 Heterogenous activation of paraffins 9

1.1.3.1 Catalytic cracking 10

1.1.3.2 Oxidative dehydrogenation (ODH) 12

1.1.4 Homogenous activation of paraffins 13

1.1.4.1 Electrophillic addition 14

1.1.4.2 Oxidative addition 15

1.1.4.3 Sigma bond metathesis 17

1.1.4.4 Metalloradical activation 19

1.1.4.5 1,2-addition 19

1.2 Conclusion 20

1.3 References 21

Chapter Two 24

Introduction to PNP pincer complexes and their application in catalysis 24

2.1 Pincer ligands 24

2.1.1 Pincer ligands and their applications 25

2.1.1.1 The role of pincer ligands as gas sensors 26

2.1.1.2 The role of pincer ligands as switches 26

2.1.1.3 The role of pincer ligands in self assembled systems (supramolecular structures) 27

2.1.2 Pincer complexes of iridium and cobalt and their applications in the activation of C–H bonds 29

2.1.2.1 Iridium 29

2.1.2.2 Cobalt 32

2.1.3 Characterization techniques 33

2.1.3.1 ^{31}P NMR spectroscopy 34

2.1.3.2 Infrared (IR) spectroscopy 34

2.1.3.3. Thermogravimetric analysis 35

2.2 Thesis scope 35

2.3 References 37

Chapter Three 40

Experimental: ligand and complex synthesis 40

3.1 General 40

3.1.1 Synthesis methods 40

3.1.2 Nuclear Magnetic Resonance (NMR) spectroscopy 40

3.1.3 Melting point determination 41

3.1.4 Fourier Transform Infra-Red (FT-IR) spectroscopy 41

3.1.5 Elemental analysis 41

3.1.6 Mass spectrometry 41

3.1.7 Thermal gravimetric analysis (TGA) 41

3.2 Synthesis of ligands 42

3.2.1 Diphosphinocyclohexylamine ($^{Ph}PN_{cyclohexyl}P^{Ph}$) (**3.1**) 42

3.2.2 Diphosphinopentylamine ($^{Ph}PN_{pentyl}P^{Ph}$) (**3.2**) 43
3.2.3 Diphosphino-*iso*-propylamine ($^{Ph}PN_{pentyl}P^{Ph}$) (**3.3**) 44
3.2.4 Diphosphinobenzylamine ($^{Ph}PN_{pentyl}P^{Ph}$) (**3.3**) 45
3.3 Synthesis of iridium complexes 46
3.3.1 Synthesis of di-μ-chlorotetrakis(cyclooctene)diiridium(I) $[IrCl(COE)_2]_2$ (**3.5**) 46
3.3.2 Synthesis of [($^{Ph}PN_{cyclohexyl}P^{Ph}$)Ir COE][$BF_4$] (**3.6**) 47
3.3.3 Synthesis of [($^{Ph}PN_{pentyl}P^{Ph}$)Ir COE][BF_4] (**3.7**) 48
3.3.4 Synthesis of [($^{Ph}PN_{iso\text{-}propyl}P^{Ph}$)Ir COE][$BF_4$] (**3.8**) 49
3.3.5 Synthesis of [($^{Ph}PN_{benzyl}P^{Ph}$)Ir COE][BF_4] (**3.9**) 50
3.4 Synthesis of cobalt complexes 51
3.4.1 Synthesis of [($^{Ph}PN_{cyclohexyl}P^{Ph}$)$CoCl_2$] (**3.10**) 51
3.4.2 Synthesis of [($^{Ph}PN_{pentyl}P^{Ph}$)$CoCl_2$] (**3.11**) 52
3.4.3 Synthesis of [($^{Ph}PN_{iso\text{-}propyl}P^{Ph}$)$CoCl_2$] (**3.12**) 53
3.4.4 Synthesis of [($^{Ph}PN_{benzyl}P^{Ph}$)$CoCl_2$] (**3.13**) 53
3.5 Synthesis of ruthenium precursor 54
3.5.1 Synthesis of triphenylphosphinedihydridocarbonyl ruthenium(II) (**3.14**) 54
3.6 References 56

Chapter Four 57

Results and Discussion 57
4.1 Ligand synthesis and characterization 57
4.2 Synthesis of iridium complexes and characterization 61
4.2.1 Synthesis and characterization of iridium precursor, di-μ-chlorotetrakis(cyclooctene)diiridium(I) $[IrCl(COE)_2]_2$, (**3.5**) 61
4.2.2 Synthesis and characterization of the iridium [($^{Ph}PNP^{Ph}$)Ir COE][BF_4] complexes (**3.6-3.9**) 62
4.3 Synthesis and characterization of the cobalt complexes [($^{Ph}PNP^{Ph}$)$CoCl_2$] (**3.10-3.13**) 67
4.4 Thermal analyses of ligands and complexes 71
4.4.1 Thermal gravimetric analyses of the ligands (**3.1-3.4**) 71
4.4.2 Thermal gravimetric analyses of the iridium complexes (**3.6-3.9**) 75
4.4.3 Thermal gravimetric analyses of the cobalt complexes (**3.10-3.12**) 81

4.5 Conclusion 85
4.6 References 86

Chapter Five 88
Catalytic testing: Oxidative functionalization of *n*-octane 88
5.1 Introduction 88
5.2 Experimental conditions 91
5.2.1 Instruments and reagents 91
5.2.2 General procedure 92
5.3 Results and discussion 93
5.3.1 Catalytic testing carried out in dichloromethane at 40 °C 93
5.3.1.1 Iridium catalysts (**3.6-3.9**) 93
5.3.1.2 Cobalt catalysts (**3.10-3.13**) 99
5.3.2 Catalytic testing carried out in acetonitrile at 80 °C 102
5.3.2.1 Cobalt catalysts (**3.10-3.13**) 102
5.3.3 *In situ* study with ruthenium precursor (**3.14**) and ligands (**3.1-3.4**) 107
5.3.3.1 Catalytic evaluation in acetonitrile performed at 80 °C 107
5.4 Conclusion 111
5.5 References 112

Chapter Six 114
Summary 114

Appendix A 116

Appendix B 134

Chapter One

Introduction

1.1 Paraffin C–H bond activation

To understand the correlation between activation, functionalisation and catalysis, Crabtree[1] provides an insightful definition, in which he describes activation as the binding of a substrate to a metal center, which is followed by functionalisation, where the substrate is altered, and regeneration of the starting metal species results in a catalytic cycle.[1] For the past 20 years, the conversion of paraffins or saturated hydrocarbons to more valuable products has drawn the interests of many scientists. This is due to the central problem, where general, selective, efficient and catalytic functionalisation reactions of unactivated paraffin C–H bonds remains unsolved.[1]

The need for paraffin activation has practical implications in the replacement of current petrochemical feedstocks (olefins) by economical and easily accessible alkanes, which can result in more efficient strategies for fine chemical synthesis and the proficient use of energy.[2,3] Paraffin activation has also ignited an interest in many environmentalists with the utilisation of methane.[4] Methane is a natural gas existing in large quantities in remote parts of the world, where there is a slight or no demand.[2,4] However, as a natural gas, the exploitation of methane becomes unfeasible due to the high cost of transportation.[2,4] Thus, indirect conversion to more valuable products involves the intermediary production of synthesis gas (carbon monoxide and hydrogen).[2] Conversion of methane to methanol (eqn (1)) or other liquid fuels makes this natural gas a viable source of energy as well a more effortless transportable liquid.[4]

$$CH_4 + \tfrac{1}{2}O_2 \rightleftharpoons CH_3OH \qquad \textbf{(1)}$$

There are many shortcomings in converting methane and other alkanes to the desired functionalised products. A major factor is the chemical inertness of the alkane, which arises due to the constituent atoms being held by strong and localized C–C and C–H bonds.[2] Furthermore, these molecules exhibit difficulty in participating in chemical reactions due to the unavailability of low energy empty orbitals or high energy filled orbitals (as seen in olefins and alkynes).[2] Another factor includes the high C–H bond strength of alkanes (*e.g.* methane, 105 kcal/mol).[5] Labinger and Bercaw[2] further articulate that the reactions of alkanes at relatively high temperatures, *e.g.* combustion, are useful in exploitation of their energy but are uncontrollable and result in products that are economically unattractive due to over oxidation, such as carbon dioxide and water, with no further use as precursors.[2,4,6] Furthermore, processes such as dehydrogenation and cracking require harsh conditions (high temperatures and pressures) and serve as another drawback in conversion.[2,3]

1.1.1 Factors that affect the activation of paraffins

In addition to the low reactivity of alkanes, as mentioned above, other factors also contribute to the difficulty in activation of C–H bonds in paraffins. These factors include:

i. Thermodynamics
ii. Selectivity
iii. Activity

Thermodynamics and kinetics show that there is a preferential activation of substrates containing sp^2 hybridized C–H bonds over sp^3 hybridized C–H bonds.[7] This is due to greater differences in the M–C bond strengths in comparison with the C–H bond strength.[7] Taking into consideration the conversion of alkanes to alkenes, which may be regarded as the reverse of the well-established alkene hydrogenation (eqn (2)), the equilibrium favours the formation of the alkane, where $\Delta H \approx -33$kcal/mol.[8]

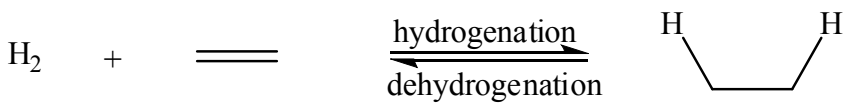

(2)

To overcome such problems, Crabtree[4] describes the use of alkenes as hydrogen acceptors (or oxidising agents) or the use of photons to drive the reaction (photochemical methods).[4,8]

Other methods include alkane hydroxylation, where insertion of an electronegative element into the C–H bond results in an exothermic reaction, which provides sufficient energy to drive the reaction.[4]

Over the past 30 years, there have been numerous attempts at trying to achieve selective activation of C–H bonds by transition metal complexes.[8] Selectivity remains a challenge where the intermediate products are more reactive than the alkane and may react more effortlessly with the metal centre.[6,9] For example, in the activation of methane to form methanol, the homolytic C–H bond energy of methane is 10 kcal/mol higher than that of methanol.[9] However, organometallic activation has illustrated that activation by the metal centre of the alkane C–H bond can be preferred over the highly reactive epoxide (eqn (3)).[2] Bond strengths (Scheme 1.1) also play a role in selective activation between different C–H bonds.[2] This is noted in the use of radicals ($HO^{\cdot}$ or $RO^{\cdot}$), where the removal of the H from the alkane is exothermic, which results in O–H bonds having bonding strengths that are similar or greater than alkane C–H bonds.[4] Examples of such include the Gif reaction[10] and Fenton Chemistry.[1,6]

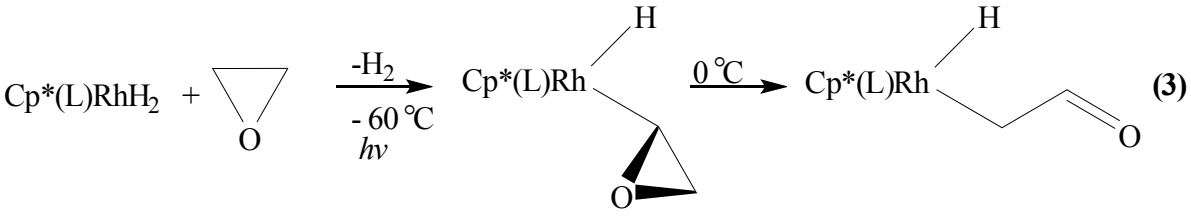

(3)

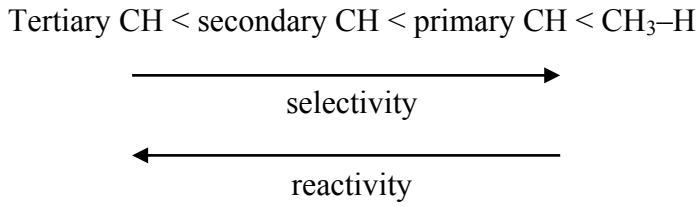

Scheme 1.1: The relationship between bond strength and selectivity as well as reactivity, where primary C–H bonds exhibit greatest selectivity and lowest reactivity in comparison to their tertiary counterparts.[4]

Selectivity for the sp^2 hybridized C–H bonds (benzylic) over sp^3 hybridized bonds occurs when:[7]

i. Steric hinderance disfavours the formation of the metal-aryl product.

ii. η^3 coordination stabilises the benzylic product.

Selectivity also poses a problem in functionalising alkanes at the terminal position, since it is the position which results in the desired product, *e.g.* commodity chemicals.[2,9] Activation of alkanes by low valent transition metals results in an alkyl metal hydride where preference for the least substituted alkyl is preferred, giving rise to a linear functionalised alkane (Scheme 1.2).[1]

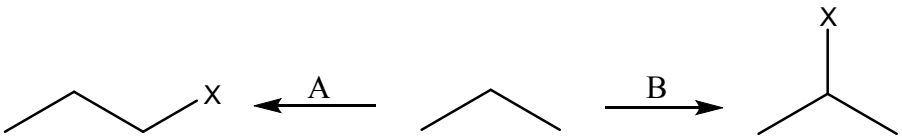

Scheme 1.2: The difference between activation by transition metals (A) and that occurring via radical or electrophilic routes (B).[1]

With an efficient and suitable design of a metal-catalysed oxidation procedure, the above selectivity problems may be avoided.[9] For example, the prefential functionalisation of primary C–H bonds becomes possible, due to the analogous bond strengths of metal–carbon bonds and C–H bonds, as well as the unfavourable steric interactions between branched alkyl groups and ancillary ligands.[9]

In terms of activity, as stated by Labinger and Bercaw, reactions which occur at a plausible rate will be valuable.[2] Furthermore, there is also a greater kinetic selectivity towards the activation of sp^3 hybridised C–H bonds, where the reaction proceeds via homolysis pathways.[7] Interestingly, a study performed on the activation of *n*-octane shows that bulkier groups on the ligand give lower reaction rates to the functionalised olefin in comparison to a less bulky analogue.[11]

1.1.2 Enzymatic paraffin activation

In most biological systems, a large variety of enzymes oxidise non-activated C-H bonds at physiological temperatures and pressures. Studies have been carried out to gain understanding of the mechanistic pathways, efficiency and selectivity of enzymatic paraffin transformation.[2,4] In this dissertation, C–H activation of alkanes will be briefly discussed using examples of cytochrome P450, methane monooxygenase and Vitamin B_{12}.

1.1.2.1 C–H activation by Cytochrome P450

Enzymes are utilised in the functionalisation of a variety of biological compounds by using dioxygen and molecular hydrogen through controlled activation of C–H bonds. An example of such an enzyme is the P450 compound I (P450-I) which consists of an iron(IV)oxo species and an oxidising group that is delocalised over the thiolate and porphyrin ligands.[12] The oxidation of alkanes by cytochrome P450 by dioxygen includes eight steps (Scheme 1.3). First, the low-spin cytochrome P450 A is converted to the high spin form B. This is followed by reduction, after which the coordination of dioxygen to iron(II) occurs. Thereafter, the formation of an oxenoid F occurs via reduction of the complex and elimination of a water molecule, which is followed by the cleavage of the C–H bond in the substrate molecule. Cleavage may occur by two mechanisms, the oxenoid and the "rebound" radical mechanism. The former includes direct insertion of the oxygen atom whilst the latter is a more widely accepted scheme. This involves a radical C–H bond cleavage with recombination in the cage.[13]

In a study to determine the C–H bond kinetics, P450-I hydroxylated the unactivated C–H bonds of lauric acid with a second-order rate constant of k_{app} = 1.1 x 10^7 mol/s at 4 °C.[12] Another study carried out by Wu and co-workers examined the activation of *n*-octane using fluorinated cytochrome P450 BM-3.[14] This particular enzyme is a water soluble monooxygenase consisting of flavin mononucleotide reductase that leads to the hydroxylation of long chain (12-20 carbon atoms) fatty acids. Together with a mutated BM-3 enzyme, it has displayed hydroxylation of *n*-octane (forming 2-, 3-, and 4-octanol). Employing fluorinated cytochrome P450 BM-3, the regioselectivity, activity and stereoselectivity of C–H activation of *n*-octane was controlled.[14]

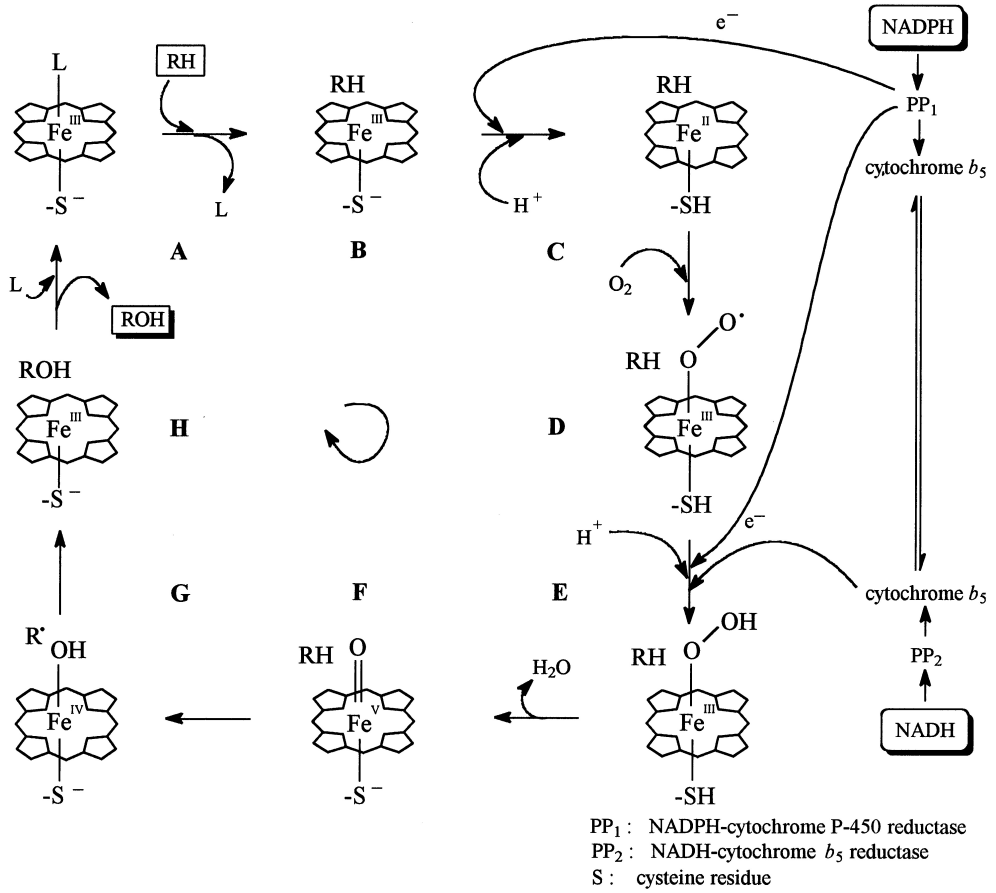

The oxenoid mechanism:

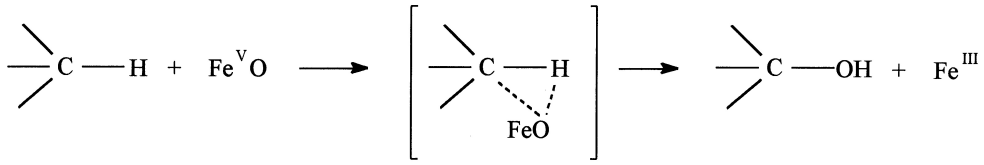

The "rebound" radical mechanism:

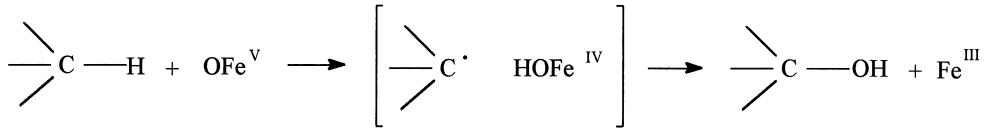

Scheme 1.3: Oxidation of alkanes by cytochrome P450.[13]

1.1.2.2 C–H activation of methane by methane monooxygenase

There is a vast and rising need for the conversion of methane to methanol by inexpensive methods, which has resulted in the development of various catalytic processes.[15] Methane monoxygenase (MMO) (Fig. 1.1) activates methane by the use of its non-heme diiron active

site. This enzyme is found in methanotropic bacteria which acquire their energy and carbon requirements by the catalytic oxidation of unreactive methane via MMO. The enzyme exisits as a six-coordinate octahedral compound, where the iron ions are bridged by a hydroxide ion, a water molecule and a carboxylate.[16]

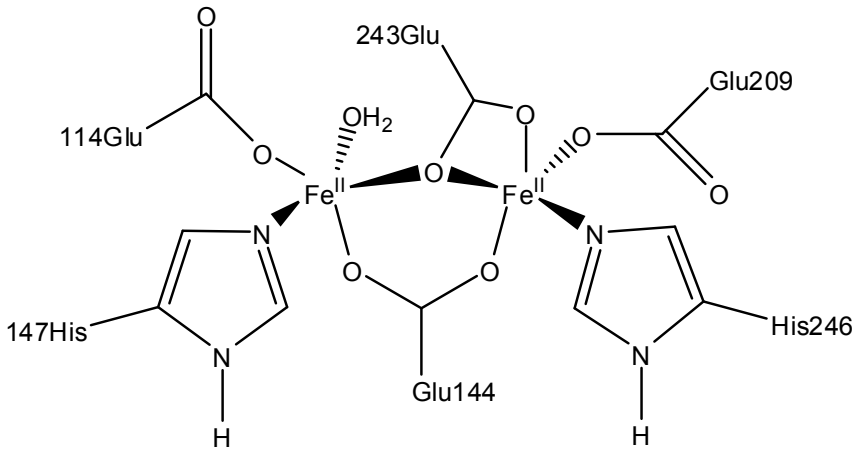

Fig. 1.1: Diagram of the active site of MMO derived from *Methylococcus capsulatus* (Bath).[16]

The enzyme functions in the reduced form (MMOH) by selectively oxidising methane to methanol, (eqn (4)).[1,16] Selectivity is achieved by the different conformations of the molecule in which the H atom is abstracted by the high valent oxoiron cluster.[1] The monoxygenase pathway operates by utilizing two equivalents of NAD(P)H (2 electrons of oxidation power), one splits the O–O bond of oxygen, where one O atom is reduced to water, whilst the remaining O atom is incorporated into the substrate.[1,16] Different classes of MMOs exist, for example, particulate MMO (pMMO), which not only catalyses the conversion of methane to methanol, but also the epoxidation and hydroxylation of small straight–chain alkanes and alkenes (five carbons in length).[15] Interestingly, Shilov and Shul'pin have shown the similarity between MMO and P450, in their mechanism of oxygen atom insertion into the C–H bond. However, MMO is less electrophilic than P450 and does not hydroxylate aromatics.[13]

$$CH_4 + O_2 + NAD(P)H + H^+ \xrightarrow{MMO} CH_3OH + NAD(P)^+ + H_2O \qquad \textbf{(4)}$$

1.1.2.3 C–H activation by coenzyme B_{12}

Coenzyme B_{12}, or 5'-deoxyadenosylcobalamin ($ADCH_2$-B_{12}), is a crowded structure (Fig. 1.2) which contains many close contacts between atoms of the 5'-deoxyadenosyl group and atoms of the substituted corrin ring.[17,18] It participates in many enzymatic reactions as a co-factor, *e.g.* the 1,2 interchange of a hydrogen atom with a substituent on the adjacent carbon atom.[17] This participation is possible through the generation of the 5'-deoxyadenosyl radical ($AdCH_3$) which results from the homolytic cleavage of the Co–C bond.[18] The radical removes the hydrogen atom from the substrate, which is then followed by the rearrangement of the resulting substrate radical as depicted in the mechanism below shown in Scheme 1.4. Its use in organometallic chemistry is quite intriguing, with the generation of free primary radicals under mild conditions.[17]

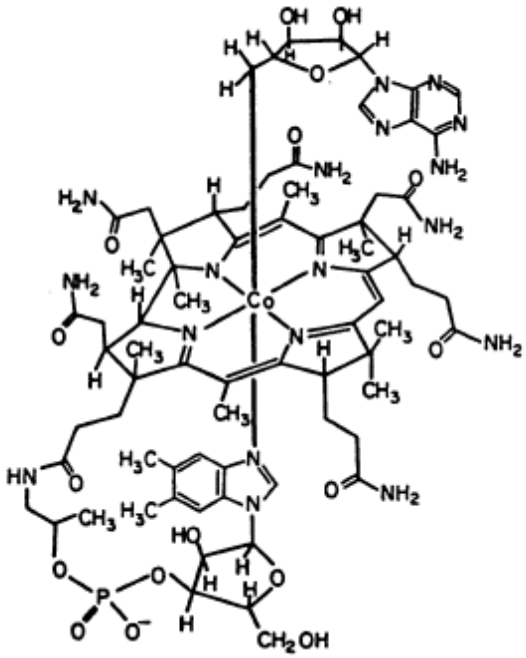

Fig.1.2: Structure of coenzyme B_{12}.[17]

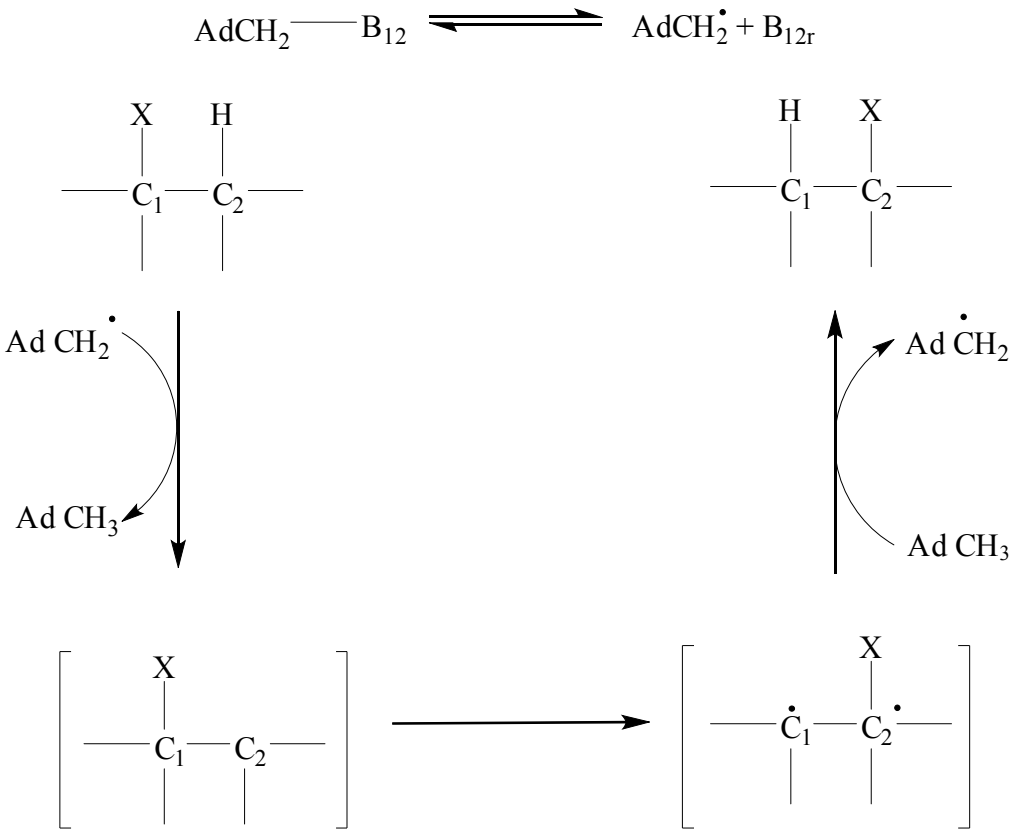

Scheme 1.4: The mechanism of coenzyme B_{12} in its 1,2 hydrogen transfer.[17]

1.1.3 Heterogeneous activation of paraffins

The substantial advances in gas to liquid processes, have led to the production of substantial amounts of *n*-paraffins.[19-21] The need to convert these paraffins to value added products has now become a major interest with the increase in the number of gas to liquid plants worldwide.[19] Processes like cracking, and oxidative dehydrogenation, have been extensively studied and are one of the major sources of olefins.[22] In this dissertation, the oxidative dehydrogenation of alkanes, as well as cracking, will be briefly discussed with appropriate examples.

1.1.3.1 Catalytic cracking

Cracking is defined "as the treatment of hydrocarbons over solid catalysts at temperatures above about 300 °C for the production of hydrocarbon materials of lower average molecular weight".[23] The precursors of plastic materials, synthetic fibers and rubbers, are light olefins and diolefins, which include ethylene, propylene, butenes and butadienes, are produced by conventional processes such as steam cracking, fluid cracking, deep catalytic cracking and thermal catalytic cracking (which is more environmentally friendly).[24]

The catalytic cracking of hydrocarbons is a chain mechanism which comprises of three steps:[25]

i. Initiation: Generation of the carbocation.

ii. Propagation: Transfer of a hydride ion to an adsorbed carbenium ion from the reactant molecule.

iii. Termination: Formation of the olefin after the desorption of the carbenium ion.

Many attempts have been postulated to elucidate the mechanism of the initiation step in the cracking of paraffins. The generation of carbenium ions was thought to occur by the use of olefins, abstaction of a hydride ion by the Lewis acid site of the catalyst, direct attack of a Brønsted acid site on a C–C bond and by zeolite electron acceptor sites.[25,26] Corma and co-workers explain that the proposed initiation is a combination of the above possiblities.[25] After extensive research it was brought forward that catalytic cracking can occur via the formation of carbonium ions which are catalyzed by the Brønsted acid sites of the zeolite framework. The authors have also shown that cracking may occur via radicals which are initiated by Lewis acid electron accepting sites of amorphous alumina. These radicals initiated the formation of olefins through dehydrogenation and/or dealkylation of paraffins. The olefins diffuse to Brønsted acid sites, forming carbenium ions. Interestingly, the authors have shown that the zeolite non-framework alumina is an effective cracking catalyst for the production of light olefins (*e.g.* propylene and butene) with lower coke products and dry gas selectivity.[25]

Irrespective of the mechanism of initiation, in chain propagation, a hydride ion is abstracted from the paraffin by the carbenium ion which then desorbs as a paraffin and the reactant is

converted to a carbenium ion that keeps the chain going by isomerizing and/or cracking.[25] The thermal catalytic cracking of *n*-hexane was carried out by a mixed metal oxide catalyst, MoO_3-CeO_2 impregnated on silica-alumina surface. The non supported catalysts (MoO_3-CeO_2) resulted in the formation of aromatics, whilst the supported catalyst conferred light olefins which varied depending on the metal loadings and the method of preparation.[24] Below is an example of acid catalysed cracking of paraffins (Fig. 1.3).[25]

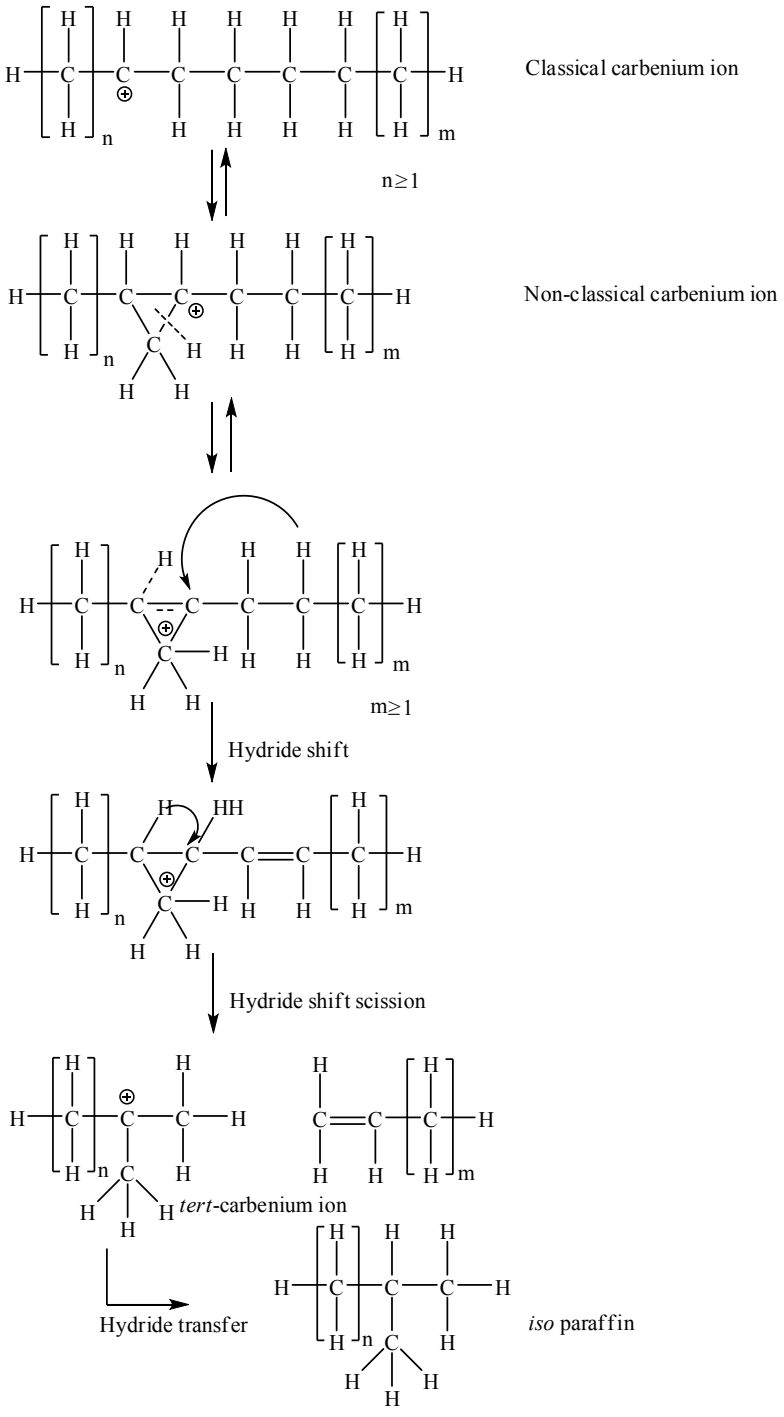

Fig. 1.3: Acid–catalyzed cracking of paraffins.[25]

This application is useful in the petroleum industry, for the conversion of heavy oils and the acid treated solid catalysts usually include clays (montmorillonite) and solid oxides (combination of alumina and silica).[23,25] One of the first fixed bed catalytic processes to reach large scale use was the Houdry Process. The Houdry plant consists of several reactors which manifold together to maintain a continous flow of the oil. This process has been been supplanted by the continuous flow of the catalyst (from the reactor vessel to a regenerator and back) and is observed in fluid catalytic cracking, thermal catalytic cracking and Houdry flow. Modifications to the Houdry plant gave the "Orthoflow" design, where the spent catalyst was regenerated by employing a reactor above the regenerator.[23]

1.1.3.2 Oxidative dehydrogenation (ODH)

" Oxidative dehydrogenation involves the removal of hydrogen from the reactant molecules by oxygen of the feed to form the corresponding olefins without parallel or consecutive oxidation reactions giving carbon monoxide or dioxide as non-selective products." [27]

The ODH of alkanes has been of interest to many researchers due to the following reasons suggested by Cavani and co-workers.[22]

i. In cracking, ethylene is the preferred product over propylene (product in demand) and thus it does not satisfy the market demand for the desired olefins.
ii. In dehydrogenation, catalyst deactivation is brought upon by coking and thermodynamic constraints limit alkane conversion. Therefore the oxygen in ODH counteracts these constraints.
iii. Improved energy efficiency since ODH is exothermic, whilst cracking and dehydrogenation are endothermic.

Many studies have been performed with vanadium based catalysts (VMgO) for the ODH of alkanes.[19-21] VMgO catalysts have been well established for the oxidative conversion of shorter alkanes to their corresponding olefins or dienes.[19,21] Different vanadium loadings were exploited which illustrated their effects on the textural and chemical properties of the catalyst. The varied loadings were also effective in determining the preeminent catalytic activity and selectivity towards the desired products.[19] A similar study was undertaken on the same substrate but with hydrotalcite-like compounds containing vanadium and magnesium

(at different ratios) synthesised by various techniques. The dominant product was styrene, and at a ratio 2.3 of Mg/V, the maximum selectivity and yield of styrene was obtained.[21] Interestingly, Comite and co-workers showed the ODH of propane on vanadium oxide catalysts ($V_2O_5/TiO_2/SiO_2$) which were prepared by different methods of grafting titanium and vanadium alkoxides on silica.[28] A comparitive study was undertaken inorder to establish which preparative method resulted in greatest catalytic activity and selectivity.[28] Studies have also been undertaken with molybdena supported on different oxides for the ODH of propane. Oxides that were exploited in this study included niobia, alumina, zirconia, silica, magnesia and titania out of which titania displayed improved selectivity towards propene.[27] Cavani and co-workers have established that the molybdenum catalysts are less active than the vanadia-based catalysts.[22] Factors such as the formation of MoO_3 crystallites results in the loss of accessibility to the active Mo species. Electronic and catalytic properties are influenced by the presence of alkalis, which affect the MoOx domains and cause a decrease in the ODH turnover rates.[22]

1.1.4 Homogenous activation of paraffins

This area of catalysis focuses on organometallic species and their different modes of alkane C–H bond activation. Crabtree[4] has shown that organometallic complexes which act as catalysts focus on three goals:[4]

i. Simple complexation to the alkane without C–H bond cleavage.
ii. Stoichiometric alkane reactions.
iii. Catalytic alkane conversion.

The two main classes in which C–H activation proceeds is electrophilic activation and oxidative addition. These two reactions proceed through a sigma-bond complexed intermediate.[6] In this dissertation, a distinction between electrophilic activation and oxidative addition will be made, together with other classes of activation listed below:

i. Electrophilic activation
ii. Oxidative activation
iii. Sigma-bond metathesis
iv. Metalloradical activation

v. 1,2-addition

1.1.4.1 Electrophilic addition

This type of reaction is classified as proceeding directly to the functionalised alkane and the term "electrophilic" was coined due to the substitution of a metal for a proton in the intermediate product (eqn (4)).[2] The stabilization of the leaving group, H^+, by solvation in the polar media, serves as the driving force for the reactions shown below. These reactions have been reported with late transition metals and by lanthanide and actinide metal centers (eqn (5)). In the latter two cases, the ligand acts as a base and assists the reaction.[9]

$$LnM^{x+2}X_2 + R\text{-}H \longrightarrow [LnM^{x+2}(R)(X)] + H\text{-}X \qquad \textbf{(4)}$$

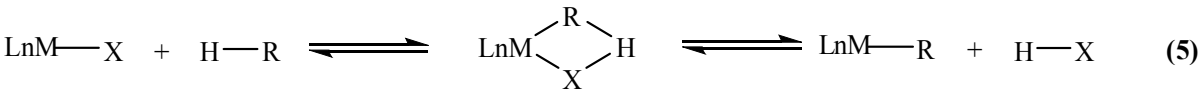

(5)

One of the earliest reactions which described the activation of methane by platinum chloride via electrophilic activation was published by Shilov in 1972.[6] Interestingly, this reaction showed the compatibility of transition metal electrophiles with oxidants and allowed the design of an oxidation procedure based on the initial electrophillic C–H cleavage step.[9] In trying to explore the mechanistic feature of this system, Stahl and co-workers[29] have proposed a catalytic cycle (Scheme 1.5) which takes place with three individual steps; generation of the alkylplatinum(II) intermediate by the electrophilic activation (by Pt(II)) of the alkane; oxidation of alkylplatinum(II) to generate alkylplatinum(IV) and functionalisation by reductive elimination.[6,29] The practical utility of this system has been prevented by various features, however, it still remains as one of the core routes to paraffin activation.[29]

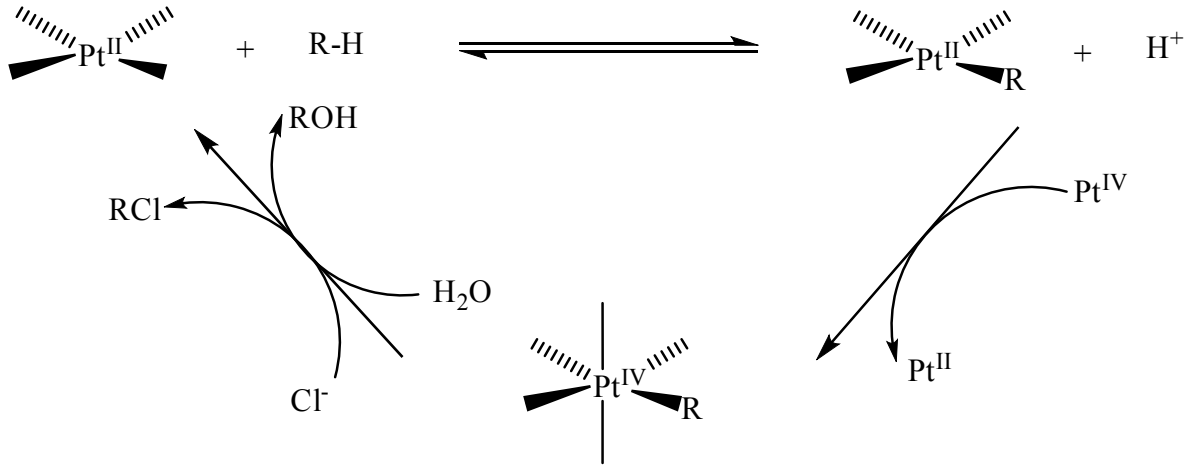

Scheme 1.5: The catalytic cycle for alkane activation by Pt(II) species.[29]

Sen has shown that by using strong acidic media (sulphuric acid), the electrophilicity of the metal ion is enhanced *e.g.* the oxidation of methane to methyl sulphate by Hg(II).[9] This is attributed to the poorly coordinating conjugate base of the strong acid. Overoxidation of the alcohol (the primary product of alkane oxidation) is prevented by esterification. [9]

1.1.4.2 Oxidative addition

Oxidative addition reactions of C–H bonds to late transition metals were discovered in the 1980s[30], where regioselectivity was an important aspect which favoured the reaction of stronger C–H bonds: CH_4 > 1° > 2° >> 3° C–H bonds .[11] Thereafter, the transfer of hydrogen from paraffins to olefinic hydrogen acceptors, was discovered using soluble late-transition metal complexes. Although low yields and ligand degradation were observed, unusual kinetic regioselectivity and dehydrogenation of the less substituted alkanes was noted.[11]

Oxidative addition reactions are characteristic for electron rich, low valent transition metals (*e.g.* Re, Fe, Ru, Os, Rh, Ir, and Pt) and are an attractive way of activating unreactive C–H bonds (eqn (6)).[2,31] In the oxidative addition of H_2, an interaction occurs between the bonding σ-orbitals of hydrogen with the unoccupied acceptor orbital of the complex, as well as between the anitbonding σ*-orbital of the hydrogen with the occupied donor orbital of the complex. These interactions strengthen the M–H bond and weaken the H–H bond via the electron transfer from the $\sigma_g(H_2)$-orbital to the ML_n and from the donor orbital to the σ_u*-orbital. Ligands play a crucial role in the activation of paraffin C–H bonds (Scheme 1.6).[13]

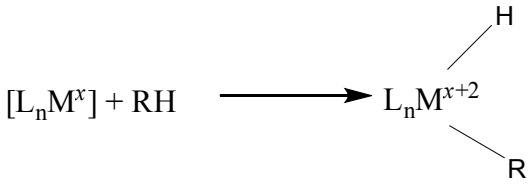

(6)

Those which are a hydride or contain a lone pair with minimal π-bonding are ideal, as noted in the reaction between methane and ruthenium and rhodium complexes. These ligands do not or partially participate in covalent bonding (unlike halide ligands) thereby improving the exothermicity of the reaction.[13]

$$PPh_3 \cong py < DMSO < CN^- < NO_2^- < NH_3 < I^- < Br^- < Cl^- < F^- \cong H_2O$$

Scheme 1.6: Reactivity of Pt(II) ligands on the rate of H-D exchange.[13]

Renkema and co-workers report the transfer dehydrogenation of cyclooctane (COA)/*tert*-butylethene (TBE) (Scheme 1.7).[32] These reactions were catalyzed by iridium complexes, containing pincer ligands, to give cyclooctene and 2,2-dimethylbutane. [32 32 32] Mechanistic studies have shown that the "difficult" or rate determining step was the C–H elimination of the hydrogenated alkane product.[32] Jenson and co-workers have extensively explored the field of the activation of octane, using iridium pincer complexes.[11,33] These authors were the first to establish a catalytic system for the efficient and selective dehydrogenation of *n*-octane to give the corresponding α-olefins.[11,33,34] These ligands are robust and extraordinarily active for alkane dehydrogenation reactions.[34] The C–H activation of paraffins by pincer complexes will be discussed in detail in Chapter two of this dissertation.

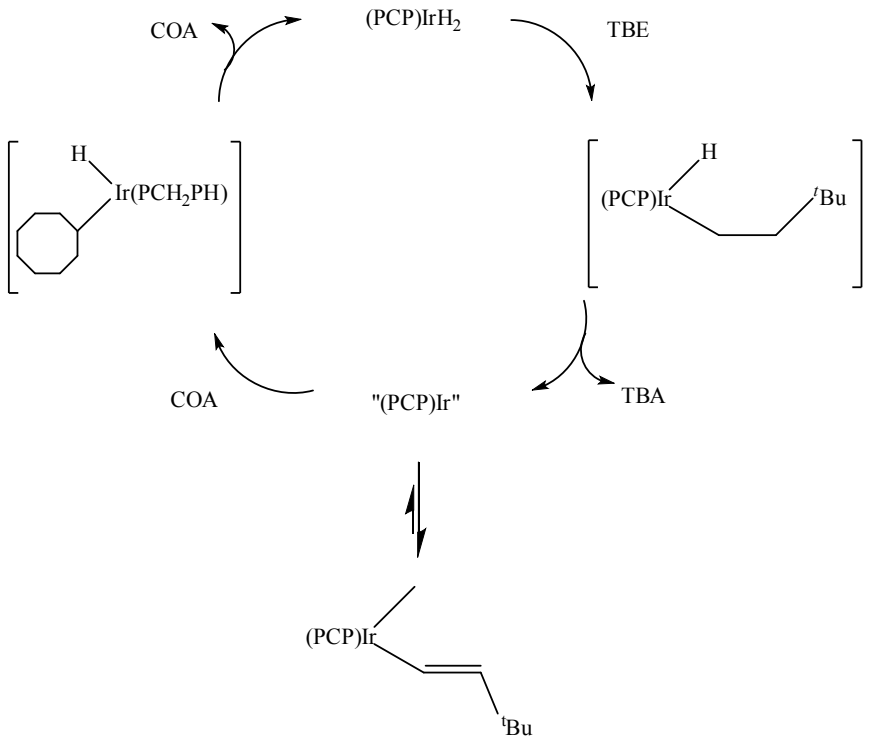

Scheme 1.7: The mechanism of transfer dehydrogenation by an iridium pincer complex. (TBA = *tert*-butylethane and COA = cycloctane).[32]

1.1.4.3 Sigma bond metathesis

In simple terms, sigma bond metathesis is where the C–H bond of the alkane adds across a bond to an electropositive metal, which forms the intermediate that ultimately results in a new hydrocarbon and a new metal alkyl species.[35] Metathesis of alkanes was discovered using a tantalum hydride supported on silica by the group of Basset.[36] In general, alkane metathesis has several advantages over other natural sources and processes such as the Fischer-Tropsch Process and catalytic cracking. For example, metathesis allows the production of high molecular weight (MW) alkanes as well as the production of low MW products from high MW reactants. Metathesis also has the advantage of higher selectivity under less severe conditions.[37]

A notable difference exists between paraffin and olefin metathesis which illustrates the lack of selectivity observed in alkane activation. In the former, cleavage and recombination of

several sp^3 C–C bonds occurs, whilst the latter deals with one sp^2 C=C. Basset and co-workers have shown that selectivity obeys the following order: $C_{n+1} > C_{n+2} > C_{n+3}...$; $C_{n-1} > C_{n-2} > C_{n-3}$ and is related to the mechanism of activation which occurs as follows:[36]

i. Formation of the metal-alkyl which leads to the formation of the olefin and metal hydride species by paraffin dehydrogenation via the activation of the C–H bond.

ii. α-H elimination from the metal-alkyl.

iii. The new olefin on the metal-hydride undergoes hydrogenation.

Crabtree provided an informative portrayal of this mode of activation, where the sigma bond between the metal and the alkane does not compensate for the back donation of charge from the metal to the C–H with that from the C–H to the metal. A reduction of the electron density on the C–H bond results in acidification of the C–H proton. This is due to the fact that one lobe of the C–H σ*-orbital is available for back donation, whilst the other lobe is isolated from the metal. The alkane acidification is therefore imperative in the metathesis pathway, in that an exchange of the R' group (substrate) with that present on the metal M–R occurs due to the transfer of the proton from the substrate to the basic alkyl group on the metal.[1] This phenomenon has been reported to occur with d^0 transition metals (lanthanides or actinides) (eqn (7)).[1-3]

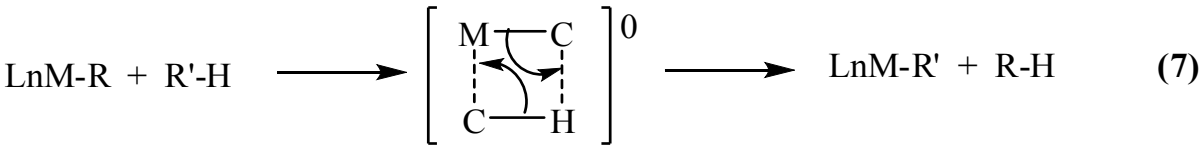

(7)

An example of sigma bond metathesis is shown by the iridium complex $[Cp^*(PMe_3)Ir(CH_3)(OTf)]$ (Cp^* = pentamethylcyclopentadienyl; OTf = OSO_2CF_3) which reacts with several alkanes (*e.g.* methane), as well as the Si–H of silanes. An NMR study of the complex in the activation of methane shows the incorporation of the ^{13}C labelled methane and the formation of CH_4 with time (eqn (8)).[38]

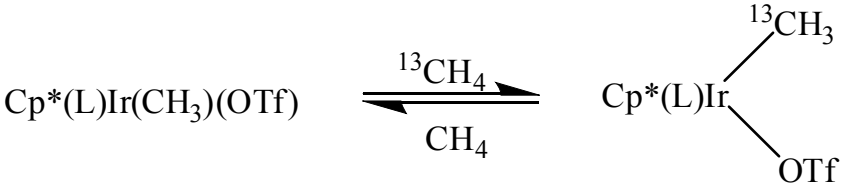

(8)

Pincer - ligated iridium complexes have been used as catalysts in the metathesis of *n*-alkanes and cycloalkanes (COA and COD = cylcooctane and cyclodecane) to give cycloalkanes with different carbon numbers. The major products were dimers with decreasing amounts of cyclooligomers.[39] Metathesis of cycloalkanes is widely employed in the pharmaceutical industry, since the partial oxidation of large saturated rings serve as the building blocks for pharmaceutical intermediates.[39] More recently these catalysts were able to effect the metathesis of *n*-alkanes (conversion of C_n *n*-alkanes to C_{2n-2} *n*-alkanes and ethane) based on molecular weight selectivity.[40]

Basset and co-workers have commented on the impact of alkane metathesis on the processing of fuels (natural gas and crude oil), which may be a solution to the various challenges faced by modern society which correlate to the production of energy and its effects on the environment.[36]

1.1.4.4 Metalloradical activation

This type of activation is characteristic of the interaction of two metalloradicals with a substrate (H_2 or CH_4), that occurs through a termolecular transition state (Fig. 1.4).[41-43] This type of transition state is analogous to that of oxidative addition to single metal centers.[42] Cui and Wayland articulate that the transition states synchronize the breaking of the substrate bond with the formation of two new weaker bonds.[42] Many studies have been undertaken to gain an understanding of the mechanistic pathways of these reactions using rhodium(II) porphyrins (eqn (9)).[41-45] Rhodium(II) porphyrins are particularly interesting since they only activate saturated hydrocarbons and their active centre affords an open site for substrate one-electron oxidative addition reactions by acting as a weak acid in a non donor environment. They also restrict the range of transition state structures due to sterics.[42]

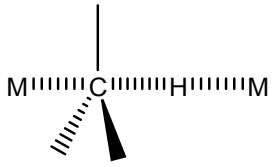

Fig. 1.4: The termolecular transition state of metalloradical alkane activation.[43]

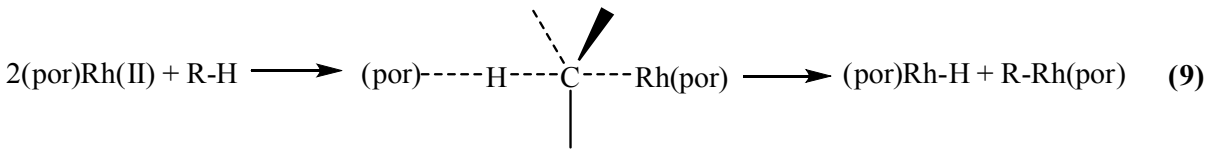

(9)

1.1.4.5 1,2-addition

This type of reaction involves alkane addition across a doubly bonded metal and a non metal.[2] One of the earliest studies was performed on a zirconium imide alkyl complex in which C–H activation occurred through thermolysis of each of the alkyl complexes (eqn (10)). Interestingly, Cummins and co workers noticed that the interaction of the nitrogen 2*pπ* and the zirconium *dp* hybrid orbitals, in the trigonal plane, are weak.[46] The combined electron density on the nitrogen, together with the electrophilicity of the zirconium center renders the C–H bond of the alkane susceptible to activation.[46]

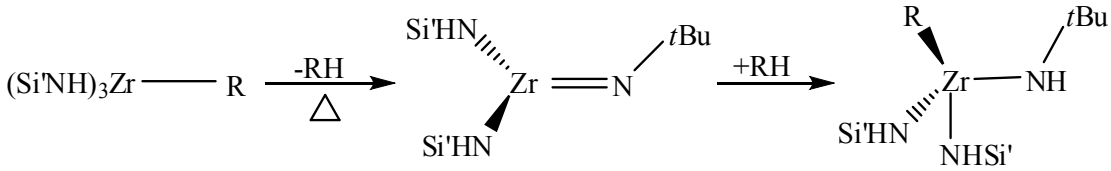

(10)

Si'= (^{t}Bu$_3$Si)

1.2 Conclusion

From the early onset of the mechanisms proposed by Shilov to the present day, it is noted that C–H bond activation has entered the mainstream, and has now become a common interest and focal point of scientists around the world. One of the major setbacks is the fine tuning of a robust and stable metal complex that will not only allow functionalisation of the alkane, but considerable selectivity towards the desired product. However, with the low reactivity of alkanes and their inert nature, the development of alkane C–H bond activation will remain in focus for the years to come.

1.3 References

(1) Crabtree, R. H. *Journal of Organometallic Chemistry* **2004**, *689*, 4083.

(2) Labinger, J. A.; Bercaw, J. E. *Nature* **2002**, *417*, 507.

(3) Klei, S. R.; Tan, L.; Golden, J. T.; Yung, C. M.; Thalji, R. K.; Ahrendt, K. A.; Ellman, J. A.; Tilley, T. D.; Bergman, R. G. In *Activation and Functionalization of C-H Bonds*; American Chemical Society: **2004**; Vol. 885, p 46.

(4) Crabtree, R. H. *Journal of the Chemical Society-Dalton Transactions* **2001**, 2437.

(5) Jia, C.; Kitamura, T.; Fujiwara, Y. *Accounts of Chemical Research* **2001**, *34*, 633.

(6) Goldman, A., S.; Goldberg, K., I. In *Activation and Functionalization of C-H Bonds*; American Chemical Society: **2004**; Vol. 885, p 1.

(7) Zhu, Y. J.; Fan, L.; Chen, C. H.; Finnell, S. R.; Foxman, B. M.; Ozerov, O. V. *Organometallics* **2007**, *26*, 6701.

(8) Crabtree, R. H.; Mellea, M. F.; Mihelic, J. M.; Quirl, J. M. *Journal of the American Chemical Society* **1982**, *104*, 107.

(9) Sen, A. *Accounts of Chemical Research* **1998**, *31*, 550.

(10) Barton, D. H. R.; Doller, D. *Accounts of Chemical Research* **1992**, *25*, 504.

(11) Liu, F.; Pak, E. B.; Singh, B.; Jensen, C. M.; Goldman, A. S. *Journal of the American Chemical Society* **1999**, *121*, 4086.

(12) Rittle, J.; Green, M. T. *Science* **2010**, *330*, 933.

(13) Shilov, A. E.; Shul'pin, G. B. *Chemical Reviews* **1997**, *97*, 2879.

(14) Wu, L.-L.; Yang, C.-L.; Lo, F.-C.; Chiang, C.-H.; Chang, C.-W.; Ng, K. Y.; Chou, H.-H.; Hung, H.-Y.; Chan, S. I.; Yu, S. S. F. *Chemistry – A European Journal* **2011**, *17*, 4774.

(15) Chan, S. I.; Yu, S. S. F. *Accounts of Chemical Research* **2008**, *41*, 969.

(16) Westerheide, L.; Pascaly, M.; Krebs, B. *Current Opinion in Chemical Biology* **2000**, *4*, 235.

(17) Halpern, J. *Science* **1985**, *227*, 869.

(18) Geno, M. K.; Halpern, J. *Journal of the American Chemical Society* **1987**, *109*, 1238.

(19) Elkhalifa, E. A.; Friedrich, H. B. *Applied Catalysis A: General* **2010**, *373*, 122.

(20) Friedrich, H. B.; Govender, N.; Mathebula, M. R. *Applied Catalysis A: General* **2006**, *297*, 81.

(21) Friedrich, H. B.; Mahomed, A. S. *Applied Catalysis A: General* **2008**, *347*, 11.

(22) Cavani, F.; Ballarini, N.; Cericola, A. *Catalysis Today* **2007**, *127*, 113.

(23) Emmett, P. H. *Catalysis*; Reinhold Pub. Corp., 1958.

(24) Al-Yassir, N.; Le Van Mao, R. *Applied Catalysis A: General* **2006**, *305*, 130.

(25) Corma, A.; Orchillés, A. V. *Microporous and Mesoporous Materials* **2000**, *35-36*, 21.

(26) Narbeshuber, T. F.; Brait, A.; Seshan, K.; Lercher, J. A. *Applied Catalysis A: General* **1996**, *146*, 119.

(27) Meunier, F. C.; Yasmeen, A.; Ross, J. R. H. *Catalysis Today* **1997**, *37*, 33.

(28) Comite, A.; Sorrentino, A.; Capannelli, G.; Di Serio, M.; Tesser, R.; Santacesaria, E. *Journal of Molecular Catalysis A: Chemical* **2003**, *198*, 151.

(29) Stahl, S. S.; Labinger, J. A.; Bercaw, J. E. *Journal of the American Chemical Society* **1996**, *118*, 5961.

(30) Janowicz, A. H.; Bergman, R. G. *Journal of the American chemical Society* **1982**, *104*, 352.

(31) Weng, W.; Guo, C.; Moura, C.; Yang, L.; Foxman, B. M.; Ozerov, O. V. *Organometallics* **2005**, *24*, 3487.

(32) Renkema, K. B.; Kissin, Y. V.; Goldman, A. S. *Journal of the American Chemical Society* **2003**, *125*, 7770.

(33) Belli, J.; Jensen, C. M. *Organometallics* **1996**, *15*, 1532.

(34) Jensen, C. M. *Chemical Communications* **1999**, 2443.

(35) Arndtsen, B. A.; Bergman, R. G. *Science* **1995**, *270*, 1970.

(36) Basset, J.-M.; Coperet, C.; Soulivong, D.; Taoufik, M.; Cazat, J. T. *Accounts of Chemical Research* **2010**, *43*, 323.

(37) Goldman, A. S.; Roy, A. H.; Huang, Z.; Ahuja, R.; Schinski, W.; Brookhart, M. *Science* **2006**, *312*, 257.

(38) Burger, P.; Bergman, R. G. *Journal of the American Chemical Society* **1993**, *115*, 10462.

(39) Ahuja, R.; Kundu, S.; Goldman, A. S.; Brookhart, M.; Vicente, B.; Scott, S. L. *Chemical Communications* **2008**, 253.

(40) Haibach, M. C.; Kundu, S.; Brookhart, M.; Goldman, A. S. *Accounts of Chemical Research* **2012,** *currently in press*.

(41) Sherry, A. E.; Wayland, B. B. *Journal of the American Chemical Society* **1990**, *112*, 1259.

(42) Cui, W.; Wayland, B. B. *Journal of the American Chemical Society* **2004**, *126*, 8266.

(43) Zhang, X.-X.; Wayland, B. B. *Journal of the American Chemical Society* **1994**, *116*, 7897.

(44) Cui, W.; Zhang, X. P.; Wayland, B. B. *Journal of the American Chemical Society* **2003**, *125*, 4994.

(45) Wayland, B. B.; Ba, S.; Sherry, A. E. *Journal of the American Chemical Society* **1991**, *113*, 5305.

(46) Cummins, C. C.; Baxter, S. M.; Wolczanski, P. T. *Journal of the American Chemical Society* **1988**, *110*, 8731.

Chapter Two

Introduction to PNP pincer complexes and their application in catalysis

2.1 Pincer ligands

The fundamental criterion for a metal-mediated process is that it should operate in a catalytic manner and it ought to be fast, clean, efficient and selective.[1] To achieve this, the transition metals that are used in catalysis need to be controlled and modified, which is attained by well-designed and appropriate ligand systems.[1,2] Pincer ligands have gained much interest in that they are part of a system which displays high stability, activity and variability.[1-3].

Pincer ligands are terdentate (Fig. 2.1).[4] They consist of two electronic donor atoms, which coordinate to the metal centre in a meridional fashion creating a bond on opposite sides of the metal.[1,4] The donor atoms consist typically of nitrogen (amines (NR_2), sulphur (thioethers (SR_2), oxygen (ethers (OR)), phosphines (PR_2), as well as arsines (AsR_2), N-heterocyclic carbenes (NHCs) and selenoethers (SeR).[1,5] Unidentical donor atoms can also be present.[6] The central anionic atom constitutes the sigma bond between the metal and the ligand.[4] This usually consists of nitrogen, carbon, silicon or a functional group ranging from pyridine to a benzene ring, giving rise to neutral and anionic pincer ligands.[1,5] The donor atoms may also be connected to the central anionic atom through linkers or spaces, which can be *e.g.* methylene groups, amine, silicon or oxygen atoms.[1,7] These types of ligands are more flexible and have a lower preference to the meridional geometry than those ligands lacking the linkers.[7] For example, PNP (aminodiphosphine) ligands, which consist of *ortho*-arylene linkers, prevent the dissociation of the electron rich amide from the low valent electron rich transition metal and it offers increased rigidity.[5,7] The lack of β-hydrogens prevents decomposition of the amide and moisture-sensitive functionalities.[5,7] By varying the donor and central anionic atoms as well as the linker groups, the activity of the metal can be tailored without significantly changing the bonding pattern.[4,8] This allows the reactions of the metal ions to be selective and limited, due to the high demand that these pincer ligands place on the stereochemistry of the complex.[4]

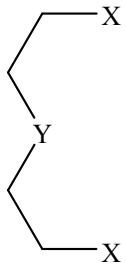

Fig. 2.1: Schematic structure of the pincer ligand showing the donor atoms (X) and central anionic atom (Y).[4]

In this dissertation, the aminodiphosphine (phosphazane) ligands or "PNP" ligands, which consist of an alkyl or arylamine nitrogen atom doubly connected to two diorganyl phosphine ends will be extensively discussed with appropriate examples.[9] These were synthesized in the early 1970s[10] and consist of a combination of two soft donor atoms (phosphorous) and one hard central anionic atom (nitrogen).[9] They offer a range of considerable scope and versatility in that they allow the possibility to investigate the steric and electronic requirements through modification of the functional groups on the phosphine and nitrogen by using bulky or electron withdrawing/donating groups respectively.[8,9,11] This results in changes in the P-N-P angle and conformation around the phosphine.[11] Since these changes allow significant adjustments in the coordination behaviour and the structural properties of the complexes (their ability to create vacant coordination sites at the metal centre), these ligands have been designed for use in catalytic and stoichiometric processes.[9,11]

2.1.1 Pincer ligands and their applications

The first pincer ligands were synthesised in the 1970s by Moulton and Shaw, where they have reported the *ortho* metallation of a bulky 1, 3 bis[(di-*t*-butylphosphino)methyl benzene ("PCP") ligand to the transition metals, nickel, palladium, iridium and rhodium.[12] Due to their versatile nature and robustness, pincer ligands and their respective complexes have seen applications in various fields of chemistry. The applications of pincer complexes as gas sensors, switches and their role in supramolecular chemistry will be discussed briefly with focus on paraffin activation by iridium and cobalt complexes.

2.1.1.1 The role of pincer ligands as gas sensors

Several natural occuring and man induced processes are responsible for the emission of sulphur containing compounds into the earth's atmosphere. For example, sulphur dioxide (SO_2) oxidises in the presence of hydrogen peroxide, sunlight and/or ozone forming SO_3, which reacts with water to form sulphuric acid (acid rain). It is therefore important that there are methods to detect SO_2, even in minute quanitites.[13] Certain platinum NCN complexes undergo a color change from colorless to bright orange upon the co ordination of SO_2 (Scheme 2.1).[8] Sulphur bonds to d^8 metals (*e.g.* platinum(II) and nickel(II) species) through the HOMO and LUMO (2_b^1) of SO_2 and either the filled d_{xz} or d_{yz} orbital of the transition metal.[13] The recognition of SO_2 to platinum is selective and not disturbed by the presence of other gases in the atmosphere.[8] Enhanced selectivity is achieved by fine-tuning the system, with a change in ligand properties (incorporating electron withdrawing or donating substituents of the aryl ring or by changing the basicity on the donor atoms). This increases the accessbility of the metal to sulphur.[13]

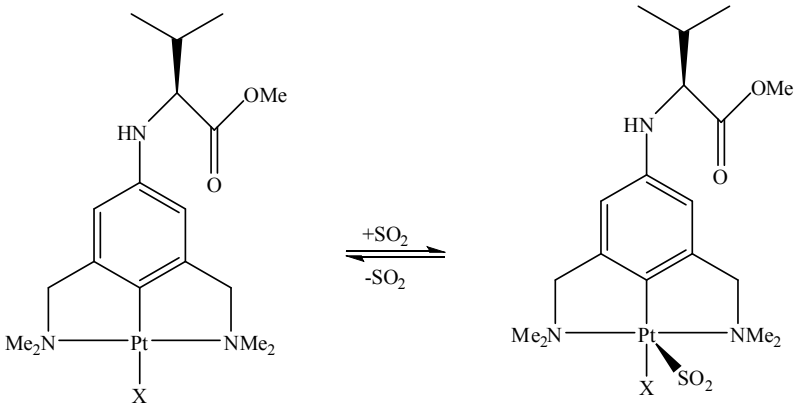

Scheme 2.1: Binding of SO_2 on pincer complexes of NCN with the formation of five-coordinate adducts.[8]

2.1.1.2 The role of pincer ligands as switches

Platinum pincer complexes, mentioned in Section 2.1.1.1, function as a SO_2 gas sensors. However, the same type of complex serves as a gas-triggered crystalline switch that is based on the self assembly of the pincer complex [PtX(R^1-NCN)] (R^1= H; X= Cl, Br, I) in the solid

state.[8] These pincer complexes operate by forming an adduct upon exposure to SO_2 gas, which is noted by using characterisation techniques such as IR spectroscopy and XRD and a change in color. Notably, PCP-ruthenium complexes (eqn (1)) have applications in solvent-triggered molecular switches, where in polar solvents (MeOH and acetone) it develops into a zwitterionic yellow species, whilst in less polar solvents (THF and benzene), it exists as a red metallaquinone with a ruthenium-carbene unit. These properties are due to the functionalization of the arene moeity of the PCP ligand with an acidic hydroxy group.[8]

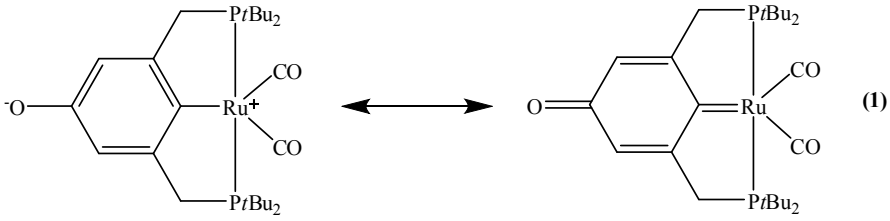

(1)

2.1.1.3 The role of pincer ligands in self assembled systems (supramolecular structures)

Due to their excellent stability, metal complexes containing PNP ligands can serve as the building blocks of 1D, 2D and 3D assemblies and which, by controlled self assembly, can give rise to products that resemble metal organic frameworks.[3,8] Interestingly, d^8 square planar pincer complexes respresents the core unit in non covalent metallodendrimer synthesis (Scheme 2.2). Functionalising the anionic atom of the ligand with a nitrile group creates a bifunctional ligand that has the ability to co ordinate to another ligand's anionic atom and to the metal center.[8,14] This eventually leads to a 5th generation dendritic structure that occurs through halide abstraction and addition of further complexes (AB_2 building blocks).[8]

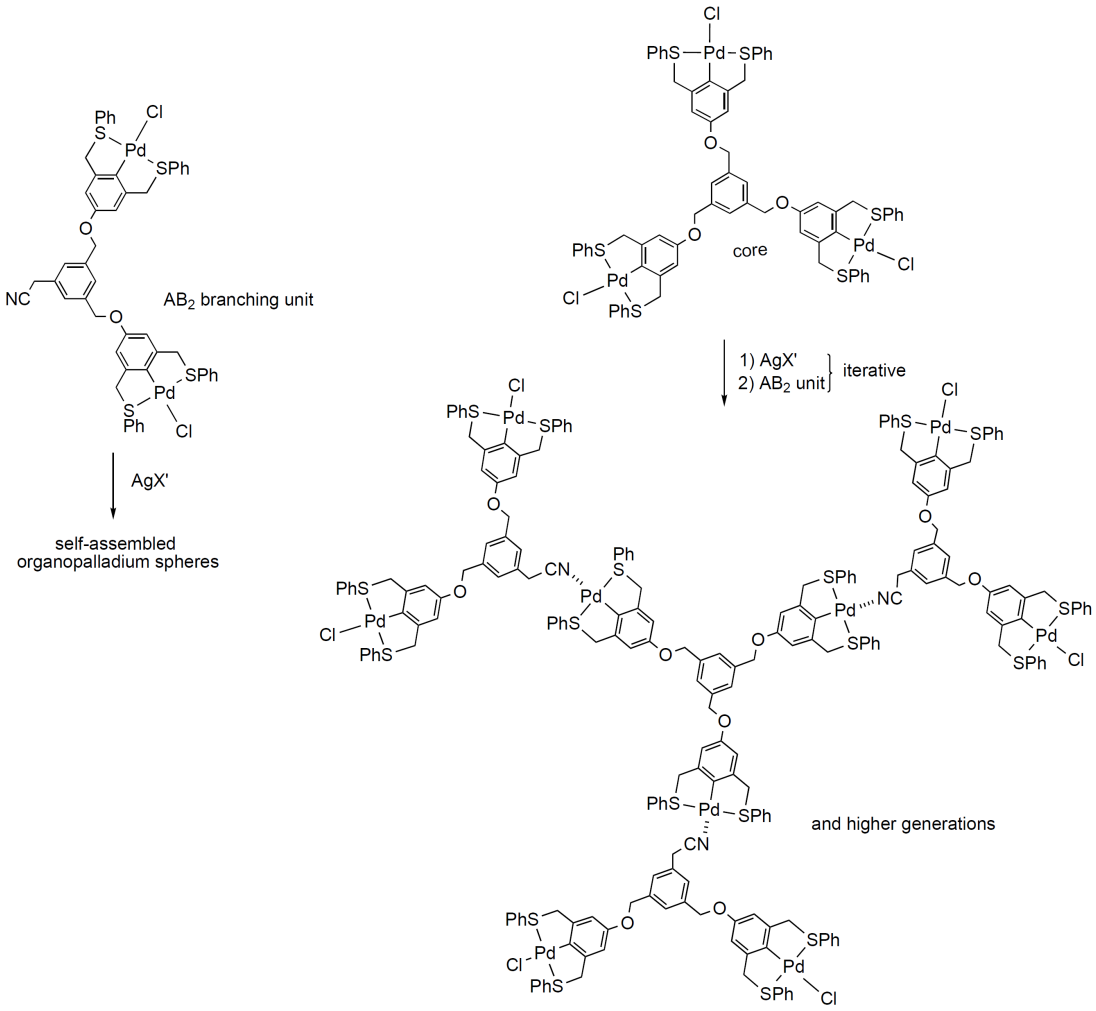

Scheme 2.2: Self assembly of SCS pincer complexes containing palladium.[8]

Studies have been undertaken where palladium pincer complexes are used for host guest interactions.[15] The pincer complexes serve as the respective host or receptors for the nitrile and pyridine guests (Scheme 2.3).[8,15] Enhanced selectivity is achieved through modification of the ligand, for example, a change in the ring size of the calixarene subtituents allow optimization of the binding pockets of these receptors.[8]

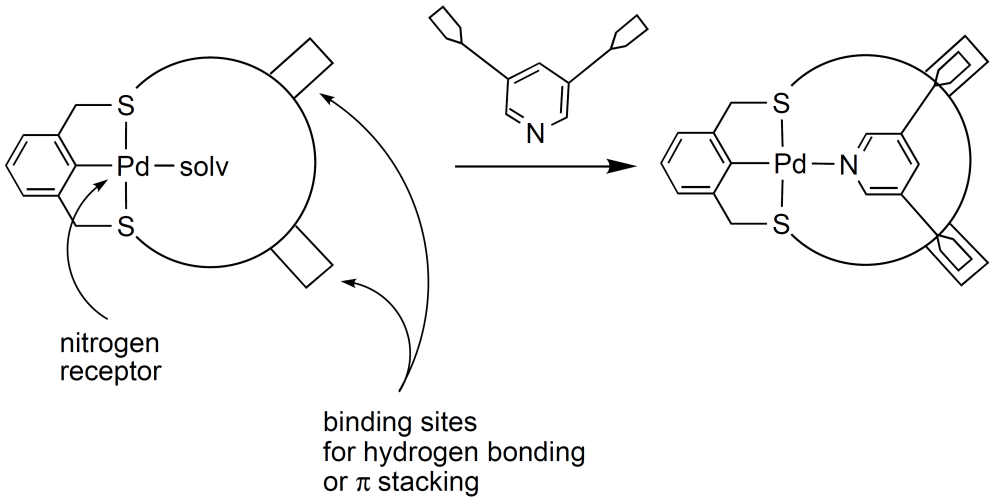

Scheme 2.3: Functionalized palladium SCS pincer complexes for substrate discrimination.[8]

2.1.2 Pincer complexes of iridium and cobalt and their applications in the activation of C–H bonds

2.1.2.1 Iridium

In the dehydrogenation of methane gas, iridium ions (Ir^+) display very high reactivity which can be attributed to three characteristic and unique features:[16]

i. Its ability to change spin.

ii. The strength of the Ir–C and Ir–H bonds

iii. Its ability to form up to four covalent bonds.

Jensen and co-workers have undertaken extensive research on the transfer dehydrogenation of octane using the PCP-Ir complex shown in Fig. 2.2.[17-20] The major kinetic product is the α-olefin, with initial yields of ≥ 90% 1-octene. It was also observed that the overall reaction rate was insensitive to the concentration of the hydrogen acceptor used, for example, 0.2M and 0.5M solutions norbornene gave analogous product distribution and percentage yields. However, when *tert*-butylethene was used, lower selectivity of 1-octene was observed.[18]

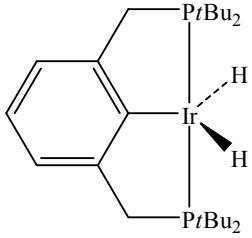

Fig. 2.2: Structure of the iridium pincer complex used by Jensen and co-workers.[18]

Jensen further explains the mechanism of alkane dehydrogenation, which involves three steps (Scheme 2.4):[17]

i. Oxidative addition of a paraffin C–H bond (enhanced selectivity towards the terminal H).

ii. β-hydrogen elimination from the resulting alkyl group.

iii. Dissociation of the alkene and regeneration of the catalyst.

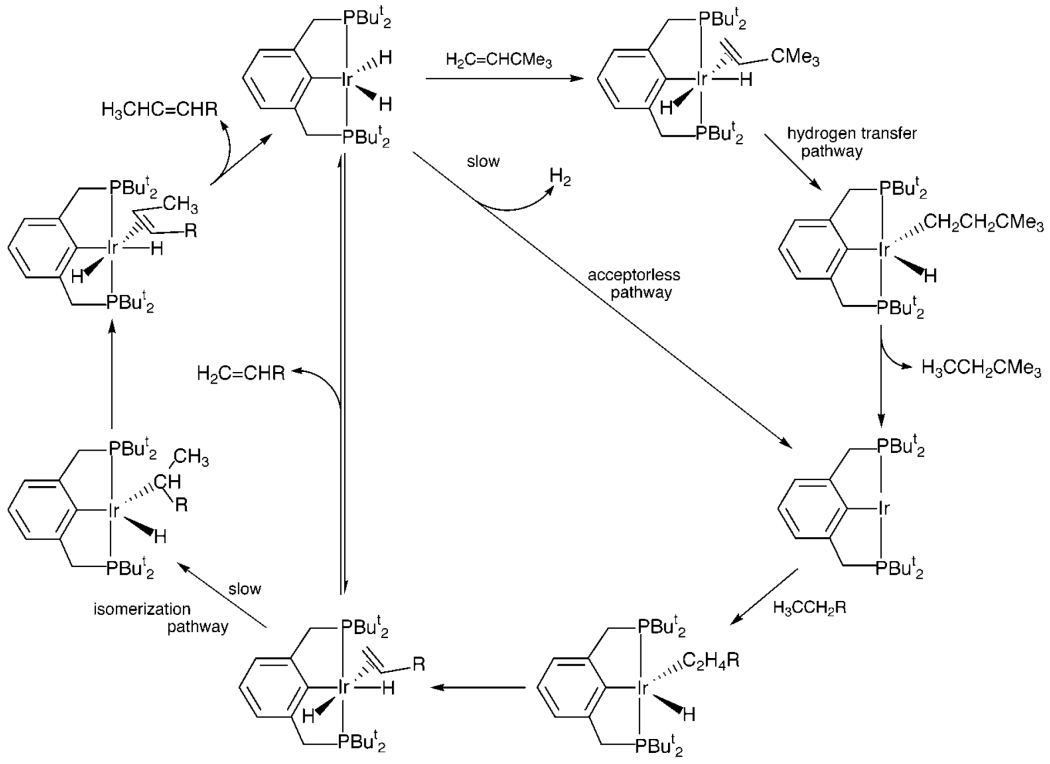

Scheme 2.4: Mechanism of alkane dehydrogenation of linear alkanes proposed by Jensen.[17]

In the case of linear alkanes, the mechanism gets complicated by the secondary alkene isomerization reaction.[17] This complication arises from the competition between the initial

terminal alkene and the hydrogen acceptor for coordination to the metal center.[17] This theory is evidentially substantiated when 1-decene is used as the hydrogen acceptor, where high concentrations of terminal alkenes are obtained in the first 15 minutes of the dehydrogenation reaction.[18] The mechanism shows a kinetic preference for the production of terminal alkenes, which may be attributed to the steric constraints provided by the pincer ligand.[17] Interestingly, when *t*-butyl is used as the respective R group instead of *iso*-propyl, lower fractions of 1-octene were obtained. This reflects the competition between isomerization and transfer hydrogenation.[18] The mechanism also illustrates the acceptorless pathway, which occurs by the direct reductive elimination of H_2 at elevated temperatures.[17]

Studies on the dehydrogenation of cycloctane by the pincer complex shown in Fig. 2.2 have also been undertaken, with *tert*-butylethylene as the hydrogen acceptor , which proceeds at a rate of 82 turnovers h^{-1}.[19,20] This research has shown the long term stability of pincer complexes under catalytic conditions (150 °C with no decomposition over up to one week).[20]

Extensive research has been carried out on the activation of C–H bonds by cationic complexes of iridium, which have shown to be stabilized by solvent molecules and agostic interactions involving the C–H bonds.[21-26] Meiners and co-workers have reported the double C–H activation of THF (eqn (2)) by a sterically modified PNP pincer complex.[22] Firstly, the cyclooctene undergoes reversible intramolecular oxidative addition as well as intermolecular formation of Fischer–carbenes by dehydrogenation of THF.[22]

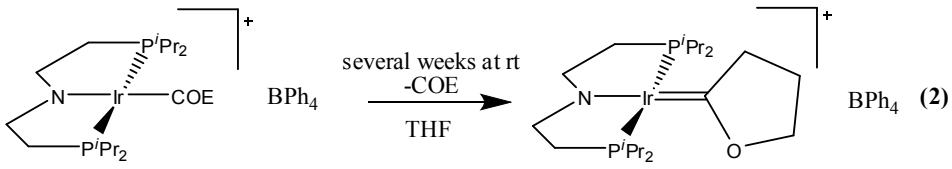

(2)

Ben-Ari and co-workers have reported the C–H activation of benzene (Scheme 2.5) which forms an Ir(I)-Ph complex, which undergoes an oxidation process to form an Ir(III) complex upon treatment with CO.[23] This process involves the migration of the proton from the ligand "arm" to the metal. A DFT study carried out by Ben-Ari and co-workers has shown that the rate determining step in the activation process of benzene is the dissociation of cyclooctene (COE) to form a 14 electron species.[24] Calculations have shown that C–H cleavage occurs after the rate determining step.[24]

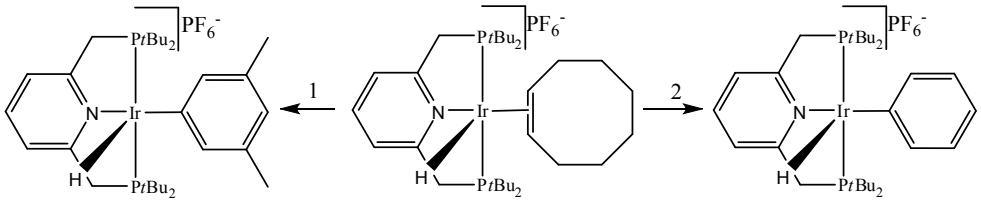

1 = m-Xylene; 1h, 50 °C

2 = Benzene; 1h, 50 °C

Scheme 2.5: C–H activation of benzene by iridium PNP pincer complex.[24]

2.1.2.2 Cobalt

Four distinct stereochemical configurations are associated with cobalt(II), namely, tetrahedral, octahedral, trigonal bypramidal and square planar.[27] To date no research has been carried out in the activation of C–H bonds by pincer complexes of cobalt and a limited number of cobalt PNP complexes have been synthesized. One of the initial studies carried out by Dahlhoff and co-workers describes the bonding of two PNP ligands (2-bis(diphenylphosphino)methyl-6-methylpyridine and 2-[-2-diphenylphosphino-1-(diphenylphosphinomethyl)ethyl]-6-methylpyridine) to cobalt.[28] Interestingly, they have concluded through vibrational and electronic spectra that for various metal ions such as Fe^{II}, Co^{II}, Ni^{II}, Pd^{II}, Zn^{II}, Cd^{II}, and Hg^{II} the ligand bonds either through both the phosphorous atoms or through one of the phosphorous atoms and the nitrogen.[28] More recently, Dong and co-workers have shown how the cobalt PNP pincer complexes exhibit a dual coordination, tetrahedral and square pyramidial, by utilizing ethylene linkers instead of a rigid pyridial moiety (Fig. 2.3).[29] Romerosa and co-workers have elucidated the tetrahedral coordination of the cobalt atom to the PNP ligand by making use of spectroscopic methods and single crystal XRD analysis.[9]

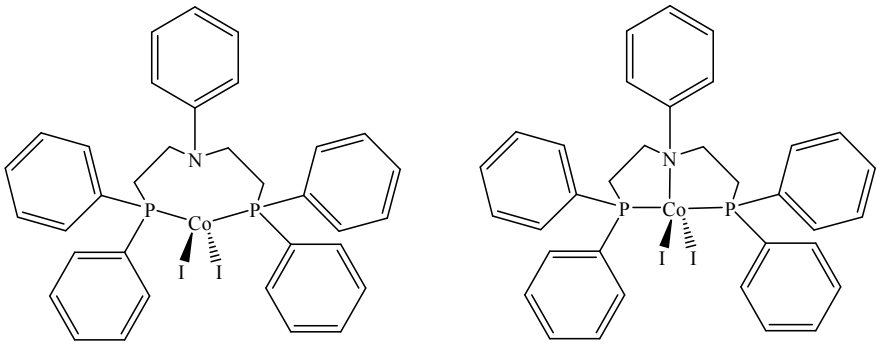

Fig. 2.3: Dual coordination modes of the cobalt pincer complexes.[29]

Dubois and Dubois have used cobalt pincer complexes as catalysts for hydrogen formation and oxidation.[30] The cobalt catalyst, using bromoanilinium tetraflouoroborate, was an active electrocatalyst for hydrogen production as well as for the reduction of protons to hydrogen. More recently, Wiedner and co-workers have also used cobalt PNP pincer complexes as hydrogen oxidation and production catalysts.[31] In contrast to the work performed by Dubois and Dubois[30], Weidner and co-workers have introduced the electron-donating tert-butyl substituent on the phosphorous in the hope that it will promote higher electrocatalytic activity.[31] Their findings have shown a turnover frequency of 160 s^{-1} and an overpotential of 160 mV in comparison to the data obtained by Dubois and Dubois with a turnover frequency of 90 s^{-1} and an over potential of 285 mV.[31]

2.1.3 Characterization techniques

Several characterization techniques are available for the elucidation of ligand and metal complex structures. One of the most useful techniques for phosphorous compounds is ^{31}P NMR. Furthermore, spectroscopic analysis such as IR is effective in establishing the shift in the bands of the functional groups upon complexation to the respective metal.

2.1.3.1 ^{31}P NMR spectroscopy

^{31}P NMR is a useful technique in the characterization and assignment of structures of phosphorous ligands with coordination compounds. Coupling constants can be an informative tool in the investigation of bonding in coordination compounds. With an increase in the electronegativity of the substituents (*e.g.* N, O, S, or halogen) on the phosphorous atom, the s character of the phosphorous donor orbital (α^2_P) increases, which results in an increase in the coupling constants $^1J_{M\text{-}P}$.[32] Furthermore, a chemical shift of less than 100 ppm is observed. For trivalent compounds, positive chemical shifts are observed, as are for penta- and hexacoordinate phosphorous compounds.[33]

The factors responsible for the ^{31}P chemical shift:[33]

i. Shielding from the electrons in the 3p orbitals (sometimes in the 3d orbitals).
ii. The coordination number also affects the environment of the phosphorous atom, as it determines the shape of the phosphorous molecule. (Phosphorous has a coordination number from three to six).
iii. Substituents on the phosphorous atom protect it from magnetic and electronic effects brought upon by its surrounding environment (*e.g.* solvent).

Upon varying the substituent on the phosphorous atom, the change in chemical shift is pronounced due to the distribution of electron density, between the substituent and phosphorous in the σ bonds, difference in bond lengths and angles about phosphorous, change in electronegativity (relative to phosphorous).[33,34]

2.1.3.2 Infrared (IR) spectroscopy

Through the years, IR spectroscopy has become a useful tool in a variety of applications. This is due to the fact that IR spectrometers use a combination of high acquisition speed with excellent spectral sensitivity, as well as its cost effectiveness allowing repetitive and automated analyses.[35]

In this study of pincer complexes, the shift in the $\nu_{P\text{-}N}$ and $\nu_{P\text{-}Ph2}$ band was observed upon

complexation to iridium and cobalt, which occurs at 995 cm^{-1} and 1435 cm^{-1}.[36] Furthermore, for the iridium complexes that contain the counter ion, BF_4^-, a broad band is expected between 1083 and 1015 cm^{-1}.[37]

2.1.3.3 Thermogravimetric analysis

Thermal analysis techniques are useful in studying the thermal behaviour of metal complexes. In thermogravimetic techniques, the complexes are decomposed which causes their bonds to break as a result of the applied heat.[38] Phase transformations are observed through each inflection on the thermogravimetric (TG) curves and the endo and/or exothermic peaks on the (differential scanning calorimetry) DSC curves.[39] TG curves were obtained which indicate the loss in mass of the sample with an increase in temperature. The DSC curves reflect the endothermic thermal event (melting), which is indicated by a negative peak (ΔH is positive) and illustrates that increased heat is being transferred to the sample.[40] In this study, thermogravimetric analysis will be useful in determining the temperature at which the ligands and the complexes decompose.

2.2 Thesis scope

There were several aims of this project. First, to synthesize and characterize PNP pincer ligands with the general formula of $[((Ph)_2P)_2NR]$ (Fig. 2.4), with various functional groups on the nitrogen atom. To investigate the steric effects on the metal centre by varying the subtituent on the nitrogen atom (cyclic group (cyclohexyl), straight chain (pentyl), branched chain (*iso*-propyl) and an aromatic group (benzyl)).

Second, to complex the ligands to the transition metals (iridium and cobalt) and characterize using elemental analysis, infrared spectrocopy and high resolution mass spectrometry. The thermal behaviour of the complexes and the manner in which they decompose upon heating was investigated using thermogravimentric analysis.

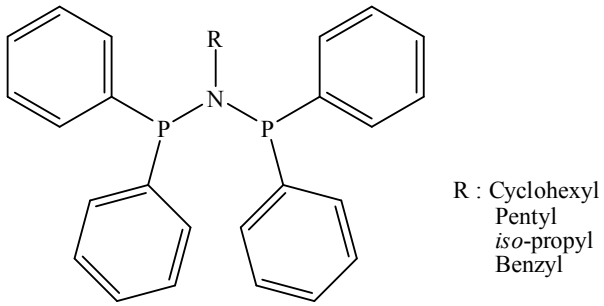

Fig. 2.4: Structure of the PNP pincer complex with the different R functional groups.

Third, to investigate the catalytic behaviour of the iridium and cobalt complexes for the oxidation of *n*-octane using two solvent systems, namely DCM and MeCN at 40 and 80 °C respectively. To investigate the effects of two oxidants, *tert*-butyl hydroperoxide and hydrogen peroxide, on the catalytic behaviour of the metal complexes. To determine the optimum ratio of substrate to oxidant in each solvent system for best conversion and selectivity. To investigate the catalytic behaviour of a ruthenium precursor with the ligands mentioned above in the *in situ*, single pot, oxidation of *n*-octane.

2.3 References

(1) Benito-Garagorri, D.; Kirchner, K. *Accounts of Chemical Research* **2008**, *41*, 201.

(2) van der Boom, M. E.; Milstein, D. *Chemical Reviews* **2003**, *103*, 1759.

(3) Benito-Garagorri, D.; Alves, L. G. A.; Puchberger, M.; Mereiter, K.; Veiros, L. F.; Calhorda, M. J.; Carvalho, M. D.; Ferreira, L. P.; Godinho, M.; Kirchner, K. *Organometallics* **2009**, *28*, 6902.

(4) Xu, X.; Xi, Z.; Chen, W.; Wang, D. *Journal of Coordination Chemistry* **2007**, *60*, 2297.

(5) Winter, A. M.; Eichele, K.; Mack, H.-G.; Potuznik, S.; Mayer, H. A.; Kaska, W. C. *Journal of Organometallic Chemistry* **2003**, *682*, 149.

(6) Fryzuk, M. D.; Berg, D. J.; Haddad, T. S. *Coordination Chemical Reviews* **1990**, *99*, 137.

(7) Fan, L.; Foxman, B. M.; Ozerov, O. V. *Organometallics* **2004**, *23*, 326.

(8) Albrecht, M.; van Koten, G. *Angewandte Chemie International Edition* **2001**, *40*, 3750.

(9) Romerosa, A.; Saraiba-Bello, C.; Serrano-Ruiz, M.; Caneschi, A.; McKee, V.; Peruzzini, M.; Sorace, L.; Zanobini, F. *Dalton Transactions* **2003**, 3233.

(10) Dahlhoff, W. V.; Nelson, S. M. *Journal of Chemical Society* **1971**, *A*, 2184.

(11) Balakrishna, M. S.; Prakasha, T. K.; Krishnamurthy, S. S.; Siriwardane, U.; Hosmane, N. S. *Journal of Organometallic Chemistry* **1990**, *390*, 203.

(12) Moulton, C. J.; Shaw, B. L. *Journal of the Chemical Society, Dalton Transactions* **1976**, 1020.

(13) Albrecht, M.; Gossage, R. A.; Lutz, M.; Spek, A. L.; van Koten, G. *Chemistry – A European Journal* **2000**, *6*, 1431.

(14) Huck, W.; Snellink-Ruël, B.; van Veggel, F. C. J. M.; Reinhoudt, D. N. *Organometallics* **1997**, *16*, 4287.

(15) Kickham, J. E.; Loeb, S. J. *Inorganic Chemistry* **1994**, *33*.

(16) Shilov, A. E.; Shul'pin, G. B. *Chemical Reviews* **1997**, *97*, 2879.

(17) Jensen, C. M. *Chemical Communications* **1999**, 2443.

(18) Liu, F.; Pak, E. B.; Singh, B.; Jensen, C. M.; Goldman, A. S. *Journal of the American Chemical Society* **1999**, *121*, 4086.

(19) Belli, J.; Jensen, C. M. *Organometallics* **1996**, *15*, 1532.

(20) Gupta, M.; Hagen, C.; Flesher, R. J.; Kaska, W. C.; Jensen, C. M. *Chemical Communications* **1996**, 2083.

(21) Dorta, R.; Goikhman, R.; Milstein, D. *Organometallics* **2003**, *22*, 2806.

(22) Meiners, J.; Friedrich, A.; Herdtweck, E.; Schneider, S. *Organometallics* **2009**, *28*, 6331.

(23) Ben-Ari, E.; Leitus, G.; Shimon, L. J. W.; Milstein, D. *Journal of American Chemical Society* **2006**, *128*, 15390.

(24) Ben-Ari, E.; Cohen, R.; Gandelman, M.; Shimon, L. J. W.; Martin, J. M. L.; Milstein, D. *Organometallics* **2006**, *25*, 3190.

(25) Hermann, D.; Gandelman, M.; Rozenberg, H.; Shimon, L. J. W.; Milstein, D. *Organometallics* **2002**, *21*, 812.

(26) Bernskoetter, W. H.; Hanson, S. K.; Buzak, S. K.; Davis, Z.; White, P., S.; Swartz, R.; Goldberg, K. I.; Brookhart, M. *Journal of American Chemical Society* **2009**, *131*, 8603.

(27) Young, R. S. *Cobalt: Its Chemistry, Metallurgy and Uses.*; Reinhold Pub. Corp., New York **1960;** Vol. 149.

(28) Dahlhoff, W. V.; Dick, T. R.; Ford, G. H.; Kelly, W. S. J.; Nelson, S. M. *Journal of the Chemical Society A: Inorganic, Physical, Theoretical* **1971**, 3495.

(29) Dong, Q.; Rose, M. J.; Wong, W.-Y.; Gray, H. B. *Inorganic Chemistry* **2011**, *50*, 10213.

(30) DuBois, M. R.; DuBois, D., L. *Chemical Society Reviews* **2009**, *38*, 62.

(31) Wiedner, E. S.; Yang, J. Y.; Dougherty, W. G.; Kassel, W. S.; Bullock, R. M.; DuBois, M. R.; DuBois, D. L. *Organometallics* **2010**, *29*, 5390.

(32) Pidcock, A. In *Catalytic Aspects of Metal Phosphine Complexes*; American Chemical Society, Washington, D.C **1982**; Vol. 196, p 1.

(33) Emsley, J.; Dennis, H. *The Chemistry of Phosphorus: Environmental, organic, inorganic, biochemical, and spectroscopic aspects.*; Harper and Row, London **1976**.

(34) Bosque, R.; Joaquim, S. *Journal of Chemical Information of Computer Sciences* **2001**, *41*, 225.

(35) Shaw, R. A.; Mantsch, H. H. In *Encyclopedia of Analytical Chemistry*; John Wiley & Sons, Ltd: **2006**.

(36) Slawin, A. M. Z.; Milton, H. L.; Wheatley, J.; Woollins, J. D. *Polyhedron* **2004**, *23*, 3125.

(37) M'thiruaine, C. M.; Friedrich, H. B.; Changamu, E. O.; Bala, M. D. *Inorganica Chimica Acta* **2011**, *366*, 105.

(38) Modi, C.; Patel, M. *Journal of Thermal Analysis and Calorimetry* **2008**, *94*, 247.

(39) Pansuriya, P.; Mohan, P.; Mehul, C.; Pinakin, D.; Vasudev, T. *Journal of Coordination Chemistry* **2008**, *61*, 3336.

(40) Brown, M. E. *Introduction to thermal analysis: Techniques and applications*; Chapman and Hall, London **1988**.

Chapter Three

Experimental: ligand and complex synthesis

3.1 General

3.1.1 Synthesis methods

All experiments were performed using standard Schlenk techniques under inert conditions in moisture free reaction glassware with anhydrous solvents. All solvents were analytical grade. To render the reaction glassware moisture free, it was heated with a heat gun followed by cycles of vacuum and nitrogen pressure. The solvents utilized were dry unless otherwise stated. Diethyl ether, tetrahydrofuran and hexane were distilled from sodium benzophenoneketyl under nitrogen. DCM was distilled from P_2O_5, and ethanol and methanol from magnesium turnings. Deuterated solvents were used as received and stored in a vacuum desiccator.

3.1.2 Nuclear Magnetic Resonance (NMR) spectroscopy

The NMR spectra were recorded at 400 MHz (^{1}H), 100 MHz (^{13}C) and 162 MHz (^{31}P) using a Bruker ultrashield 400 MHz spectrometer at 25 °C in a 5 mm diameter NMR tube with $CDCl_3$ as the respective solvent. ^{1}H NMR and $^{13}C\{^1H\}$ NMR chemical shifts are reported in parts per million (ppm) downfield from tetramethylsilane. ^{1}H NMR and $^{13}C\{^1H\}$ NMR signals were referenced to the residual hydrogen signal of $CDCl_3$ (7.26 ppm) and (77.16 ppm) respectively. ^{31}P NMR chemical shifts were reported in parts per million (ppm) from triphenylphosphine (-17.6 ppm).

3.1.3 Melting point determination

The melting points of the ligands were obtained using a Stuart Scientific melting point apparatus, SMP3. The melting point of the complexes was obtained using an Ernst Leitz Wetzlar WR 461086 melting point apparatus.

3.1.4 Fourier Transform Infra-Red (FT-IR) spectroscopy

The FT-IR spectra were recorded using a Perkin Elmer Universal Attenuated Total Reflection (ATR) Sampling Accessory attached to the FT-IR series 100. Spectra were recorded in the region of 4000–380 cm^{-1}. The sample was placed on the diamond window and pressurized.

3.1.5 Elemental analysis

Elemental analyses were carried out on a LECO CHNS-932 elemental analyzer and standardized with acetanilide. Approximately 2 mg of the sample is accurately weighed into a tin foil cup, placed on an auto sampler and combusted. The products of combustion are CO_2, H_2, N_2 and SO_2. The percentage of carbon, hydrogen and nitrogen in the sample are displayed on the screen.

3.1.6 Mass spectrometry

Mass spectra of the ligands and iridium complexes were recorded using a Bruker Micro TOF-Q11 with electron spray ionization technique.

3.1.7 Thermal gravimetric analysis (TGA)

Thermal gravimetric analysis of the ligands and their respective complexes was carried out using a TA Instruments, SDTQ 600, under a flow rate of 100 ml/min

under nitrogen. The samples were placed on an aluminum pan and the ramping rate was 10 °C covering from 0 °C to 1000 °C.

3.2 Synthesis of ligands

Reagents used in the synthesis of **3.1**–**3.4**:

i). Chlorodiphenylphosphine ($C_{12}H_{10}ClP$), Merck
ii). Triethylamine ($C_6H_{15}N$), Riedel-de Haën
iii). Cyclohexylamine ($C_6H_{11}NH_2$), Aldrich
iv). Pentylamine ($C_5H_{11}NH_2$), Merck
v). *iso*-propylamine ($C_3H_7NH_2$), Fluka
vi). Aniline ($C_6H_5NH_2$), uniLab

3.2.1 Diphosphinocyclohexylamine ($^{Ph}PN_{cyclohexyl}P^{Ph}$) (3.1)

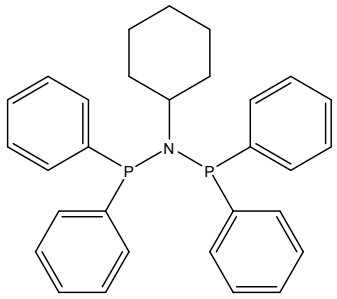

The syntheses of the ligands (**3.1**–**3.4**) were adapted from literature.[1] To a nitrogen saturated Schlenk tube, 30 ml of DCM together with cyclohexylamine (5.6mmol, 0.65 ml) were added. This was followed by the drop-wise addition of triethylamine (7.5 ml). Thereafter, chlorodiphenylphosphine (5.6 mmol, 1.0 ml) was added drop-wise to the amine solution held at -78 °C. The solution was allowed to stir for 30 minutes, after which a second aliquot of chlorodiphenylphosphine (5.6 mmol, 1.0 ml) was added drop-wise. The mixture was allowed to reach rt and was stirred for approximately 14 hours. The solution was filtered via cannula for the removal of the triethylammonium hydrochloride salt. Diethyl ether was added to the filtrate for further precipitation of the salt. The product was isolated after filtering twice through a short column packed carefully with neutral alumina. The column was washed with

diethyl ether. The solvent was removed under reduced pressure and product was allowed to dry overnight under vacuum.

Yield:	53%; 1.38 g (white powder)
Mp:	132.7-134.8 °C
^{1}H NMR (400 MHz, $CDCl_3$) δ:	0.99-1.05 (qui *J*= 11.92 Hz, 2H), 1.32-1.46 (br d, 2H),1.53-1.60 (br m, 4H), 1.82-1.88 (q *J* = 12.38 Hz, 2H),3.18-3.25 (m, 1H), 7.24-7.39 (br m, 17H).
^{13}C NMR (100 MHz, $CDCl_3$) δ:	25.52 (s, 1C), 26.17 (s, 1C), 35.0-35.13 (t, 2C), 60.33-60.49 (t, 1C), 127.93-128.0 (d, 8C), 128.52 (s, 4C), 132.70-132.90 (d, 8C), 140.05-140.18 (d, 2C).
^{31}P NMR (162 MHz, $CDCl_3$) δ:	50.01 (s, 2P).
IRν_{max} (ATR)/cm^{-1}:	3070 (*w*), (ar), 3050 (*w*), (ar), 2926 (*m*), (CH_2), 2851 (*m*), (CH), 1584 (*w*), (ar), 1477 (*m*), (CH_2), 1450 (*m*), (CH_2), 1433 (*s*), (P-Ph_2), 1347 (*w*), (CH), 1179 (*w*), (C-N), 1055 (*s*), (cyclohexane ring), 982 (*m*), (P-N), 741 (*s*), $(CH_2)_n$, 694 (*s*), (Ph).
HRMS (ESI):	Calculated for $C_{30}H_{31}NP_2$: 467.5383; Found: 468.1853 *m/z* (*M* + H)

3.2.2 Diphosphinopentylamine ($^{Ph}PN_{pentyl}P^{Ph}$) (3.2)

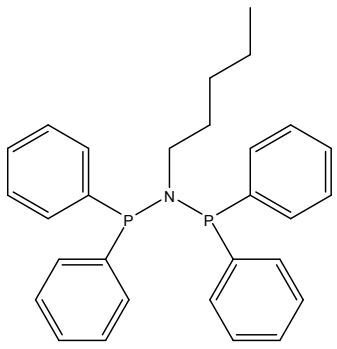

Diphosphinopentylamine was synthesized according to the procedure described for diphosphinocyclohexylamine **(3.1)**, in that pentylamine (5.6 mmol, 0.65 ml) was used as the respective amine.

Yield: 32%; 0.82g (white powder)

Mp: 90.0-92.8 °C

^{1}H NMR (400 MHz, $CDCl_3$) δ: 0.63-66 (t *J* = 7.28 Hz, 3H), 0.81-0.89 (m, 2H), 0.94-1.01 (d *J*= 7.08 2H), 1.03-1.10 (m *J* = 7.78 Hz, 2H), 3.12-3.25 (m, 2H), 7.23-7.40 (br m, 20H).

^{13}C NMR (100 MHz, $CDCl_3$) δ: 13.95 (s, 1C), 22.13 (s, 1C), 28.95 (s, 1C), 30.98-31.01 (t, 1C), 52.97-53.19 (t, 1C), 127.98-128.67 (t, 7C),128.67 (s, 4C), 132.61-132.83 (t, 7C), 139.61-139.75 (d, 2C).

^{31}P NMR (162 MHz, $CDCl_3$) δ: 62.37 (s, 2P)

IRν_{max} (ATR)/cm^{-1}: 3070 (*w*), (ar), 3050 (*w*), (ar), 2943 (*m*), (CH_3), 2934 (*m*), (CH_2), 2856 (*m*), (CH_2), 1584 (*w*), (ar), 1570 (*w*), (ar),1478 (*m*), (CH_2) 1467 (*w*), (CH_2), 1455 (*w*), (CH_2), 1432 (*s*), (P-Ph_2), 1375 (*w*), (CH_3), 1185 (*w*), (C-N), 1164, (*w*) (C-N), 978 (*m*), (P-N), 739 (*s*), $(CH_2)_n$, 690 (*s*), (Ph).

HRMS (ESI): Calculated for $C_{29}H_{31}NP_2$: 455.5271; Found: 478.3859 *m/z* (*M* + Na)

3.2.3 Diphosphino-*iso*-propylamine ($^{Ph}PN_{iso\text{-}propyl}P^{Ph}$) (3.3)

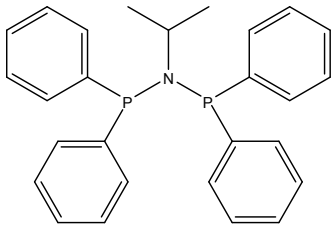

Diphosphino-*iso*-propylamine was synthesized according to the procedure described for diphosphinocyclohexylamine **(3.1)**, in that *iso*-propyl amine (5.6 mmol, 0.50 ml) was used as the respective amine.

Yield: 55%; 1.32g (white powder)

Mp: 129.3-131.8 °C

^{1}H NMR (400 MHz, $CDCl_3$) δ: 1.06-1.0 (d *J* = 6.48 Hz, 6H), 3.63-3.72 (m, 1H),

7.18-7.28 (br m, 20 H).

^{13}C NMR (100 MHz, $CDCl_3$) δ: 24.33-24.47 (t, 2C), 51.93-52.03 (t, 1C), 127.98-128.05 (d, 8C), 128.54 (s, 4C), 132.77-132.99 (d, 8C), 139.84-139.97 (d 2C).

^{31}P NMR (162 MHz, $CDCl_3$) δ: 48.84 (s, 2P).

IRν_{max} (ATR)/cm^{-1}: 3068 (*w*), (ar), 3050 (*w*), (ar), 2966 (*m*), (CH_3), 2863 (*w*), (CH_3), 2863 (*w*), (CH_3), 1585 (*w*), (ar), 1462 (*w*), (CH_3), 1478 (*m*), (CH_3), 1432 (*s*), (P-Ph_2), 1376 (*m*), (CH_3), 1359 (*m*), (CH),1202 (*w*), (C-N), 1171 (*m*), (C- N), 986 (*m*), (P-N), 690 (*s*), (Ph).

HRMS (ESI): Calculated for $C_{27}H_{27}NP_2$: 427.4727; Found: 428.1679 *m/z* (*M* + H)

3.2.4 Disphosphinobenzylamine ($^{Ph}PN_{benzyl}P^{Ph}$) (3.4)

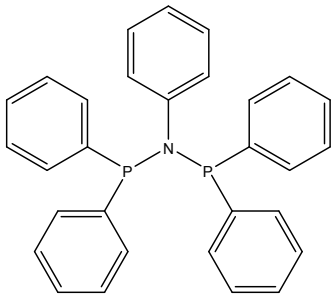

Diphosphinobenzylamine was synthesized according to the procedure described for diphosphinocyclohexylamine **(3.1)**, in that the aniline was distilled thrice before use. Other changes that were made to the synthesis was that 50 ml of DCM together with aniline (11.2 mmol, 1.0 ml) were added. This was followed by the drop wise addition of triethylamine (15 ml). Thereafter, chlorodiphenylphosphine (11.2 mmol, 2.0 ml) was added drop wise to the amine solution held at -78 °C. The solution was allowed to stir for 30 minutes after which a second aliquot of chlorodiphenylphosphine (11.2 mmol, 2.0 ml) was added drop wise. The rest of the synthesis was carried out as that for **3.1**.

Yield: 44%; 2.27g (white powder)

Mp: 128.0-130.0 °C

^{1}H NMR (400MHz, $CDCl_3$) δ: 6.59-6.61 (d, *J* = 6.53Hz, 2 H), 6.89-6.90 (m, 3H), 7.21-7.33 (br m, 20H)

^{31}P NMR (162MHz, $CDCl_3$) δ: 68.48 (s, 2P)

IRν_{max} (ATR)/cm^{-1}: 3056 (*w*), (ar), 1589 (*m*), (ar), 1433 (*s*), (P-Ph_2), 1208 (s), (C-N), 1188 (*w*), (C-N), 1177 (*w*), (C-N), 1161 (*w*), (C-N), 988 (*w*), (PN), 689 (*s*), (Ph)

HRMS (ESI): Calculated for $C_{30}H_{25}NP_2$: 461.4903; Found: 484.3329 *m/z* (*M* +Na)

3.3 Synthesis of iridium complexes

Reagents used in the synthesis of **3.5-3.9**:

i). Iridium trichloride hydrate ($IrCl_3.nH_2O$), Heraeus.

ii). 2-Propanol ($C_3H_8O_2$), Aldrich

iii). *cis*-Cyclooctene (C_8H_{14}), Aldrich

iv). Silver tetrafluoroborate ($AgBF_4$), Merck

3.3.1 Synthesis of di-μ-chlorotetrakis(cyclooctene)diiridium(I)[IrCl(COE)$_2$]$_2$ (3.5)

The synthesis of **3.5** was adapted from literature.[2] A three-necked round bottom flask was equipped with a reflux condenser and a nitrogen inlet and was charged with hydrated iridium chloride ($IrCl_3.xH_2O$) (6.7 mmol, 2.0 g), 22 ml of 2-propanol, 8 ml of deionized water and cyclooctene (COE) (4 ml). A slow stream of nitrogen was allowed to pass through the system. The solution was stirred at room temperature for five minutes and was thereafter brought to reflux at 78 °C for three hours during which the solution turns from a dark purple to dark orange, with the precipitation of di-μ-chlorotetrakis(cyclooctene)diiridium(I). The resultant mixture was allowed to cool to room temperature, and the orange precipitate (di-μ-chlorotetrakis(cyclooctene)diiridium(I)) was collected by quick filtration using a

Büchner funnel with a constant flow of nitrogen over the mouth of the funnel. The precipitate was rapidly washed with cold methanol for the removal of unreacted COE and dried overnight in *vacuo* at room.

Yield: 52 %; 1.05 g (orange powder)

Mp: > 148 °C (decomposes); literature[2] 150 °C (decomposes)

$C_{32}H_{56}Cl_2Ir_2$ (calculated): C: 43.1%; H: 5.9% (C: 42.9%; H: 6.3%)

IRν_{max} (ATR)/cm^{-1}: 2971 (*m*), (CH), 2907 (*s*), (CH_2), 2844 (*s*), (CH_2), 1463 (*s*), (CH_2) 1446 (*s*), (CH_2), 1355 (*s*), (CH),738 (*m*), $(CH_2)_n$.

3.3.2 Synthesis of [($^{Ph}PN_{cyclohexyl}P^{Ph}$)Ir COE][$BF_4$] (3.6)

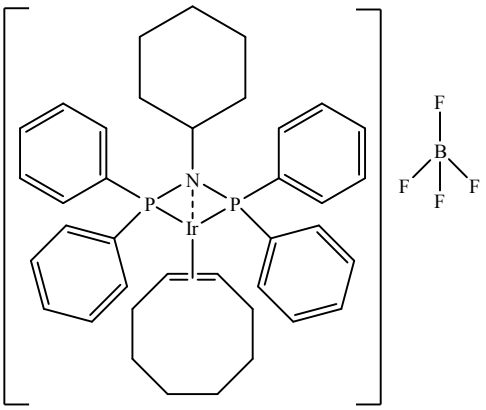

To a nitrogen saturated Schlenk tube, 15 ml of DCM and $[IrCl(COE)_2]_2$ (0.5 mmol, 0.45g), **(3.5)**, was added and purged with nitrogen for 10 minutes. To another pre-dried nitrogen saturated Schlenk tube, 2 ml of DCM and $AgBF_4$ (1.5 mmol, 0.30g) were added and purged with nitrogen for 15 minutes. The $AgBF_4$ solution was added drop-wise to the iridium solution at -30 °C. The solution turned from orange to red and was left to stir until the bath reached room temperature (approximately 8 hours). Thereafter, the solution was filtered twice, under nitrogen, through celite for the removal of silver chloride. The celite was washed with DCM. The resultant filtrate was reduced to a ¼ its volume by the removal of DCM under reduced pressure. ($^{Ph}PN_{cyclohexyl}P^{Ph}$) (1.5 mmol, 0.70g), **(3.1)**, was dissolved in 1 ml of DCM and added drop wise to the iridium-tetrafluoroborate solution. The resultant mixture was allowed to stir for 15 minutes and reduced to half its volume under reduced pressure.

Hexane was added to allow precipitation of the yellow solid. The solid was washed several times with hexane and diethyl ether for the removal of unreacted starting material {monitored by TLC- solvent system; hexane:DCM (1:1)}. The solvent was removed via cannula after each wash and the precipitate was dried overnight at room temperature under high vacuum.

Yield:	58%; 0.50 g (orange powder)
Mp:	> 185 °C (decomposes)
$C_{38}H_{45}BF_4IrNP_2$ (calculated):	C: 53.4%; H: 5.3%;N: 1.8%
	(C: 53.3%; H: 5.3%; N: 1.6%)
IRν_{max} (ATR)/cm^{-1}:	3056 (*w*), (ar), 2931 (*w*), (CH_2), 2856 (*w*), (CH), 1587 (*w*), (ar), 1572 (*w*), (ar), 1480 (*m*), (CH_2), 1435 (*s*), (P-Ph_2), 1307 (*w*), (CH), 1183 (*w*), (C-N), 1151 (*w*), (C-N),1049 (br s), (BF_4), 997 (*m*), (P-N), 731 (*s*), $(CH_2)_n$, 692 (*s*) (Ph).
HRMS (ESI):	Calculated for $C_{38}H_{45}IrNP_2$: 769.9569; Found: 768.2663 *m/z* (*M* - H)

3.3.3 Synthesis of [($^{Ph}PN_{pentyl}P^{Ph}$)Ir COE][BF_4] (3.7)

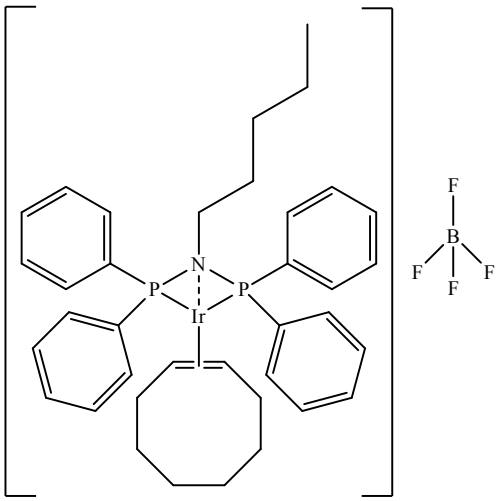

[($^{Ph}PN_{pentyl}P^{Ph}$)Ir COE][BF_4] was synthesized according to the procedure described for [($^{Ph}PN_{cyclohexyl}P^{Ph}$)IrCOE][$BF_4$] **(3.6)**, in that, $AgBF_4$ (1.4 mmol, 0.27g) and ($^{Ph}PN_{pentyl}P^{Ph}$) (1.2 mmol, 0.55g), **(3.2)** were used.

Yield: 44 %; 0.38 g (orange powder)

Mp: 160-163 °C

$C_{37}H_{45}BF_4IrNP_2$ (calculated): C: 50.5%; H: 5.3%; N: 1.6%

(C: 52.6%; H: 5.4%; N: 1.7%)

IRν_{max} (ATR)/cm^{-1}: 3057 (*w*), (ar), 2927 (*m*), (CH_2), 2867 (*m*), (CH_2), 1587 (*w*), (ar), 1572 (*w*), (ar), 1481 (*w*), (CH_2) 1466 (*w*), (CH_2), 1435 (*s*), (P-Ph_2), 1378 (*w*), (CH_3), 1187 (*w*), (C-N), 1048 (br *s*), (BF_4), 997 (*s*), (P-N), 746 (*s*), $(CH_2)_n$, 690 (*s*), (Ph).

HRMS (ESI): Calculated for $C_{37}H_{45}IrNP_2$: 757.9457; Found: 756.2658 *m/z* (*M* - H)

3.3.4 Synthesis of [($^{Ph}PN_{iso\text{-}propyl}P^{Ph}$)Ir COE][$BF_4$] (3.8)

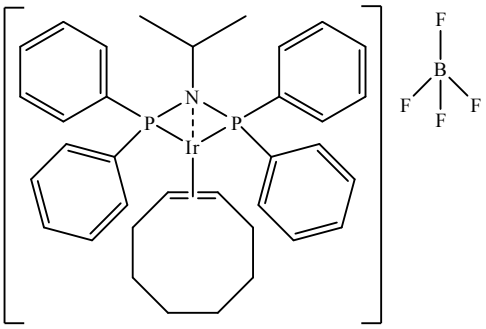

[($^{Ph}PN_{iso\text{-}propyl}P^{Ph}$)Ir COE][$BF_4$] was synthesized according to the procedure described for [($^{Ph}PN_{cyclohexyl}P^{Ph}$)IrCOE][$BF_4$] **(3.6)**, in that $AgBF_4$ (1.4 mmol, 0.27g) and ($^{Ph}PN_{iso\text{-}propyl}P^{Ph}$) (1.2 mmol, 0.51g), **(3.3)** were used.

Yield: 47 %; 0.38 g (orange powder)

Mp: > 155 °C (decomposes)

$C_{35}H_{41}BF_4IrNP_2$ (calculated): C: 51.0%; H: 5.1%; N: 1.8%

(C: 51.5%; H: 5.1%; N: 1.7%)

IRν_{max} (ATR)/cm^{-1}: 3059 (*w*), (ar), 2963 (*w*), (CH_3), 1587 (*w*), (ar), 1481 (*w*), (CH_3), 1436 (*s*), (P-Ph_2), 1372 (*w*), (CH), 1175 (*m*),

(C-N), 1038 (br *s*), (BF_4), 997 (*s*), (P-N), 744 (*s*), ($(CH_2)_n$, 692 (*s*) (Ph).

HRMS (ESI): Calculated for $C_{35}H_{41}IrNP_2$: 729.8913; Found: 728.2334 *m/z* (*M* - H)

3.3.5 Synthesis of [($^{Ph}PN_{benzyl}P^{Ph}$)Ir COE][BF_4] (3.9)

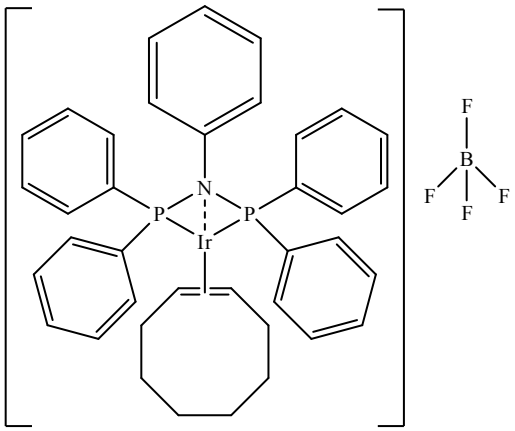

[($^{Ph}PN_{benzyl}P^{Ph}$)Ir COE][BF_4] was synthesized according to the procedure described for [($^{Ph}PN_{cyclohexyl}P^{Ph}$)IrCOE][$BF_4$] **(3.6)**, in that $AgBF_4$ (1.6 mmol, 0.30g) and ($^{Ph}PN_{benzyl}P^{Ph}$) (1.2 mmol, 0.55g), **(3.4)** were used.

Yield: 77 %; 0.65 g (orange powder)

Mp: 168-170 °C

$C_{38}H_{39}BF_4IrNP_2$ (calculated): C: 51.9%; H: 4.2%; N: 1.8%
(C: 53.7%; H: 4.7%; N: 1.7%)

IRν_{max} (ATR)/cm^{-1}: 3055 (*w*), (ar), 1588 (*m*), (ar), 1435 (*s*), (P-Ph_2), 1208 (*m*), (C-N), 1161 (*w*), (C-N), 1052 (br *s*), (BF_4), 996 (*m*), (P-N), 690 (*s*), (Ph).

HRMS (ESI): Calculated for $C_{38}H_{39}IrNP_2$: 763.9089; Found: 762.2045 *m/z* (*M* - H)

3.4. Synthesis of cobalt complexes

Reagents used in the synthesis of **3.10-3.13**:

i). Cobalt chloride ($CoCl_2.6H_2O$), Associated Chemical Enterprise.

3.4.1 Synthesis of [($^{Ph}PN_{cyclohexyl}P^{Ph}$)$CoCl_2$] (3.10)

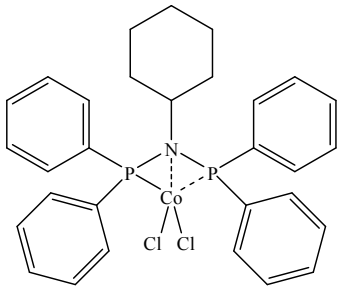

The synthesis of **3.10-3.13** was adapted from a known procedure in literature.[3] To a 100 ml two necked round bottom flask, 10 ml of ethanol was added and purged with nitrogen for 10 minutes. Thereafter, $^{Ph}PN_{cyclohexyl}P^{Ph}$ (0.62 mmol, 0.290 g), **(3.1)**, and $CoCl_2.6H_2O$ (0.63 mmol, 0.15 g) were added. The solution was slowly stirred at room temperature. The round bottom flask was equipped with a condenser and the solution was brought to reflux at 77 °C. After 15 minutes under reflux the solution changed color from blue to green. After 24 hours under reflux, the solvent was removed under reduced pressure resulting in the crude product. For the removal of unreacted ligand, the green solid was washed several times with diethyl ether {monitored by TLC-solvent system;hexane:DCM(1:1)} and dried under high vacuum overnight.

Yield:	59 %; 0.22 g (green powder)
Mp:	175-179°C
$C_{30}H_{31}Cl_2CoNP_2$ (calculated):	C: 60.3%; H: 5.2%; N: 2.3%
	(C: 60.3%; H: 5.2%; N: 2.3%)
IRν_{max} (ATR)/cm^{-1}:	3404 (*br*), (OH), 3055 (*w*), (ar), 2931 (*w*), (CH_2), 2854 (*w*), (CH), 1586 (*w*), (ar), 1480 (*m*) (CH_2), 1434 (*s*), (P-Ph_2), 1372 (*w*), (CH), 1187 (*w*), (C-N),1153 (*w*), (C-N), 1068 (*s*), (cyclohexane ring), 1027 (*w*)

(cyclohexane ring), 998 (*m*), (P-N), 744 (*s*), $(CH_2)_n$, 690 (*s*), (Ph).

3.4.2 Synthesis of [($^{Ph}PN_{pentyl}P^{Ph}$)$CoCl_2$] (3.11)

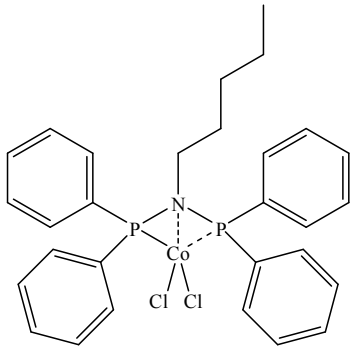

[($^{Ph}PN_{pentyl}P^{Ph}$)$CoCl_2$] was synthesized according to the procedure described for [($^{Ph}PN_{cyclohexyl}P^{Ph}$)$CoCl_2$] **(3.10)** in that $^{Ph}PN_{pentyl}P^{Ph}$ (0.62 mmol, 0.28 g), **(3.2)** was used.

Yield:	45 %; 0.16 g (green powder)
Mp:	217-222 °C
$C_{29}H_{31}Cl_2CoNP_2$ (calculated):	C: 58.6%; H: 6.0%; N: 2.2%
	(C: 59.5%; H: 5.3%; N: 2.4%)
IRν_{max} (ATR)/cm^{-1}:	3382 (*br*), (OH), 3055 (*w*), (ar), 2946 (*m*), (CH_3), 2862 (*w*), (CH_2), 1586 (*w*), (ar), 1480 (*m*), (CH_2) 1466 (*w*), (CH_2), 1433 (*s*), (P-Ph_2), 1377 (*w*), (CH_3), 1210 (*w*), (C-N), 1190 (*w*), (C-N), 997 (*m*), (P-N), 740 (*s*), $(CH_2)_n$, 691 (*s*), (Ph).

3.4.3 Synthesis of [(^{Ph}PN$_{iso\text{-propyl}}$P^{Ph})CoCl$_2$] (3.12)

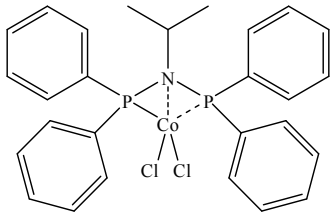

[(^{Ph}PN$_{iso\text{-propyl}}$P^{Ph})CoCl$_2$] was synthesized according to the procedure described for [(^{Ph}PN$_{cyclohexyl}$P^{Ph})CoCl$_2$] **(3.10)** in that^{Ph}PN$_{iso\text{-propyl}}$P^{Ph} (0.62 mmol, 0.27 g) **(3.3)** was used.

Yield:	61 %; 0.21g (green powder)
Mp:	160-162°C
$C_{27}H_{27}Cl_2CoNP_2$ (calculated):	C: 58.0%; H: 5.2%; N: 2.4%
	(C: 58.2%; H: 4.9%; N: 2.5%)
IRν_{max} (ATR)/cm^{-1}:	3420 (*br*) (OH), 3055 (*w*), (ar), 2974 (*w*), (CH_3), 1586 (*w*), (ar), 1481 (m), (CH_3), 1434 (*s*), (P-Ph$_2$), 1370 (*m*) (CH), 1170 (*m*), (C-N), 998 (*m*), (P-N), 743 (*s*), (CH_2)$_n$, 692 (*s*), (Ph).

3.4.4 Synthesis of [(^{Ph}PN$_{benzyl}$P^{Ph})CoCl$_2$] (3.13)

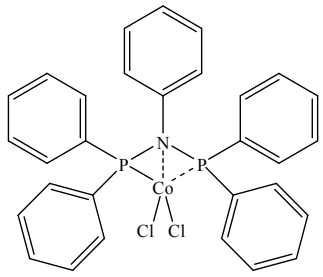

[(^{Ph}PN$_{benzyl}$P^{Ph})CoCl$_2$]was synthesized according to the procedure described for [(^{Ph}PN$_{cyclohexyl}$P^{Ph})CoCl$_2$] **(3.10)** in that^{Ph}PN$_{benzyl}$P^{Ph} (0.62 mmol, 0.27 g), **(3.4)** was used.

Yield: 76 %; 28 g (green powder)

Mp: 113-115 °C

$C_{30}H_{25}Cl_2CoNP_2$ (calculated): C: 60.4%; H: 4.9%; N: 2.0%

(C: 60.9%; H: 4.3%; N: 2.4%)

IRν_{max} (ATR)/cm^{-1}: 3329 (*br*), (OH), 1590 (*w*), (ar),1434 (*s*), (P-Ph_2), 1210 (*s*), (C-N), 1189 (*m*), (C-N), 1174 (*w*), (C-N), 1160 (*w*), (C-N), 999 (*m*), (P-N), 687 (*s*) (Ph).

3.5. Synthesis of the ruthenium precursor

3.5.1 Synthesis of triphenylphosphinedihydridocarbonylruthenium(II) (3.14)

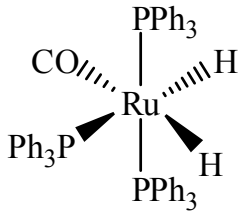

Reagents used in the synthesis of **3.14**:

i. Ruthenium trichloride hydrate ($RuCl_3.xH_2O$), Aldrich
ii. Triphenylphosphine($C_{18}H_{15}P$), BDH Laboratory Reagents
iii. Formaldehyde (CH_2O), BDH Laboratory Reagents
iv. Potassium hydroxide (KOH), Saarchem

The synthesis of **3.14** was performed as reported in the literature.[4] A three-necked round bottom flask was equipped with a nitrogen inlet, a reflux condenser and purged with nitrogen for 10 minutes. Thereafter, triphenylphosphine (3.2 g, 12 mmol) and 100 ml degassed MeOH were added. The mixture was heated at a rapid reflux for 10 minutes. In quick sequence, a solution of ruthenium trichloride hydrate (0.5 g, 2 mmol) in 40 ml MeOH aqueous formaldehyde (37 % w/v, 20 ml) and potassium hydroxide (0.6 g, 10.7 mmol) in 20 ml MeOH, were added to the mixture. The reaction was held at reflux for an hour during which a grey precipitate formed. The reaction was allowed to reach room temperature, cooled in an ice bath and left to stir for 30 minutes. The grey precipitate was filtered under vacuum using a Büchner

funnel and washed, in sequence, with absolute ethanol (25 ml), water (25 ml), absolute ethanol (25 ml) and hexane (25 ml). The crude precipitate was left to dry under vacuum and thereafter dissolved in toluene and filtered through a short column packed with neutral alumina. The column was washed with toluene. The solvent was concentrated under vacuum, after which MeOH was added, which resulted in the precipitation of the white product. The solvent was removed via cannula and the product was left to dry overnight in *vacuo* at room temperature.

Yield:	33%; 0.6 g (white powder)
Mp:	159 °C (Literature[4]: 161 °C)
^{1}H NMR (400 MHz, $CDCl_3$) δ:	-9.08 to -8.74 (m, 1H), -7.05 to -6.84 (m, 1H), 6.83-7.18 (m, 45H)
^{31}P NMR (162 MHz, $CDCl_3$) δ:	44.71 (t 1P), 57.0 (d, 2P)
IRν_{max} (ATR)/cm^{-1}:	1941 (*s*), (ν_{CO})

3.6 References

(1) Blann, K.; Bollmann, A.; de Bod, H.; Dixon, J. T.; Killian, E.; Nongodlwana, P.; Maumela, M. C.; Maumela, H.; McConnel, A. E.; Morgan, D. H.; Overette, M. J.; Pŕetorius, M.; Kuhlmann, S.; Wasserscheid, P. *Journal of Catalysis* **2007**, *249*, 244.

(2) Parshall, G. W. *Inorganic Syntheses*; McGraw Hill, New York, **1974**.

(3) Romerosa, A.; Saraiba-Bello, C.; Serrano-Ruiz, M.; Caneschi, A.; McKee, V.; Peruzzini, M.; Sorace, L.; Zanobini, F. *Dalton Transactions* **2003**, 3233.

(4) Marimuthu, T.,*The preparation and novel application of diphosphorous xanthenes family ligands in homogenous catalysis* PhD Thesis, University of KwaZulu-Natal, **2011**, p 89.

Chapter Four

Results and Discussion

4.1 Ligand synthesis and characterization

The PNP ligands (**3.1-3.4**) were synthesized by deprotonating the respective amine with triethylamine, followed by the addition of two equivalents of chlorodiphenylphosphine at -78 °C (Scheme 4.1). This was to allow complete reaction of the amine, but at the same time the amine reacts relatively slowly (low temperature) so as to prevent unwanted side products. Moderate yields were obtained, due to the numerous required filtrations through the alumina column for removal of oxidized phosphine ((P=O), ^{31}P NMR = ~30 ppm). The product was isolated as a white powder and was fairly crystalline, as noted by the sharpness of the melting point (Chapter 3, Section 3.2) and the sharp endothermic peak in the DSC plot (Section 4.5.1).

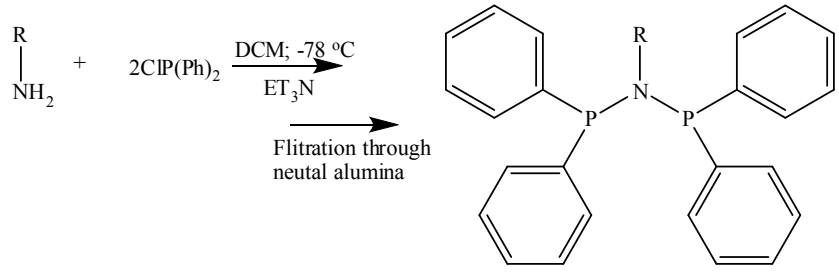

Scheme 4.1: Synthetic procedure for ligands **3.1-3.4**.
(R: cyclohexyl (**3.1**); pentyl (**3.2**); *iso*-propyl (**3.3**); benzyl (**3.4**)).

In the ^{1}H NMR spectra, the peaks integrated to the correct number of protons for the respective ligand (Appendix A, Figs 1A, 4A, 7A, 10A, and Chapter 3, Section 3.2). Noticeably, the proton attached to the carbon directly bonded to the nitrogen atom (proton (1)) (Fig. 4.1) was of keen interest, so as to establish whether bonding of the phosphorous atom to the amine occurred. The peak shift for these respective protons for ligands **3.1** to **3.3** are shown in Table 4.1. These protons occur furthest downfield, in the aliphatic region, in relation to the other protons since it is attached to the

nitrogen atom. Interestingly, all peak shifts are within the same magnitude, irrespective of the type of amine. This may be due to the fact that the other atoms (phosphorous) attached to the nitrogen are identical.

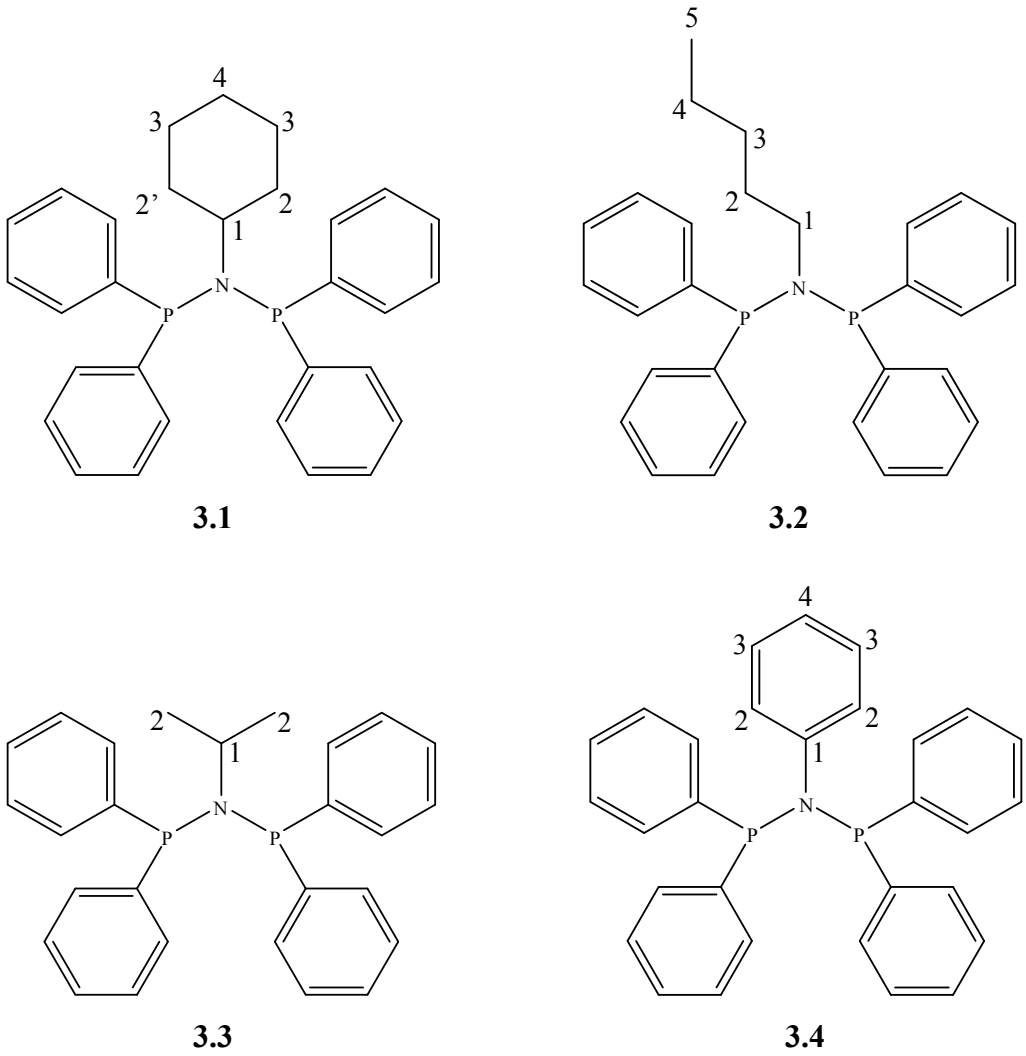

3.1 **3.2**

3.3 **3.4**

Fig. 4.1: Assignment of the protons of ligands **3.1**–**3.4**.

Table 4.1: Peak shifts of the proton on carbon (1) of ligands **3.1–3.3**.

Ligand	δ ^{1}H NMR peak ($CDCl_3$)/ ppm	Proton Integration
3.1	3.18	Multiplet, 1H
3.2	3.12	Multiplet, 2H
3.3	3.63	Multiplet, 1H

For ligand **3.1** the protons on carbon (4) occur furthest upfield, since it is furthest away from the heteroatom (N). The protons on carbon (2) (δ 1.32 ppm) and (2') (δ 1.82 ppm) appear at different positions, one as a broad doublet and the other as a

quartet, respectively. This could be attributed to the side in which the proton on carbon (1) lie conferring different multiplicities of protons on carbons (2) and (2'). However, the protons on carbon (3) (δ 1.53 ppm) are not affected and appear as a broad multiplet integrated for 4H. The protons of the aromatic region cannot be integrated individually and displayed as a broad multiplet. (This is observed for all ligands). For ligand **3.2**, the methyl protons on carbon (5), (δ 0.63 ppm), appear as a triplet furthest downfield, since they are furthest away from the nitrogen heteroatom. The methylene protons on carbons (2) (δ 0.81 ppm), (3) (0.94) and (4) (1.03 ppm)) appear as multiplets, integrated to the correct number of protons. For ligand **3.3**, the protons on carbon (2) (δ 1.06 ppm) are equivalent and appear as a doublet integrated for 6 protons. For ligand **3.4**, the protons on carbons (2) and (4) (δ 6.89 ppm) occur further downfield than the protons on carbon (3) (δ 6.59 ppm). This could be attributed to the electron delocalization effects on the aromatic ring, thus protons on carbons (2) and (4) are in a similar environment and hence have similar peak shifts.

Upon observation of the ^{13}C NMR of the ligands **3.1**-**3.3** (Appendix A, Figs. 2A, 5A, 8A and Chapter 3, Section 3.2), all aromatic carbons appeared in the region of 127 ppm to 140 ppm. For ligands **3.1**-**3.3**, the carbon directly attached to nitrogen, carbon at position 1 (Fig. 4.1), occurs as a triplet due to coupling with the phosphorous and is furthest upfield. As noted with the ^{1}H NMR for ligand **3.1**, the carbons at position 2 and 2' occur at different peak shifts, whilst the carbon at position 3 remain unaffected and appear as a triplet which could be attributed to the gamma substituent effect.[1]

The ^{31}P NMR of the ligands (Appendix A, Figs. 3A, 6A, 9A, 11A and Chapter 3, Section 3.2) was compared to that in literature and is shown in Table 4.2. This was used as the principal technique to confirm the synthesis of the ligands. It can be observed that the peak shifts obtained in literature[2] are in accordance with those obtained experimentally. The singlet at 81.8 ppm in the ^{31}P NMR for chlorodiphenylphosphine (Appendix A, Fig. 12A) shifts upfield upon complexation to the amine. This peak shift is due to the electron rich environment created by the amine, which result in a shielding effect, shifting the phosphorous peak upfield.[3] The alkyl group attached to the nitrogen may cause the difference in the peak shifts of ligands relative to each other. A more branched alkyl group (**3.1** and **3.3**) has a

greater electron donating effect, resulting in greater shielding, hence the peak shifts for these respective ligands are further upfield in comparison to ligands **3.2** and **3.4**.[3-5] Upon observation of the IR data (Chapter 3, Section 3.2), ligand **3.1** shows strong cyclohexane ring vibrations at 1055 cm^{-1}.[6] A distinctive feature of long-chain linear aliphatic groups is the presence of a strong methylene band at 1470 cm^{-1} and a weak methyl band at 1380 cm^{-1} and a band 750-720 cm^{-1} which is due to the methylene rocking vibration.[6] Such features are clearly observed with ligand **3.2**. Another interesting observation for ligands **3.2** and **3.3** is that the bands at 1478 cm^{-1} and 739 cm^{-1} respectively are split into two bands and this is attributed to the crystallinity of the ligand.[6]

Table 4.2: ^{31}P NMR shifts of the ligands **3.1-3.4**.

Ligand	**^{31}P NMR peak ($CDCl_3$)/ ppm**	
	Experimental	**Literature[2]**
3.1	50.0	50.7
3.2	62.4	62.3
3.3	48.8	50.1
3.4	68.5	62.3

The HRMS (High Resolution Mass Spectrometry) (Chapter 3, Section 3.2) of the ligands were in agreement with those calculated, with the addition of either a hydrogen (**3.1** and **3.3**) or sodium ion (**3.2** and **3.4**). This is commonly noted, where adduct ions, such as hydrogen $[M + H]$, sodium $[M + Na]^-$ (or potassium $[M + K]^+$ in some cases) are prominent.[7]

4.2 Synthesis of iridium complexes and characterization

4.2.1 Synthesis and characterization of the iridium precursor, di-μ-chlorotetrakis(cyclooctene)diiridium(I) $[IrCl(COE)_2]_2$, (3.5)

The synthesis of the iridium complexes required the prior synthesis of the iridium precursor, di-μ-chlorotetrakis(cyclooctene)diiridium(I) $[IrCl(COE)_2]_2$, (**3.5**) (Chapter 3, Section 3.3.1) (eqn (**4.1**)).[8]

$$2IrCl_3 + 4C_8H_{14} + 2(CH_3)_2CH(OH) \longrightarrow Ir_2Cl_2(C_8H_{14})_4 + 4HCl + 2(CH_3)_2CO \quad \textbf{(4.1)}$$

This was carried out as reported in the literature[8], where cyclooctene (COE), *iso*-propanol and iridium chloride are brought to reflux for three hours affording an orange precipitate. The NMR spectrum of the precursor (**3.5**) could not be undertaken, even under inert conditions, due to rapid decomposition. However, the melting point was in accordance with literature values. The elemental analyses (%C and %H) obtained experimentally were within the accepted range (< 0.5%) of the calculated values and this was thus a confirmation that the precursor was successfully synthesized. A comparison of the IR data between uncomplexed COE and the precursor was also undertaken (Table 4.3) in order to confirm the synthesis of the precursor. Upon complexation to the metal, the bands associated with the *cis* double bond disappear, i.e. the medial *cis* C–H stretch and out of plane bend and the alkenyl C=C stretch. There is also the distinct shift in the bands associated with the methylene and methyne C–H bonds.

Table 4.3: Comparison of IR data of COE and $[IrCl(COE)_2]_2$, (**3.5**)

Functional group/assignment[6]	**ν/cm^{-1} of COE**	**ν/cm^{-1} of the precursor (3.5)**
Medial *cis* C–H stretch	3015	-
Methyne C–H stretch	-	2971, 2907
Methylene C–H asym. stretch	2916	-
Methylene C–H sym. stretch	2850	2844
Alkenyl C=C stretch	1650	-
Methyne C–H bend	1340	1355
Methylene $(CH_2)_n$- rocking ($n \geq 3$)	750	738
cis C–H out of plane bend	701	-

4.2.2 Synthesis and characterization of [(^{Ph}PNP^{Ph})IrCOE][BF_4] complexes (3.6-3.9)

The synthesis of the iridium complexes (**3.6-3.9**) (Chapter 3, Section 3.3.2) was undertaken according to the generalized Scheme 4.2. Excess silver tetrafluoroborate was added to the iridium precursor (**3.5**) at -30 °C in DCM, resulting in a color change from orange to brick red. After stirring the solution for approximately eight hours (room temperature was reached), a grey precipitate formed (silver chloride) which was removed via filtration through celite. Excess ligand was added to the filtrate and the mixture stirred, after which hexane and diethyl ether were added which resulted in precipitation of the cationic complex. The synthetic procedure was based on literature procedures,[9,10] but modifications were made (Section 3.2.2). The percentage yields were calculated based on the assumption that 100% of the intermediate (**1**) formed, which was used as the limiting reagent for the calculations.

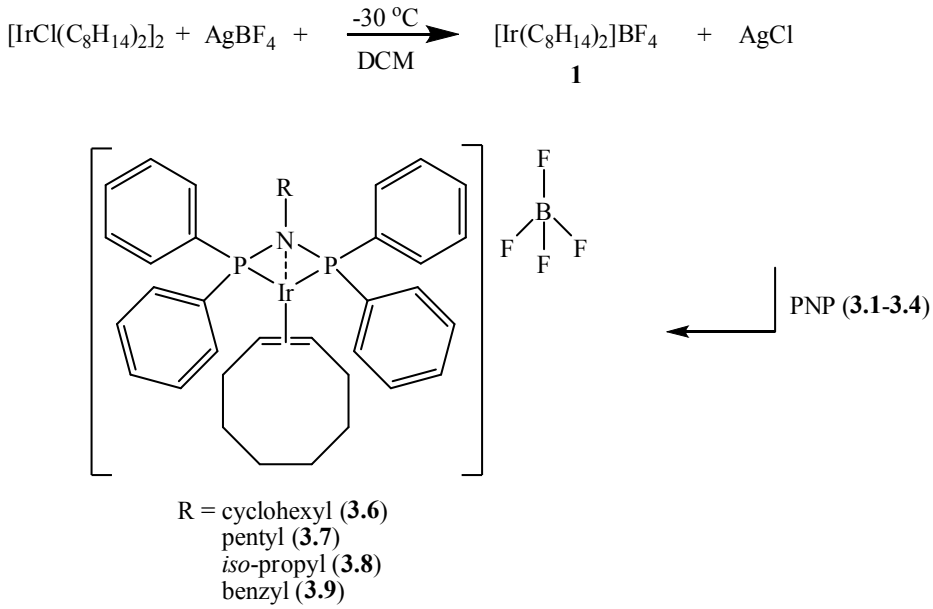

Scheme 4.2: Synthesis of the iridium complexes **3.6**–**3.9**.

Only two complexes had a distinct melting point (**3.7** and **3.9**), whilst the others (**3.6** and **3.8**) turned black at the indicated temperature signifying decomposition. The NMR spectra of similar iridium complexes containing a different type of PNP ligand have been reported in literature[10-14]; however, in this study the NMR spectra could not be elucidated due to rapid decomposition of the complex in deuterated solvents. Possible methods of elucidating the NMR spectra of the iridium complexes included working at low temperatures (-25 °C) and in nitrogen-saturated solvents in nitrogen filled NMR tubes. However, all methods investigated proved unsuccessful. Therefore, elemental analyses were used as a supporting technique to establish complexation between the ligand to the metal precursor. For all complexes the calculated percentages of carbon, hydrogen and nitrogen were in agreement (<0.5%) with those obtained experimentally. Furthermore, the molecular ion peaks that were obtained by HRMS corresponded to those calculated for the expected products, with either the subtraction or addition of hydrogen. Noticeably, the mass calculated excluded the counter ion, $[BF_4]^-$. IR analysis was also beneficial in showing the presence of the counter ion $[BF_4]^-$ in the complex with a broad band at 1049 cm^{-1} for complex **3.6**, 1048 cm^{-1} for **3.7**, 1038 cm^{-1} for **3.8** and 1052 cm^{-1} for **3.9**.[15]

The infrared band shifts of the complexes are discussed in relation to their respective ligand and only those bands that showed a significant shift, from the ligand to the

metal complex, are mentioned and shown in Table 4.4. It is theoretically possible that for complex **3.6** the ligand binds in a tridentate manner to the metal (i.e. via the two phosphorous and the nitrogen atoms). Since there is a significant shift in the bands associated with the functional groups present on all three of these respective atoms, this bonding mode cannot be excluded. The magnitude of the shift associated with the methyne C–H bend (from 1347 cm^{-1} to 1307 cm^{-1}) from ligand to complex is large. There is thus either a much stronger inductive effect caused by the coordinating phosphorous atoms than that observed for the equivalent cobalt complex (**3.10**, Section 4.3), or there is a close approach of the nitrogen to the iridium. Also noted is the shift of the bands associated with the methylene C–H bond (from 741 cm^{-1} to 731 cm^{-1}) and the disappearance of the band at 1450 cm^{-1} and the appearance of a new band associated with the tertiary C–N stretch (1151 cm^{-1}) of the complex. To ascertain as to whether the metal coordinates to the phosphorous atoms, the shift in the bands associated with P–N bond (from 982 cm^{-1} to 997 cm^{-1}) and the aromatic C–H is a clear indication. For the aromatic C–H, one band observed for the free ligand (3070 cm^{-1}) is not seen in the complex, while a shift in the other band associated with the same assignment (from 3050 cm^{-1} to 3056 cm^{-1}) as well as the appearance of another band related to the C=C–C of the aromatic ring (1572 cm^{-1}) are observed.

For complex **3.7** (Table 4.5) there is the disappearance on complexation of the band associated with the asymmetric stretch of the methyl C–H bond in the free ligand, as well as the distinct shift of the bands associated with the methylene C–H bonds. Together with the disappearance of one band associated with the C–N stretch on complexation, it may be postulated that the metal coordinates to the nitrogen atom. Alternatively, should bonding occur only via the phosphorous atoms, i.e a bidentate bonding mode, the band shifts of the functional groups on the nitrogen would have to be due to possible inductive effects (via the coordinated phosphorous atoms (see below)) or via a through space interaction (between the metal and nitrogen). To confirm the coordination of the metal to the two phosphorous atoms, the distinct shift in the band associated with the P–N bond (from 978 cm^{-1} to 997 cm^{-1}) as well as the disappearance of one of the bands related to the aromatic C–H stretch (from free ligand to complex) and a shift in the other band associated with the same assignment (from 3050 cm^{-1} to 3056 cm^{-1}).

Table 4.4: Comparison of IR data of the ligand ($^{Ph}PN_{cyclohexyl}P^{Ph}$) (**3.1**) and the respective complex [($^{Ph}PN_{cyclohexyl}P^{Ph}$)IrCOE][$BF_4$] (**3.6**).

Functional group/assignment[6]	**ν/cm^{-1} of the ligand (3.1)**	**ν/cm^{-1} iridium complex (3.6)**
Aromatic C–H stretch	3070, 3050	3056
Methylene C–H asym. Stretch	2926	2931
Methyne C–H stretch	2851	2856
Aromatic ring stretch C=C–C	1584	1587, 1572
Methylene C–H bend	1477, 1450	1480
Methyne C–H bend	1347	1307
3° amine C–N stretch	1179	1183, 1151
P–N[16]	982	997
Methylene $(CH_2)_n$- rocking ($n \geq 3$)	741	731

Table 4.5: Comparison of IR data of the ligand ($^{Ph}PN_{pentyl}P^{Ph}$) (**3.2**) and the respective complex [($^{Ph}PN_{pentyl}P^{Ph}$)IrCOE][BF_4] (**3.7**).

Functional group/assignment[6]	**ν/cm^{-1} of the ligand (3.1)**	**ν/cm^{-1} iridium complex (3.7)**
Aromatic C–H stretch	3070, 3050	3057
Methyl C–H asym. stretch	2943	-
Methylene C–H asym. stretch	2934	2927
Methylene C–H sym. stretch	2856	2867
Methylene C–H bend	1478, 1467, 1455,	1481, 1466
3° amine C–N stretch	1185, 1164	1187
P–N[16]	978	997
Methylene $(CH_2)_n$- rocking ($n \geq 3$)	739	746

Table 4.6: Comparison of IR data of the ligand ($^{Ph}PN_{iso\text{-propyl}}P^{Ph}$) (**3.3**) and the respective complex [($^{Ph}PN_{iso\text{-propyl}}P^{Ph}$)IrCOE][$BF_4$] (**3.8**).

Functional group/assignment[6]	**ν/cm^{-1} of the ligand (3.1)**	**ν/cm^{-1} iridium complex (3.8)**
Aromatic C–H stretch	3068, 3050	3059
Methyl C–H sym. stretch	2863	-
Methyl C–H asym. bend	1462, 1478	1481
Methyl C–H sym. bend	1376	-
Methyne C–H bend	1359	1372
3° amine C–N stretch	1202, 1171	1175
P–N[16]	986	997
Methylene $(CH_2)_n$- rocking ($n \geq 3$)	738	744

The coordination of the ligand to the metal in complex **3.8** (Table 4.6) via the nitrogen may be proposed through the disappearance (on complexation) of the band associated with the symmetric stretch and bend and the asymmetric bend of the methyl C–H bond and a band related to the stretch of the C–N bond in the free ligand. Furthermore, there is also a significant shift in the methyne and methylene C–H bonds. Coordination of the metal to the two phosphorous atoms is confirmed by the distinct shift of the band of the P–N bond (from 986 cm^{-1} to 997cm^{-1}) and the disappearance of a band associated with the aromatic stretch of the C–H bond and the shift of the second band (from 3050 cm^{-1} to 3059 cm^{-1}).

Table 4.7: Comparison of IR data of the ligand ($^{Ph}PN_{benzyl}P^{Ph}$) (**3.4**) and the respective complex [($^{Ph}PN_{benzyl}P^{Ph}$)IrCOE][BF_4] (**3.9**).

Functional group/assignment[6]	**ν/cm^{-1} of the ligand (3.1)**	**ν/cm^{-1} iridium complex (3.9)**
3° amine C–N stretch	1208, 1188, 1177, 1161	1208, 1161
P–N[16]	988	996

For complex **3.9** (Table 4.7), only two major comparisons could be drawn to confirm coordination of the metal to ligand **3.4**. The first, by the disappearance of two bands

associated with the C–N bond stretch on complexation followed by the distinct shift in the band related to the P–N bond.

4.3 Synthesis and characterization of the cobalt complexes [(^{Ph}PNP^{Ph})$CoCl_2$] (3.10-3.13).

The syntheses of the cobalt complexes (Chapter 3, Section 3.4) were carried out as reported in the literature[17], for the complex [$CoCl_2${$(CH_2CH_2CH_3)N(CH_2$- $CH_2PPh_2)_2$-κ^2P,P}], by refluxing the respective aminodiphosphine with $CoCl_2.6H_2O$ in ethanol (Scheme 4.3). Within 15 minutes of refluxing, the solution turns from blue to green. According to the literature method[17] for [$CoCl_2${$(CH_2CH_2CH_3)N(CH_2$- $CH_2PPh_2)_2$-κ^2P,P}], green microcrystals precipitated out of solution, however, this was not the case with the cobalt complexes with ligands **3.1**-**3.4**. After 24 hours under reflux, the solvent was removed and the green product was washed several times with diethyl ether for the removal of unreacted ligand. The complex was obtained in satisfactory yields. The NMR spectra of the complexes were not obtainable due to the paramagnetic nature of the complexes.[17] Elemental analyses were used as a confirmatory tool for the complexation of the metal to the ligand. It is observed that the experimentally obtained percentages (elemental analyses) of C, H and N are within the acceptable limits (<0.5 %) of the calculated. The infrared analyses were used to compare changes in the bond vibrations pertaining to the metal complex and the respective ligand. This can be used as an indication of complexation, as well as to confer information on the coordination of the metal to the ligand.

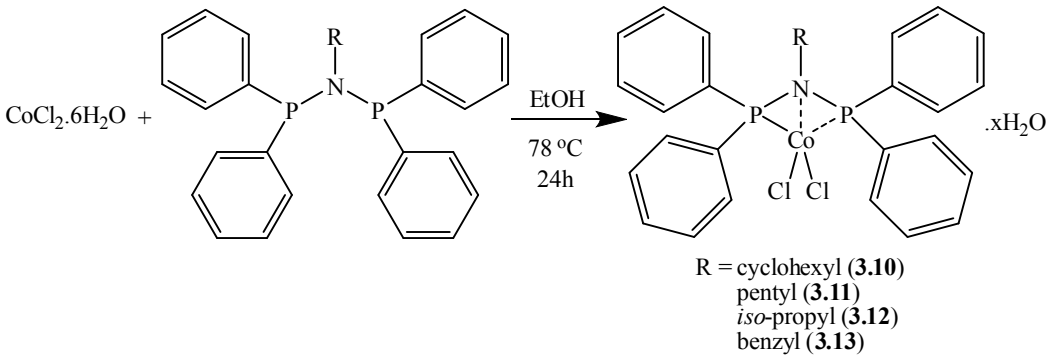

Scheme 4.3: Synthesis of the cobalt complexes (**3.10**–**3.13**).

Table 4.8: Comparison of IR data of the ligand ($^{Ph}PN_{cyclohexyl}P^{Ph}$) (**3.1**) and the respective complex [($^{Ph}PN_{cyclohexyl}P^{Ph}$)$CoCl_2$] (**3.10**).

Functional group/assignment[6]	**ν/cm^{-1} of the ligand (3.1)**	**ν/cm^{-1} cobalt complex (3.10)**
Hydroxy group, O–H stretch	-	3404
Aromatic C–H stretch	3070, 3050	3055
Methylene C–H asym. stretch	2926	2931
Methylene C–H bend	1477, 1450	1480, -
3° amine C–N stretch	1179	1187, 1153
Cyclohexane ring vibrations	1056, 1027	1068, 1027
P–N[16]	982	998

For complexes **3.10**-**3.13** (Tables 4.8-4.11), the presence of water is confirmed by the presence of the broad band at 3404 cm^{-1}, 3382 cm^{-1}, 3420 cm^{-1}, 3329 cm^{-1} respectively. This is also confirmed by the TGA of the complex (Section 4.5.3). Literature[17] states that for the related complex [($CH_3CH_2CH_2N$-$CH_2CH_2PPh_2$)$_2$], a tetrahedral geometry is observed, where cobalt is coordinated to the two chlorine atoms and to the PNP ligand via the phosphorous atoms.

Coordination is noticeable by the magnitude of the band shifts (for complex **3.10**) associated with the P–N bond (form 982 cm^{-1} to 998 cm^{-1}) and the aromatic C–H bond (from 3050 cm^{-1} to 3055 cm^{-1}). However, the shift in the bands associated with the aliphatic region, particularly that associated with the cyclohexane vibrations and the C–N stretch is more pronounced. This could mean that the cobalt coordinates via the nitrogen and one phosphorous atom or via both phosphorous atoms and the effect on the nitrogen is either a through space interaction between cobalt and the nearby nitrogen or an inductive effect from the coordinated phosphorous, adopting a tetrahedral configuration, which according to literature (using IR data) is possible.[18]
A similar condition is observed for the other cobalt complexes (**3.11**-**3.13**).

For complex **3.11** (Table 4.9), coordination of cobalt to the phosphorous atoms of the PNP ligand **3.2** is distinguished by the disappearance of the band associated with the stretching vibrations of the aromatic C–H bond and the C=C–C bond, as well as the

distinct shift of the band related to the P–N bond. Furthermore, the disappearance of the bands assigned to the methylene C–H stretch and bend and the C–N stretch, as well as the shift in the band assigned to the methylene C–H symmetric stretch, indicates possible coordination to the nitrogen atom, although these shifts may also be caused by inductive or through space effects as mentioned above.

Table 4.9: Comparison of IR data of the ligand ($^{Ph}PN_{pentyl}P^{Ph}$) (**3.2**) and the respective complex [($^{Ph}PN_{pentyl}P^{Ph}$)$CoCl_2$] (**3.11**).

Functional group/assignment[6]	**ν/cm^{-1} of the ligand (3.1)**	**ν/cm^{-1} cobalt complex (3.11)**
Hydroxy group, O–H stretch	-	3382
Aromatic C–H stretch	3070, 3050	3055
Methylene C–H asym. stretch	2934	-
Methylene C–H sym. stretch	2856	2862
Aromatic ring stretch C=C–C	1584, 1570	1586
Methylene C–H bend	1478, 1467, 1455,	1480, 1466 -
3° amine C–N stretch	1185, 1164	1210, 1190
P–N[16]	978	997

For complex **3.12** (Table 4.10), the possibility of coordination to the ligand via the nitrogen atom and a phosphorous atom cannot be excluded. This is noted by the band shifts and disappearance of bands assigned to the aliphatic region (methyl C–H stretch and bend, the methyne C–H stretch and bend and methylene rocking vibration). However, these shifts are less pronounced and may be due to inductive effects caused by the coordinated phosphorous atoms. Coordination to the phosphorous atoms is emphasized by the magnitude of the band shift associated with the P–N band.

Table 4.10: Comparison of IR data of the ligand ($^{Ph}PN_{iso\text{-}propyl}P^{Ph}$) (**3.3**) and the respective complex [($^{Ph}PN_{iso\text{-}propyl}P^{Ph}$)$CoCl_2$] (**3.12**).

Functional group/assignment[6]	**ν/cm^{-1} of the ligand (3.1)**	**ν/cm^{-1} cobalt complex (3.12)**
Hydroxy group, O–H stretch	-	3420
Aromatic C–H stretch	3068, 3050	3055
Methyl C–H asym. stretch	2966	2974
Methyl C–H sym. stretch	2863	-
Methyl C–H asym. bend	1462, 1478	1481
Methyl C–H sym. bend	1376	-
Methyne C–H bend	1359	1370
3° amine C–N stretch	1202, 1171	1170
P–N[16]	986	998
Methylene $(CH_2)_n$- rocking ($n \geq 3$)	738	743

Complex **3.13** (Table 4.11) displays a different scenario in comparison to the other ligands, in that there is no distinct shift in bands to suggest coordination by the nitrogen atom. However, the large shift in the band assigned to the P–N band is conclusive of coordination to the phosphorous atoms.

Table 4.11: Comparison of IR data of the ligand ($^{Ph}PN_{benzyl}P^{Ph}$) (**3.4**) and the respective complex [($^{Ph}PN_{benzyl}P^{Ph}$)$CoCl_2$] (**3.13**).

Functional group/assignment[6]	**ν/cm^{-1} of the ligand (3.1)**	**ν/cm^{-1} cobalt complex (3.13)**
Hydroxy group, O–H stretch	-	3329
3° amine C–N stretch	1208, 1188, 1177, 1161	1210, 1189, 1174, 1160
P–N[16]	988	999

It was established from the IR data, that the ligand coordinates to the metal center. However, the possibility of bidentate versus tridentate coordination arises. For example, the iridium complexes mentioned in Section 4.2.2 exist as a 14e$^-$ species if

bidentately coordinated (via the two phosphorous atoms) and as more stable 16e$^-$ species if tridentately coordinated (via the nitrogen and phosphorous atoms). Furthermore, all iridium complexes presented in literature display a tridentate coordination of the PNP ligand to the metal center.[9-13] The ambiguity with the coordination may be avoided with the aid of a crystal structure. However, after many attempts under varying conditions, growing of suitable crystals was unsuccessful. For the cobalt complexes, depending on the stereochemistry of the complex, coordination via the nitrogen and one phosphorous atom is possible.[18] However, in most cases coordination occurs via the two phosphorous atoms.[18-20]. Studies carried out with the same ligand structure but with the transition metal chromium, have shown coordination of chromium via the two phosphorous atoms constituting a 14e$^-$ species.[21-23]

4.4 Thermal analyses of the ligands and complexes

4.4.1 Thermal gravimetric analyses of the ligands

The thermogravimetric analyses of ligands **3.1** to **3.4**, (Appendix A, Fig. 15A–17A, Table 4.12), from 30 to 1000 °C, reveal that ligands **3.1**–**3.3** exhibit a similar decomposition pattern as proposed in Scheme 4.4.

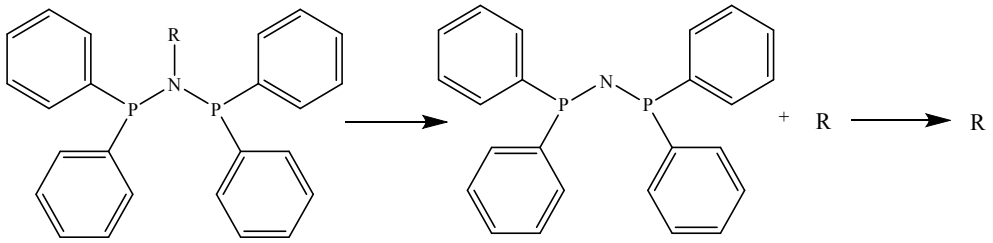

Scheme 4.4: Proposed decomposition pathway for ligands **3.1**–**3.3**.
(R: cyclohexyl (**3.1**); pentyl (**3.2**); *iso*-propyl (**3.3**))

Table 4.12: Thermoanalytical data (TGA, DSC) for the PNP ligands (**3.1- 3.4**).

Ligand	**Temperature Range/ °C**	**DSC**		**Mass loss/. %**		**Evolved moiety**
		$Peak_{max}$/ °C	**Enthalpy/ J/g**	**Observed**	**Theoretical**	
3.1	30-160	(-)50.9, (-)86.1, (-)133.9	12.7, 5.0, 38.8	1.02	-	Solvent or moisture
	160-360	(-) 356.4	62.0	83.1	82.2	$(Ph)_2$-PNP-$(Ph)_2$
	360-530 + residue			15.9	18.0	Cyclohexane
3.2	30-330	(-)56.5, (-)91.9,	8.8, 33.4	84.3	84.4	$(Ph)_2$-PNP-$(Ph)_2$
		(-) 192.6, (+)196.1,				
		(+)214.5, (-)230.5				
		(-)245.3, (+)248.3				
		(-)257.2, (+)258.3				
		(-)290.6, (-)320.5	3.2, 6.5			
	330-990			14.9	15.8	Pentane

(-) Endothermic peak

(+) Exothermic peak

continued…

Table 4.12: Thermoanalytical data (TGA, DSC) for the PNP ligands (**3.1- 3.4**)…continued

Ligand	**Temperature Range/ °C**	**DSC**		**Mass loss/. %**		**Evolved moiety**
		$Peak_{max}$/ °C	**Enthalpy/ J/g**	**Observed**	**Theoretical**	
3.3	30-160	(-)51.1, (-)56.2, (-)130.5	18.2, 4.5, 34.2	5.4		Solvent or moisture
	160-300	(+)167.4, (-)171.7,		84.4	89.9	$(Ph)_2PNP(Ph)_2$
		(+)173.1, (-)178.9,				
		(+)181.1, (-)191.8,	2.1			
		(-)249.7, (+)251.9,				
		(-)267.7, (+)269.9,				
		(-)278.6, (+)280.7				
		(-)285.8, (+)286.5				
	300-990	(-)303.1	8.8	10.7	13.6	*iso*-propyl
3.4	30-170	(-)51.1, (-)156.1.	76.7, 29.8	1.58		Solvent or moisture
	170-380	(+)343.1, (-)353.7,		58.5	59.9	$(Ph)_2PN(Ph)$
		(+)369.7				
	380-430	(-)381.6, (+)392.2		16.9	16.9	Benzene
	430-990			15.3	16.9	Benzene
	residue			7.8	6.7	Phosphorous

Ligands **3.2** and **3.3** were fully decomposed at 990 °C, whilst residual weight percentages for ligands **3.1** and **3.4** were noted at 990 °C. The first stage of weight loss is due to solvent or moisture. This could occur when working at reduced pressure, or from the effects of thermomolecular flow, or it might be due to the moisture contained in the carrier gas, which is adsorbed onto the sample.[24] Ligands **3.1**–**3.3** display a second stage of weight loss (~160 °C), which corresponds to the decomposition of the P-N-P fragment (removal of the attached substituent on the nitrogen atom). This is also noted in the DSC plot (Appendix A, Fig. 19A–21A), by the broad exothermic peak. The appearance of several endo-exo peaks in this region is indicative of the greatest decomposition of the molecule.[25] The sharpness of the endothermic peak occurring for ligands **3.1**–**3.3** (133.9 °C, 91.9 °C, 130.5 °C) correlates to the melting process (Chapter 3, Section 3.2) of these compounds and is indicative of the crystallinity of the complexes.[24] This also correlates with the IR data discussed in Section 4.1. The remaining mass loss corresponds to the substituent on the nitrogen atom, which is indicated by the endothermic peak (~300 °C) on the DSC plot. However, ligand **3.4** displays a different decomposition pattern as noted in Scheme 4.5 and Appendix A, Figs. 19A and 22A. Unlike the aforementioned ligands, the P-N-P backbone is fragmented in the second stage of weight loss. This could be due to the phenyl group (unsaturated C–H bond) attached to the nitrogen, whilst the other ligands contain a saturated substituent attached to the nitrogen.

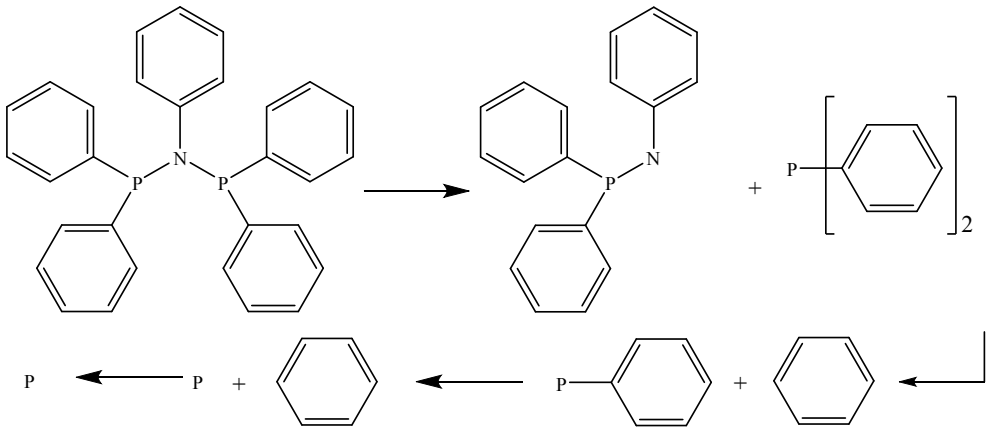

Scheme 4.5: Proposed decomposition pathway for ligands **3.4**.

4.4.2 Thermal gravimetric analyses of the iridium complexes (3.6–3.9)

The thermal decomposition of the complexes **3.6**–**3.9** commences with the gradual decomposition of P-N-P backbone as noted in Table 4.12 (Appendix A Fig. 23A-26A). The DSC curves (Appendix A Fig. 27A–30A) exhibit an endothermic peak ~30 °C, which indicates the start of decomposition. A broad exothermic peak follows this, which is as a result of the greatest weight loss of the respective compounds. The decomposition of cyclooctene (COE) follows shortly thereafter. This is expected, since COE is weakly coordinated to the iridium metal.[10] Interestingly, all iridium complexes show a residual mass at 990 °C, which corresponds to iridium metal and the counter ion, BF_4. The apparent decomposition patterns of complexes **3.6** and **3.8** (Scheme 4.6) are similar, whilst complex **3.7** (Scheme 4.7) and complex **3.9** (Scheme 4.8) display a different decomposition scheme.

Table 4.13: Thermoanalytical data (TGA, DSC) for the PNP-Iridium complexes (**3.6- 3.9**).

Complex	**Temperature Range/ °C**	**DSC**		**Mass loss/. %**		**Evolved moiety**
		$Peak_{max}$/ °C	**Enthalpy/ J/g**	**Observed**	**Theoretical**	
3.6	30-440	(-)52.7, (-)85.1, (+)185.6	37.4, 12.9	34.9	33.0	$(Ph)_2PN$(cyclohexyl)
		(-)204.1, (-)417.4, (+)431.6				
	440-990			9.6	13.1	COE
	residue			52.7	52.2	$IrP(Ph)_2 + BF_4$
3.7	30-320	(-)48.1, (-)84.4, (+)134.4	55.5, 12.6	32.9	32.1	$(Ph)_2PN$(pentyl)
		(-)179.9, (-)233.9				
	320-390			13.1	13.3	COE
	390-990			21.7	22.0	$P(Ph)_2$
	residue			31.8	33.1	$Ir + BF_4$

(-) Endothermic peak

(+) Exothermic peak

continued…

Table 4.13: Thermoanalytical data (TGA, DSC) for the PNP- Iridium complexes (**3.6- 3.9**)…continued

Complex	**Temperature Range/ °C**	**DSC**		**Mass loss/. %**		**Evolved moiety**
		$Peak_{max}$/ °C	**Enthalpy/ J/g**	**Observed**	**Theoretical**	
3.8	30-390	(-)51.9, (-)86.4, (+)146.3	33.2, 7.4	28.9	29.7	$(Ph)_2PN$(*iso*-propyl)
	390-990			15.8	13.7	COE
	residue			54.8	56.8	$IrP(Ph)_2 + BF_4$
3.9	30-360	(-)54.4, (-)88.5, (+)153.4	21,3, 10.35	31.9	32.5	$(Ph)_2PN$(benzyl)
		(-)175.3, (-)221.3, (-)267.9	16.81 6.92			
	360-470	(-)389.3	5.5	14.7	13.2	COE
	470-670			8.2	9.2	Ph
	670-990			8.8	9.1	Ph
	residue			36.2	36.4	$Ir(P) + BF_4$

(-) Endothermic peak

(+) Exothermic peak

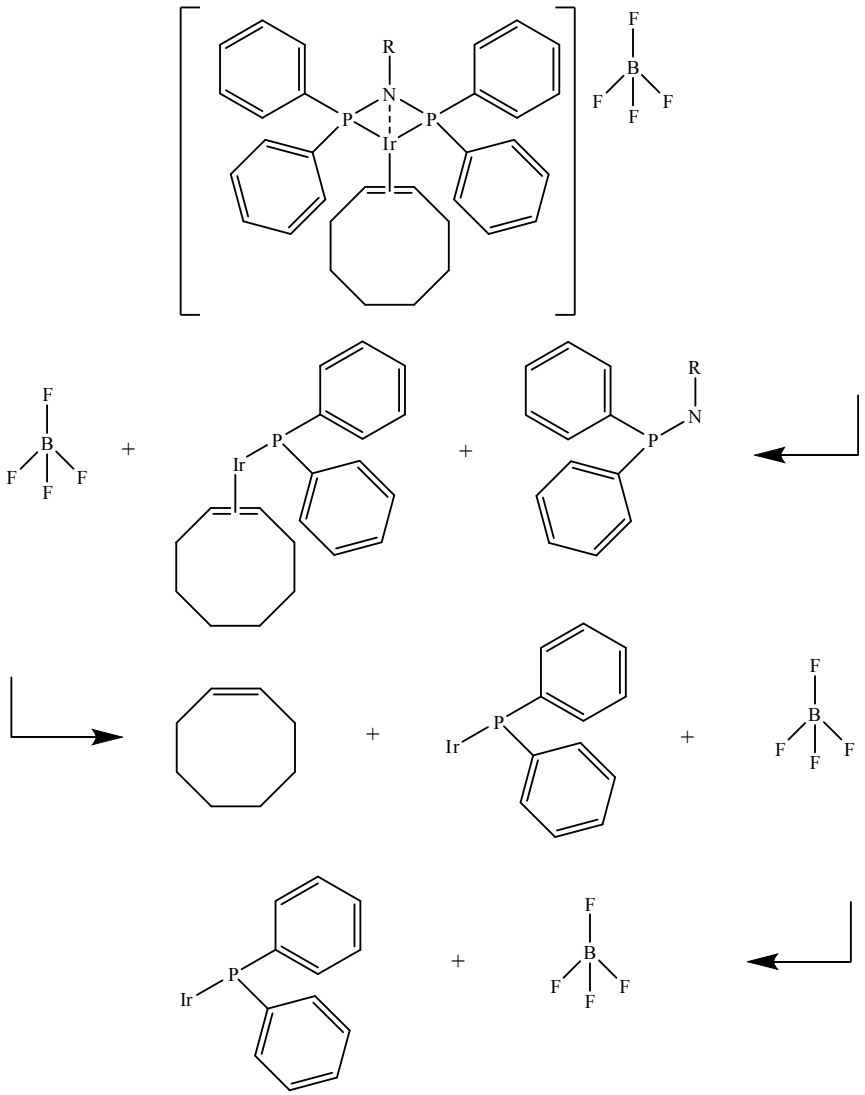

Scheme 4.6: Proposed decomposition of the iridium complex **3.6** and **3.8.**
(R= cyclohexyl (**3.6**) and *iso*-propyl (**3.8**))

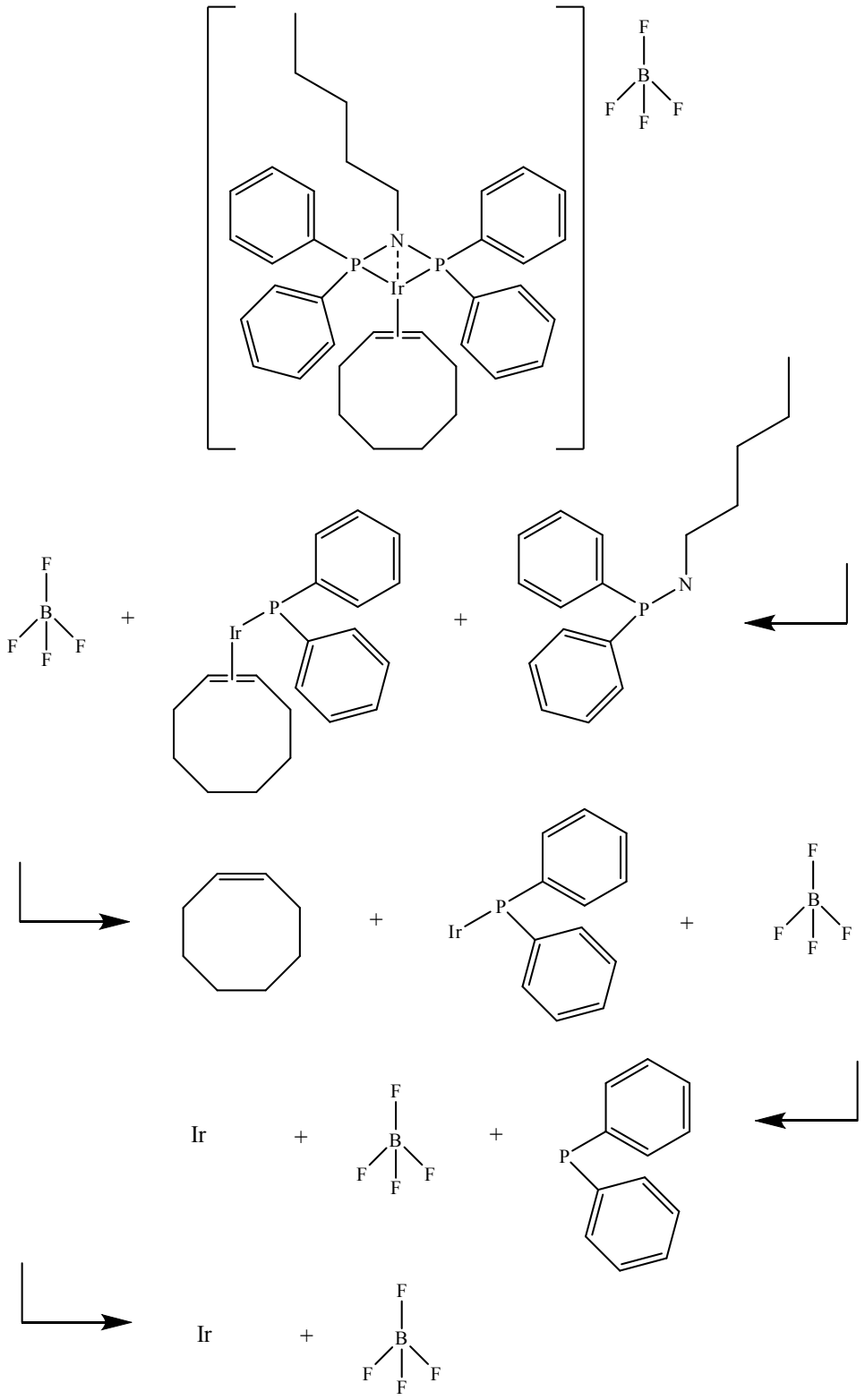

Scheme 4.7: Proposed decomposition of the iridium complex **3.7**.

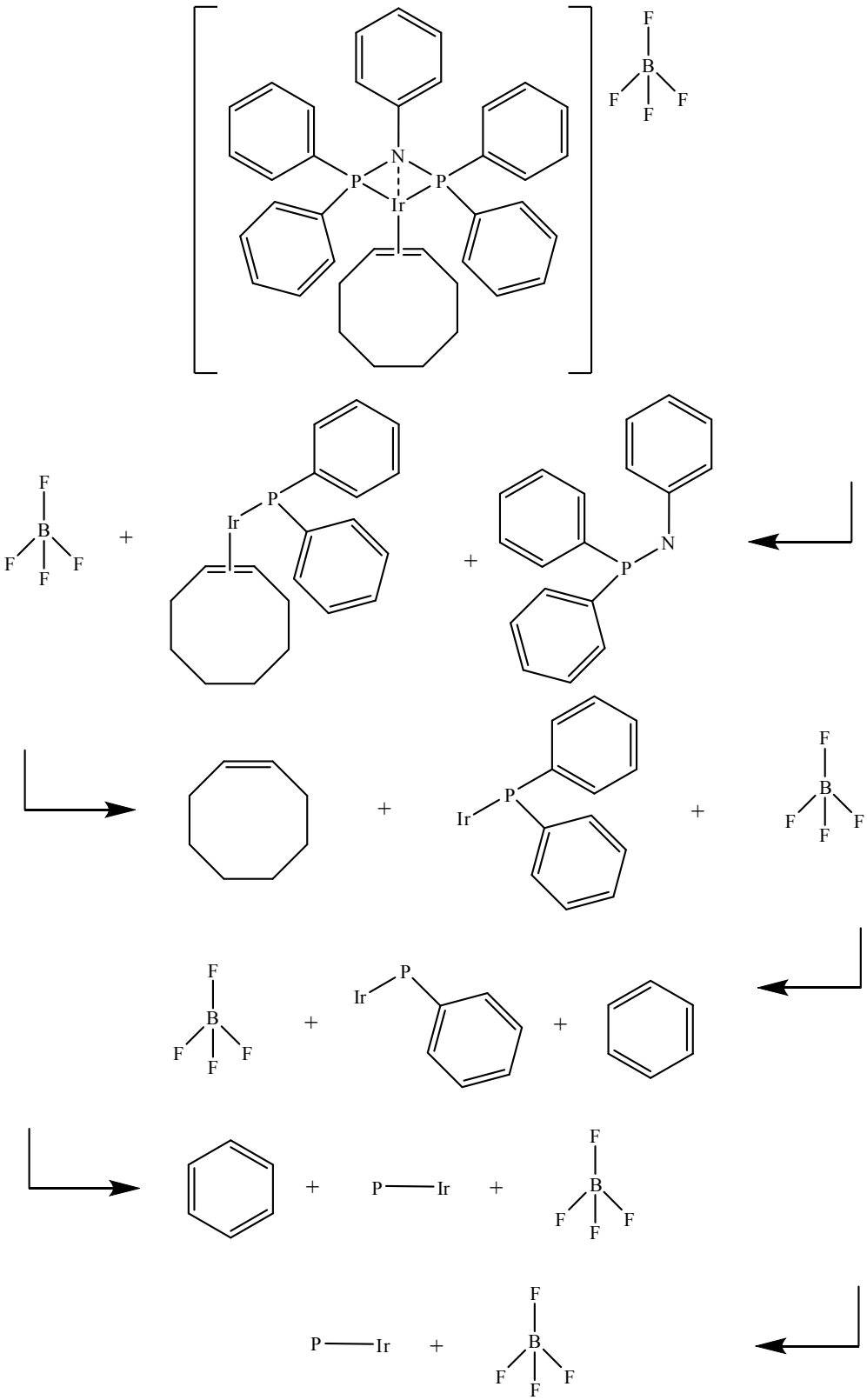

Scheme 4.8: Proposed decomposition of the iridium complex **3.9**.

4.4.3 Thermal gravimetric analyses of the cobalt complexes (3.10–3.12)

The thermal decomposition of the cobalt complexes **3.10**–**3.12** (Table 4.13) occurs in five distinct stages and this is evident in the TGA curves (Appendix A Fig 31A–33A). The first thermal event is the loss of water (~20–140 °C), which is depicted as endothermic peaks in the DSC curves (Appendix A Fig. 34A–36A).[26-28] From the broad peak shown in the IR analyses (Chapter 3, Section 3.4), it can be concluded that water coordinates to the complex. The thermal analyses provide an indication of the number of coordinating water molecules, for example, complex **3.10** has two coordinating water molecules. The second thermal loss, which is common to all of the cobalt complexes, is the decomposition of the P-N-P backbone, which is indicated as a broad exothermic peak in the DSC curves. (Schemes 4.9 and 4.10)

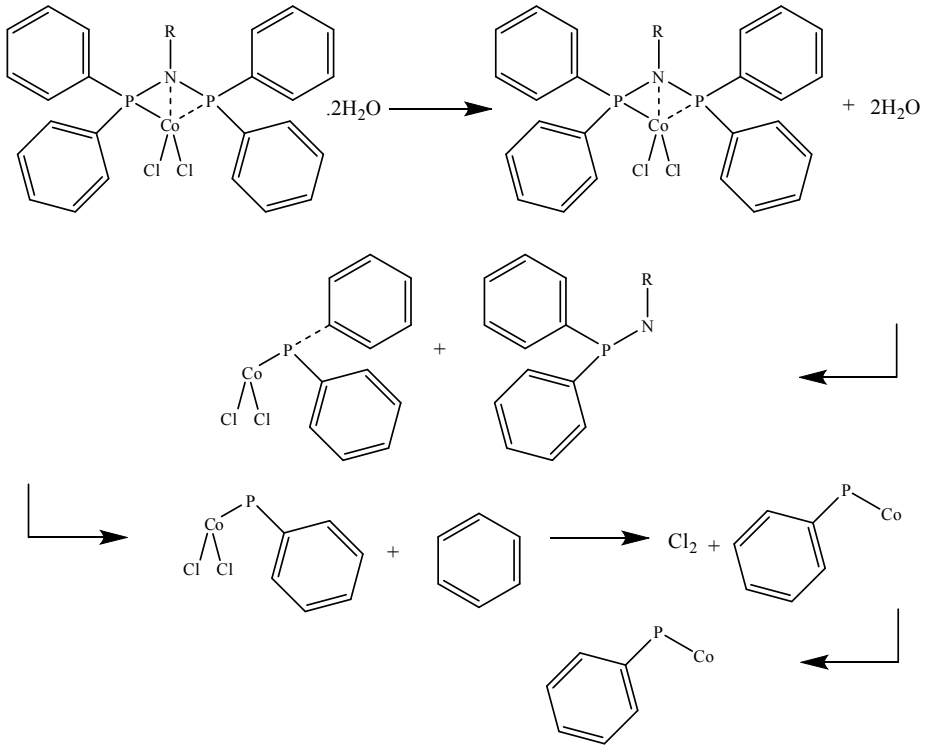

Scheme 4.9: Proposed decomposition of complex **3.10** and **3.12**.
(R= cyclohexyl (**3.10**) and *iso*-propyl (**3.12**))

The decomposition contributes to the majority of the weight loss of the complexes (>39%). Complexes **3.11** and **3.12** display similar decomposition pathways as seen

for the iridium complexes of the same type. From the ^{31}P NMR shifts (Section 4.1) of the respective ligands of these complexes, it can be established that their thermal behavior is most likely to be similar. Interestingly, the manner in which the P-N-P backbone decomposes is similar for both the iridium and cobalt complexes. It can also be observed that the chlorine atoms detach at a much higher temperature than COE, which is a reflection of stronger coordination to the metal center. The final residual mass is largely due to cobalt.

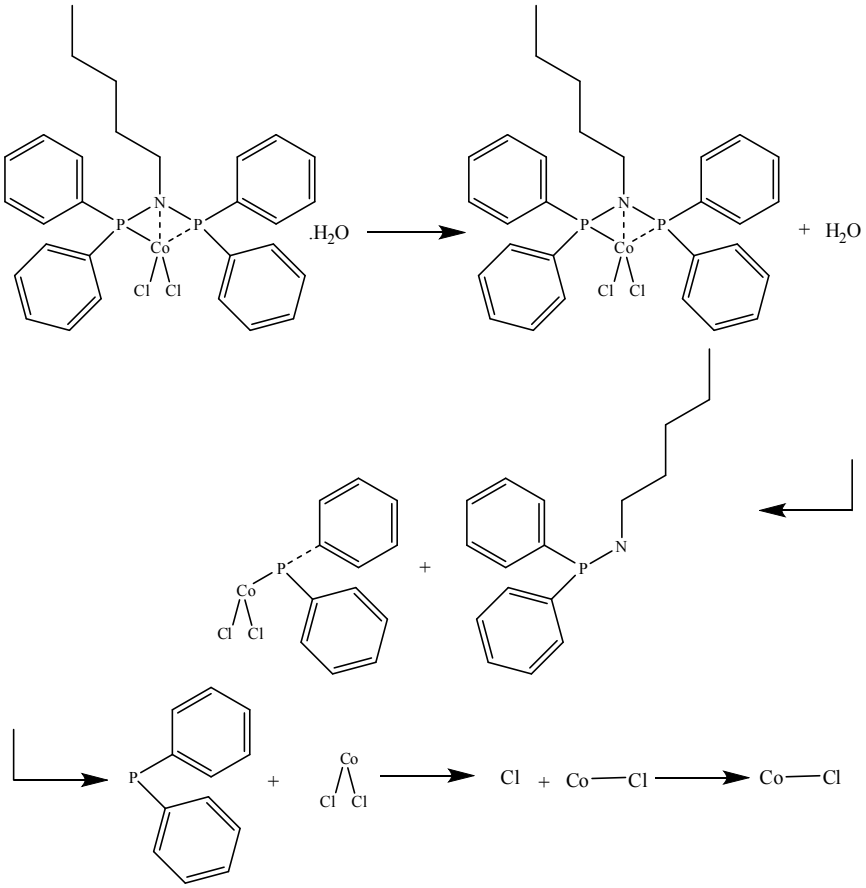

Scheme 4.10: Proposed decomposition of complex **3.11**.

Table 4.14: Thermoanalytical data (TGA, DSC) for the PNP-Cobalt complexes (**3.10- 3.12**).

Complex	**Temperature Range/ °C**	**DSC**		**Mass loss/. %**		**Evolved moiety**
		$Peak_{max}$/ °C	**Enthalpy/ J/g**	**Observed**	**Theoretical**	
3.10	20-110	(-)46.2, (-)77.3,	8.0, 29.9	5.7	5.7	$2H_2O$
	110-420	(+)111.3 (-)183.6, (+)188.9, (-)238.1, (-)289.1, (-) 339.7	46.9, 0.7, 34.4	39.47		$(Ph)_2PN$(cyclohexyl)
	420-700			18.6		Ph
	700-990			9.5		Cl_2
	residue			26.3	26.48	Ph(P)Co
3.11	30-100	(-)54.1, (-)89.7,	62,3, 10.2,	3.1	3.0	H_2O
	100-350	(-)271,9, (+)296.9, (-)323.8		42.4	44.8	$(Ph)_2PN$(pentyl)
	350-760			29.1	30.7	$P(Ph)_2$
	760-990			5.3	5.8	Cl
	residue			20.2	15.6	CoCl

(-) Endothermic peak

(+) Exothermic peak

continued…

Table 4.14: Thermoanalytical data (TGA, DSC) for the PNP- Cobalt complexes (**3.10- 3.12**)…continued

Complex	**Temperature Range/ °C**	**DSC**		**Mass loss/. %**		**Evolved moiety**
		$Peak_{max}$/ °C	**Enthalpy/ J/g**	**Observed**	**Theoretical**	
3.12	30-140	(-)48.6, (-)79.6	27.5, 41.9	6.3	6.1	$2H_2O$
	140-470	(-)230.8, (-) 318.8	56.2, 78.4	40.6	40.8	$(Ph)_2PN$(*iso*-propyl)
	470-720			14.6	13.2	Ph
	720-99			9.5	11.8	Cl_2
	residue			28.6	28.1	Ph(P)Co

(-) Endothermic peak

(+) Exothermic peak

4.5 Conclusion

The ligands (**3.1**-**3.4**) were successfully synthesized and characterized. The effect of the different substituents on the nitrogen atom is noted by the distinct shifts in the phosphorous peaks in the ^{31}P NMR spectra. The iridium complexes were synthesized by a novel method and the cobalt complexes were adapted from literature. Elemental analyses, HRMS and shifts in the IR spectra are indicative of complexation of the ligand to the metal. Furthermore, the IR data indicates a possibility that the metal binds in a tridentate manner via the nitrogen and the two phosphorus atoms of the PNP ligand for the iridium complexes and either via the two phosphorous atoms or the nitrogen and one phosphorous atom for the cobalt complexes. Thermal analyses of the ligands show that ligands **3.1**-**3.3** display similar weight loss patterns whilst ligand **3.4** is different. The decomposition pattern of complexes **3.6** and **3.8** are similar, whilst complex **3.7** and complex **3.9** display a different decomposition scheme. The cobalt complexes **3.13** display a different weight loss pattern from **3.10** and **3.13**. The major weight loss is attributed to the breaking of the PNP fragment, which is similar for the iridium and cobalt complexes.

4.6 References

(1) Bosque, R.; Joaquim, S. *Journal of Chemical Information of Computer Sciences* **2001**, *41*, 225.

(2) Blann, K.; Bollmann, A.; de Bod, H.; Dixon, J. T.; Killian, E.; Nongodlwana, P.; Maumela, M. C.; Maumela, H.; McConnel, A. E.; Morgan, D. H.; Overette, M. J.; Pŕetorius, M.; Kuhlmann, S.; Wasserscheid, P. *Journal of Catalysis* **2007**, *249*, 244.

(3) Grim, S. O.; McFarlane, W.; Davidoff, E. F. *Journal of Organic Chemistry* **1967**, *32*, 781.

(4) Pregosin, P. S.; Kunz, R. W. *^{31}P AND ^{13}C NMR of Transition Metal Phosphine Complexes.*; Springer-Verlag, Berlin **1979**.

(5) Emsley, J.; Dennis, H. *The Chemistry of Phosphorus: Environmental, Organic, Inorganic, Biochemical, and Spectroscopic aspects.*; Harper and Row, London **1976**.

(6) Coates, J. In *Encyclopedia of Analytical Chemistry*; John Wiley & Sons, Ltd: **2006**.

(7) Silverstein, R. M.; Webster, F., X *Spectrometric Identification of Organic Compounds.*; John Wiley and Sons, Inc, New York **1998**; Vol. 6.

(8) Parshall, G. W. *Inorganic Syntheses*; McGraw Hill, New York, **1974**.

(9) Meiners, J.; Friedrich, A.; Herdtweck, E.; Schneider, S. *Organometallics* **2009**, *28*, 6331.

(10) Dorta, R.; Goikhman, R.; Milstein, D. *Organometallics* **2003**, *22*, 2806.

(11) Ben-Ari, E.; Cohen, R.; Gandelman, M.; Shimon, L. J. W.; Martin, J. M. L.; Milstein, D. *Organometallics* **2006**, *25*, 3190.

(12) Ben-Ari, E.; Leitus, G.; Shimon, L. J. W.; Milstein, D. *Journal of the American Chemical Society* **2006**, *128*, 15390.

(13) Bernskoetter, W. H.; Hanson, S. K.; Buzak, S. K.; Davis, Z.; White, P., S.; Swartz, R.; Goldberg, K. I.; Brookhart, M. *Journal of the American Chemical Society* **2009**, *131*, 8603.

(14) Zhu, Y. J.; Fan, L.; Chen, C. H.; Finnell, S. R.; Foxman, B. M.; Ozerov, O. V. *Organometallics* **2007**, *26*, 6701.

(15) M'thiruaine, C. M.; Friedrich, H. B.; Changamu, E. O.; Bala, M. D. *Inorganica Chimica Acta* **2011**, *366*, 105.

(16) Slawin, A. M. Z.; Milton, H. L.; Wheatley, J.; Woollins, J. D. *Polyhedron* **2004**, *23*, 3125.

(17) Romerosa, A.; Saraiba-Bello, C.; Serrano-Ruiz, M.; Caneschi, A.; McKee, V.; Peruzzini, M.; Sorace, L.; Zanobini, F. *Dalton Transactions* **2003**, 3233.

(18) Dahlhoff, W. V.; Dick, T. R.; Ford, G. H.; Kelly, W. S. J.; Nelson, S. M. *Journal of the Chemical Society A: Inorganic, Physical, Theoretical* **1971**, 3495.

(19) Dong, Q.; Rose, M. J.; Wong, W.-Y.; Gray, H. B. *Inorganic Chemistry* **2011**, *50*, 10213.

(20) Wiedner, E. S.; Yang, J. Y.; Dougherty, W. G.; Kassel, W. S.; Bullock, R. M.; DuBois, M. R.; DuBois, D. L. *Organometallics* **2010**, *29*, 5390.

(21) Teo, S.; Weng, Z.; Hor, T. S. A. *Organometallics* **2008**, *27*, 4188.

(22) Bollmann, A.; Blann, K.; Dixon, J. T.; Hess, F. M.; Killian, E.; Maumela, H.; McGuiness, D. S.; Morgan, D. H.; Neveling, A.; Otton, S.; Overette, M.; Slawin, A. M. Z.; Wasserchеid, P.; Kihlmann, S. *Journal of the American Chemical Society* **2004**, *126*, 14712.

(23) Bowen, L. E.; Haddow, M. F.; Orpen, A. G.; Wass, D. F. *The Royal Society of Chemistry, Dalton Transactions* **2007**, 1160.

(24) Brown, M. E. *Introduction to Thermal Analysis: Techniques and Applications*; Chapman and Hall, London **1988**.

(25) Katib, S. M. A. *Journal of Thermal Analysis and Calorimetry* **2011**, *103*, 647.

(26) Panchal, P. K.; Pansuriya, P. B.; Parekh, H. M.; Chhasatia, M. R.; Patel, M. N. *Journal of Macromolecular Science, Part A: Pure and Applied chemistry* **2007**, *44*, 1.

(27) Pansuriya, P. B.; Patel, M., N. *Journal of Enzyme Inhibition and Medicinal Chemistry* **2008**, *23*, 108.

(28) Pansuriya, P. B.; Patel, M. N.; Chhasatia, M. R.; Dhandhukia, P.; Thakar, V. *Journal of Coordination Chemistry* **2008**, *61*, 3336.

Chapter Five

Catalytic testing: Oxidative functionalization of *n*-octane

5.1 Introduction

Transition metal-mediated oxidative functionalization of hydrocarbons into useful organic compounds has become an area of immense interest and has led to great advancements in large-scale industrial (Table 5.1) and synthetic organic processes.[1,2] The development of synthetic models has been biologically inspired by a number of enzymes such as methane monooxygenase and cytochrome-P450 which make use of a reactive iron-oxo species in the oxidation of a number of alkanes (Chapter 1, Section 1.1.2). [3-5]

Table 5.1: Industrial applications of oxidative functionalization of hydrocarbons.[6]

Hydrocarbon	Oxidation product	Applications
Cyclohexane	Cyclohexanol and cyclohexanone	Converted to adipic acid and caprolactam. (Polyamide precursors)
Cyclododecane	Cyclododecanol and cyclododecanone	Oxidized to dodecanedioic acid and lauryl lactam. (Polyamide precursors)
Butane	Acetic acid Maleic anhydride[7]	Solvent, vinyl acetate polymers. Unsaturated polyester resins.[7]

These catalytic oxidation processes are carried out using a variety of oxidants, namely, PhIO, NaOCl, H_2O_2, alkyl hydroperoxides, percarboxylic acids and molecular oxygen.[8] This dissertation focuses on hydrogen peroxide H_2O_2 and *tert*-butyl hydroperoxide (*t*-BuOOH) as the respective oxidants.

H_2O_2 is a commonly used oxidant due to economical and environmental considerations.[2,8,9] It operates by transferring one of its oxygen atoms to the substrate (alkane) to produce water.[9] *tert*- Butyl hydroperoxide has an advantage over H_2O_2, in that it has a higher solubility in organic solvents which contain dissolved hydrophobic hydrocarbons.[9]

The oxidation of hydrocarbons are divided into three types:[2]

I. "True" organometallic activation of the C–H bond and organometallic derivatives formed as intermediates or as the final products.

II. The metal complex functions only in the abstraction of an electron or a hydrogen atom from the hydrocarbon. Contact between the C–H bond and the metal complex occurs during C–H bond cleavage via a complex ligand.

III. The metal complex plays a role in activating the oxidant (hydrogen peroxide) to form a reactive species (hydroxyl radical), which attacks the hydrocarbon molecule, (eqn (**1**))[10].

Type III is most common, where the hydroxyl radical (HO•) abstracts hydrogen from the alkane molecule (RH) forming an alkyl radical (R•) (eqn (**2**)), which reacts with oxygen to form peroxy radicals (ROO•) (eqn (**3**).[9] The peroxy radical is converted to the alkyl peroxides (eqn (**4**)), which progressively decompose to produce alcohols and the corresponding carbonyl groups (ketones, aldehydes and acids) (eqn (**5**)).[2,9,11-13]

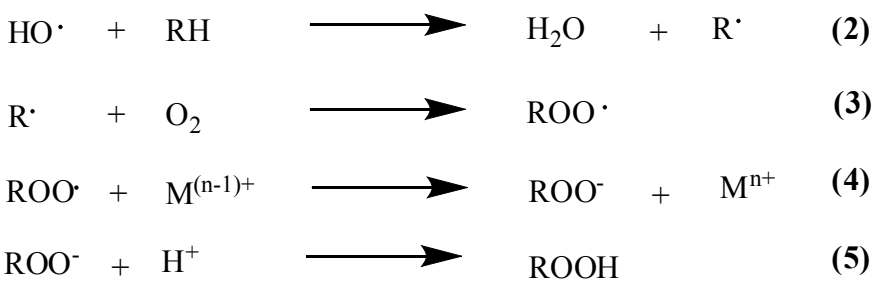

If (*t*-BOOH) is used as the oxidant, the radical *t*-BuO• is formed by the attack of the metal ion, which attacks then attacks the alkane (eqn (**6**)).[9] The reaction then proceeds as shown above in equations **3**-**5**.[9]

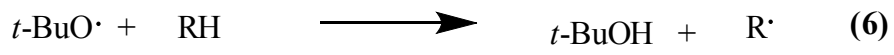

The attack on a specific bond of the hydrocarbon depends on the energy of the radical. Low energy radicals (Cl_3C• and ROO•) are more selective, stable and long lived, with preference to tertiary C–H bonds than secondary, which are more susceptible to attack than primary C–H bonds.[2] However, energetic radicals (RO•) are indiscriminate to the type of bond they attack.[2] This leads to a problem in selectivity and therefore the preferential oxidation of one carbon atom over the other is a challenging process.[14] Factors such as regioselectivity and stereoselectivity may be enhanced by modification of the metal centers by use of an appropriate ligand system, e.g. bulky ligands are important in controlling the reactivity of the metal.[8,14] Complexes which contain *N*-ligands have been reported to exhibit higher catalytic activity, where amines added to the reaction solution change the selectivity and/or accelerate the oxidation process.[4,11]

Due to the inertness of the alkane, solvents that can be oxidized easily should not be employed in reactions with hydrocarbons.[9] The solvent is important in maintaining the activity of the system.[15] Solvents such as MeCN, nitromethane, acetic acid and DCM are appropriate, in that they contain C–H bonds which are deactivated by electron-withdrawing substituents.[9] Improving the electrophilicity of metalating species is achieved with the use of strong acids, whilst water is effectively used as a green solvent and in the case of biphasic systems and in the oxidation of small chain alkanes (methane and ethane).[9]

In this study, iridium and cobalt catalysts (Chapter 3, Sections 3.3 and 3.4) were investigated in the oxidative functionalization of *n*-octane. An *in situ* study with a ruthenium precursor (**3.14**) and the respective ligands (**3.1**-**3.4**) was undertaken. Two solvent systems, namely, DCM and MeCN were employed at temperatures of 30 and 80 °C and two oxidants, *tert*-butyl hydroperoxide and hydrogen peroxide were investigated. In each of the solvent systems, optimization of substrate to oxidant was carried out in order to obtain the best conversion and selectivity.

5.2 Experimental Conditions

5.2.1 Instruments and Reagents

All catalytic reactions were performed under inert conditions in moisture free glassware with anhydrous solvents. All solvents were analytical grade. Solvents utilized were dried by standard methods, unless otherwise stated. DCM was distilled from P_2O_5. MeCN was degassed for 10-15 minutes before use. All reagents were weighed and handled in air. All products were analyzed using a Perkin Elmer Auto System gas chromatograph fitted with a Flame Ionisation Detector (FID). Specifications of the column and GC parameters are indicated in Table 5.2. The GC was calibrated with a multicomponent standard (Appendix 1B, Table B1) of the expected products and the respective RF values were calculated. Pentanoic acid was used as the internal standard. A volume of 0.5 µl of the reaction mixture were injected into the GC and quantified.

Table 5.2: Column specification and GC parameters.

Column	Pona 50 m X 0.20 mm X 0.5 µm
Injector temperature	240 °C
Detector temperature	260 °C
Split	On flow rate: 123 ml min^{-1}
Attenuation	4
Range	1
Oven Program	
Initial temperature	50 °C
Ramp one	2 °C min^{-1}
Temperature two	90 °C
Ramp two	15 °C min^{-1}
Temperature three	200 °C

Reagents used in the catalytic testing of *n*-octane:

n-octane (C_8H_{18}): Fluka

Pentanoic acid ($C_5H_{10}O_2$): Merck

Tert-butyl hydroperoxide ($C_4H_{10}O_2$): Sigma Aldrich

5.2.2 General procedure

Synthesis and properties of the catalysts (**3.6-3.13**) are described in Chapter 3, Section 3.2 and 3.3 and Chapter 4. Catalytic testing was carried out in two solvent systems, MeCN and DCM at 40 and 80 °C, using two oxidants, hydrogen peroxide and *tert*-butyl hydroperoxide. For each of the solvent systems, the substrate to oxidant ratio was varied (1:2.5; 1:5; 1:7.5; 1:10) to determine the optimum ratio for the best conversion (Appendix 2B, Tables B2 and B4). The catalyst to substrate ratio was kept constant at 1:100. Two different blank runs were carried out: one with no metal complex as the catalyst, for each of the above substrate to oxidant ratios and the other with no oxidant (Appendix 2B, Table B3 and B5).

A two-necked pear shaped flask was charged with 10 mg of the respective catalyst, pentanoic acid, octane, the respective oxidant and 10 ml of the solvent (exact masses and molar quantities are shown in Appendix 2B, Tables B6 and B8). The flask was equipped with a reflux condenser, stirred, heated to the respective temperature and maintained for 48 hours in an oil bath. After the time period, an aliquot was removed using a Pasteur pipette and filtered through cotton wool and silica gel. An aliquot (0.5 μl) was injected into the GC and quantified.

An *in situ* study was carried out using the ruthenium precursor (**3.14**) (Chapter 3, Section 3.5) and the respective ligands (**3.1-3.4**, Chapter 3, Section 3.2). The procedure was undertaken as per the general method with the exception that an equimolar quantity of the precursor and ligand was added (~1.70 $x10^{-5}$) to the two-necked flask (Appendix 3B, Table B9 and B10).

5.3 Results and Discussion

5.3.1 Catalytic testing carried out in DCM at 40 °C

5.3.1.1 Iridium catalysts (3.6-3.9)

The catalysts were completely soluble in DCM; hence it was the solvent of choice. The reaction of *n*-octane, undertaken in DCM, with *t*-BuOOH as the respective oxidant showed a conversion in the blank run (Fig. 5.1). Conversion without the catalyst is commonly noted with oxidants such as *t*-BuOOH.[13] [($^{Ph}PN_{cyclohexyl}P^{Ph}$)IrCOE][$BF_4$] (**3.6**), was used as the respective catalyst to determine the optimum ratio of substrate to oxidant to get the highest conversion. It is observed that the ratio of 1:5 of substrate to oxidant was most suitable, since the highest conversion was observed (7%). At higher concentrations of oxidant (1:7.5 and 1:10), a decrease in conversion as deeper oxidation products is observed (*e.g.* ketones). Furthermore, at these concentrations no selectivity to the alcohols was observed. The other iridium catalysts (**3.7**-**3.9**) were then tested under the same conditions using the optimum ratio of substrate to oxidant of 1:5 (Fig. 5.2). Catalyst **3.6** gave the highest conversion, followed by **3.9**. The conversion observed for **3.7** and **3.8** were rather low and in the range of the blank run. These low conversions could be attributed to the low temperature at which the reaction was taking place, contributing less energy to the activation process. The difference in conversion between the different catalysts, could be attributed to the bite angle (Donor atom-Metal-Donor atom angle)[16] of the complexes. This bite angle is known to have an impact on the activity and selectivity of catalytic reactions.[16] To establish the effect of the bite angle on the reaction conditions, the bite angles of similar complexes containing the ligands **3.1**-**3.4** was calculated from literature; for ligand **3.1** (65.95°)[17], **3.2** (70.45°)[18], **3.3** (95.8°)[19], **3.4** (66.62°)[19]. It is noted that with an increase in the size of the substituent on the nitrogen atom, the size of the bite angle decreases. An increase in steric interactions can result in a greater dissociation of the ligand (COE) from the metal center thereby increasing the reactivity of the metal.[20,21] Furthermore, van Zeist and co-workers[22] have reported that the effect of bite angle on C–X bond activation

originates from an electronic factor, where donor-acceptor orbital interactions (metal d orbitals to the substrate $\sigma^*_{c\text{-}x}$) stabilize the transition state.[22] As the metal-ligand d hybrid orbital is driven to smaller bite angles, the transition state becomes more stabilized.[22]

No conversion was observed with testing carried out with hydrogen peroxide as the respective oxidant. Although hydrogen peroxide is often a highly effective oxidant for the oxidation of alkanes, in some cases *t*-BuOOH proceeds more efficiently.[13,23] In terms of selectivity to the products of oxidation (Fig. 5.3), it is noted that the catalysts are most selective to the ketones (octanones) and least selective to octanoic acid. Literature states that when using *t*-BuOOH as an oxidant, the ketone product forms from the oxidation of the alcohol (over oxidation).[3] This is observed especially with catalyst **3.8**, which is most selective to the octanones and least selective to the alcohols and vice versa with catalysts **3.6** and **3.9**. The effect of the bite angle may also contribute to the selectivity of the alcohols, where the complexes with bulky ligands of smaller bite angles (**3.6** and **3.9**) are more selective than those complexes containing ligands of larger bite angles (**3.7** and **3.8**).[24] Furthermore, the production of the aldehyde (octanal) accounts for the decreased ketone production with catalysts **3.6** and **3.8**.

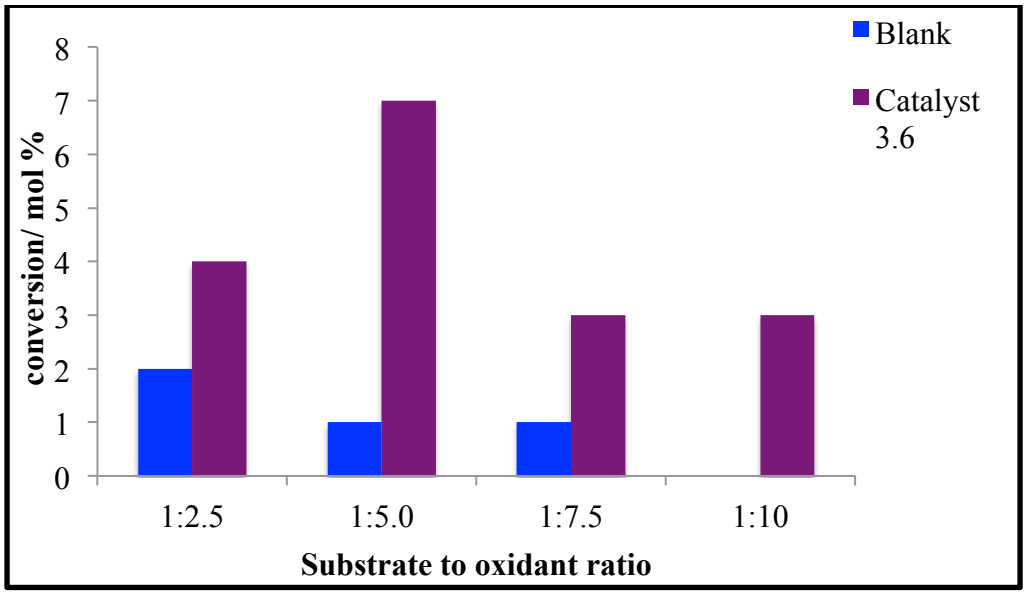

Fig. 5.1: Conversion observed for the optimization of substrate to oxidant ratio for both the catalyst ([(^{Ph}PN$_{cyclohexyl}$P^{Ph})Ir COE][BF_4] **(3.6)**) and the blank.

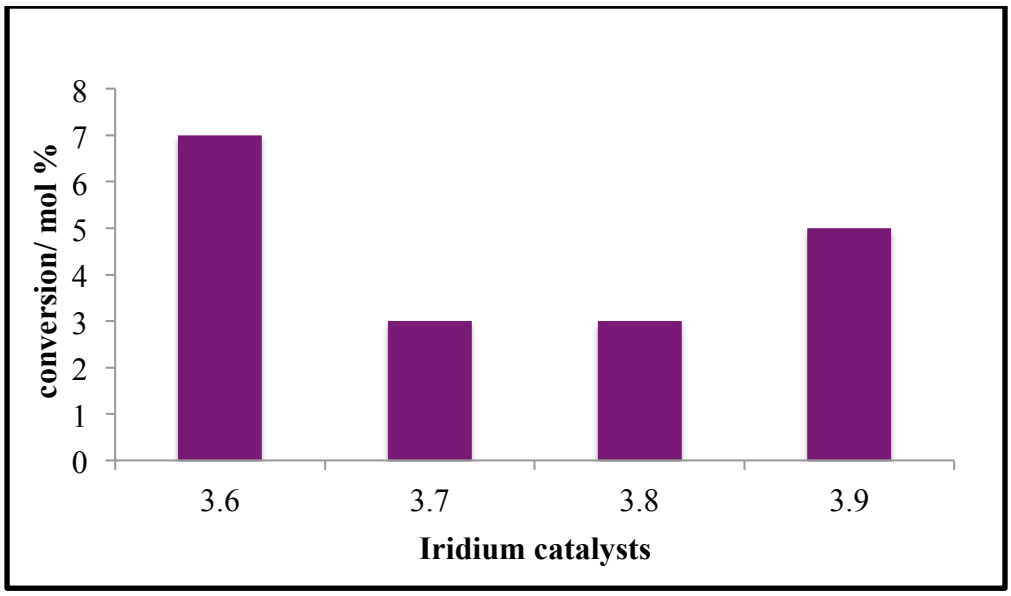

Fig. 5.2: Conversion observed for the iridium catalysts (**3.6-3.9**) at a substrate to oxidant ratio of 1:5.

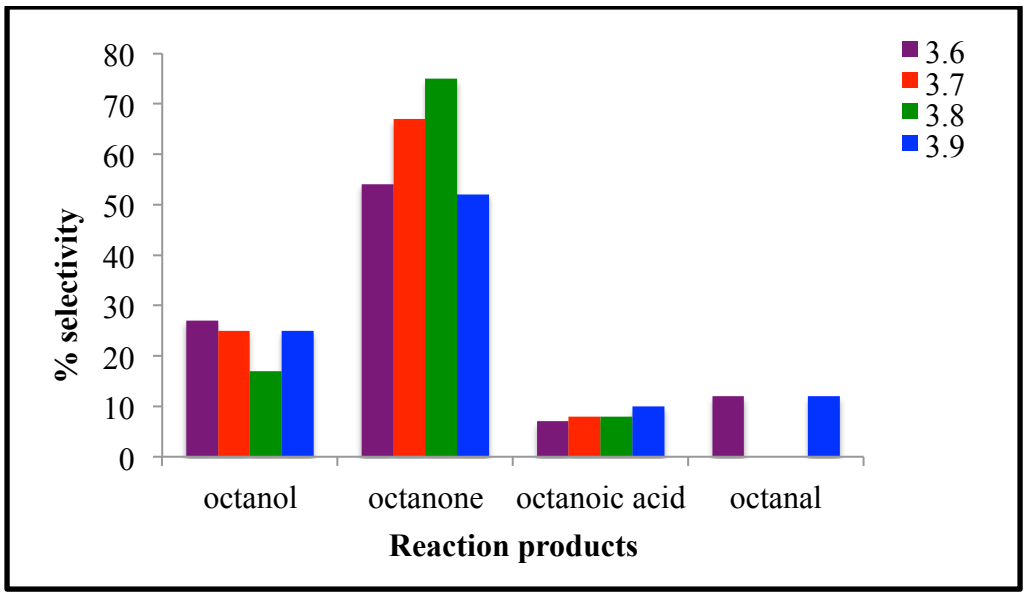

Fig. 5.3: Selectivity of the iridium catalysts (**3.6-3.9**) to the products of oxidation.

Notably, analogous reactivities are observed with catalysts **3.6** and **3.9**, and **3.7** and **3.8** at carbon positions 1-4 (Figs. 5.4-5.7 and Table 5.3). At the carbon (1) position (Fig. 5.4), all catalysts show minimal selectivity to 1-octanol and maximum selectivity to octanoic acid. This is an indication of over oxidation, which is most likely to occur since this carbon is most susceptible to attack by the oxidant since its least sterically hindered.

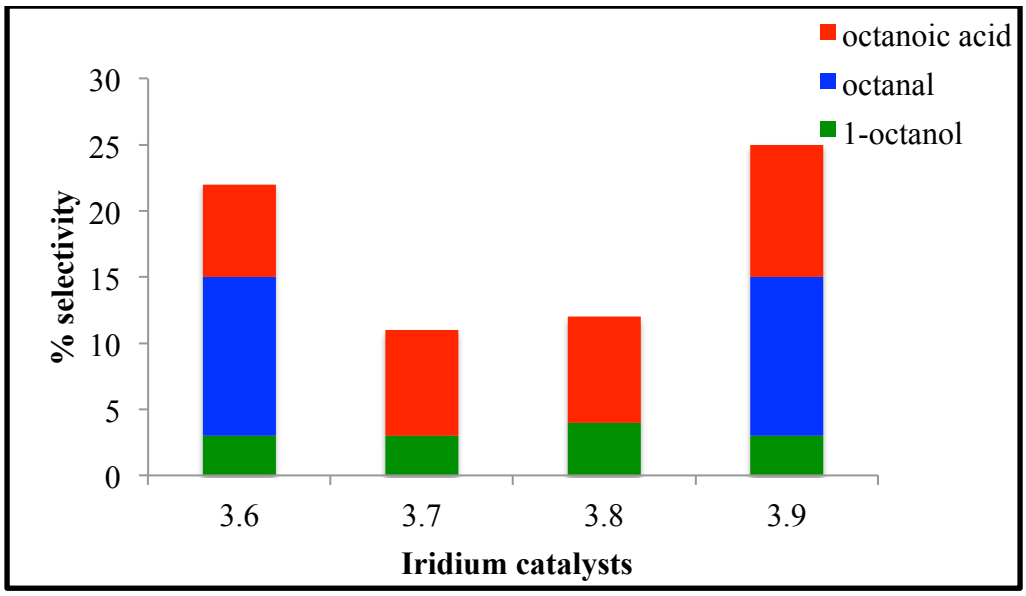

Fig. 5.4: Selectivity of the iridium catalysts (**3.6-3.9**) to C(1) products.

At carbon position (2) (Fig. 5.5), highest selectivity is noted with catalysts **3.6** and **3.9** (32 and 29% respectively). There is approximately a 1:1 ratio of alcohol to ketone production observed with these catalysts. Over oxidation occurs at this carbon position for catalysts **3.7** and **3.8,** since they are only selective to 2-octanone. However, the reverse is observed in the selectivity of the iridium catalysts at carbon position (3) (Fig. 5.6). Catalysts **3.7** and **3.8** are selective to 3-octanol and exhibit a much higher selectivity to this product than catalysts **3.6** and **3.9**, which are only selective to the ketone. Nonetheless, the production of ketones is twice as favored over the alcohols, with approximately a 1:2 ratio of alcohol to ketone. The low selectivity (towards the alcohols) observed is an indication that the oxidation reaction procedes via formation of hydroxyl radicals as shown in equations 1-6 (Section 5.1).[25]

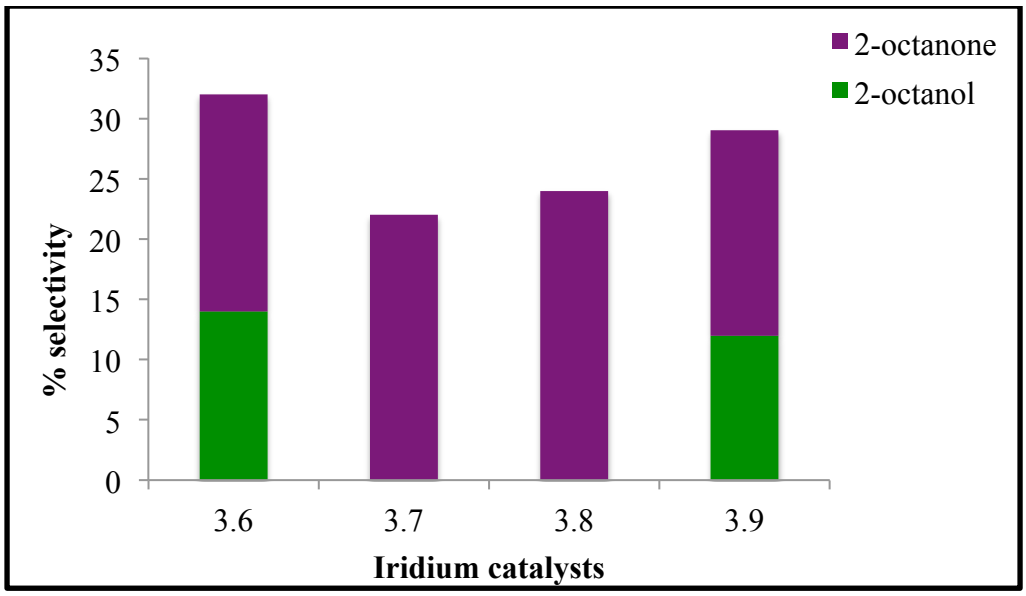

Fig. 5.5: Selectivity of the iridium catalysts (**3.6-3.9**) to C(2) products.

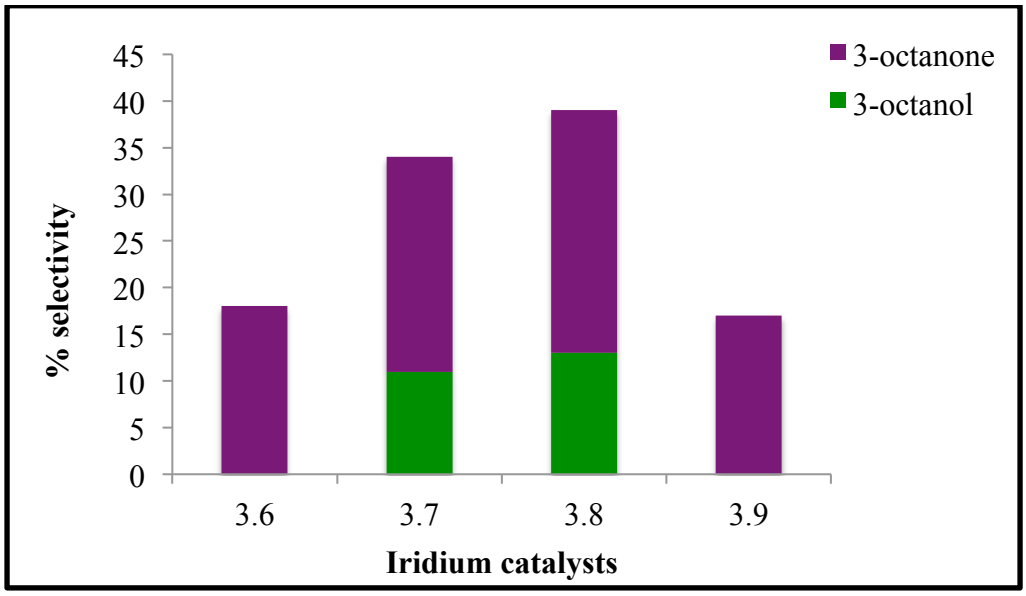

Fig. 5.6: Selectivity of the iridium catalysts (**3.6-3.9**) to C(3) products.

At carbon position 4 (Fig. 5.7), catalyst **3.6**, **3.7** and **3.9** are more selective to the ketone than the alcohol. Catalyst **3.8** displays a similar selectivity pattern as in Fig. 5.4. As observed at the other carbon positions ((2) and (3)), the alcohol production remains consistent, with the lowest being 10% and the highest, 14%.

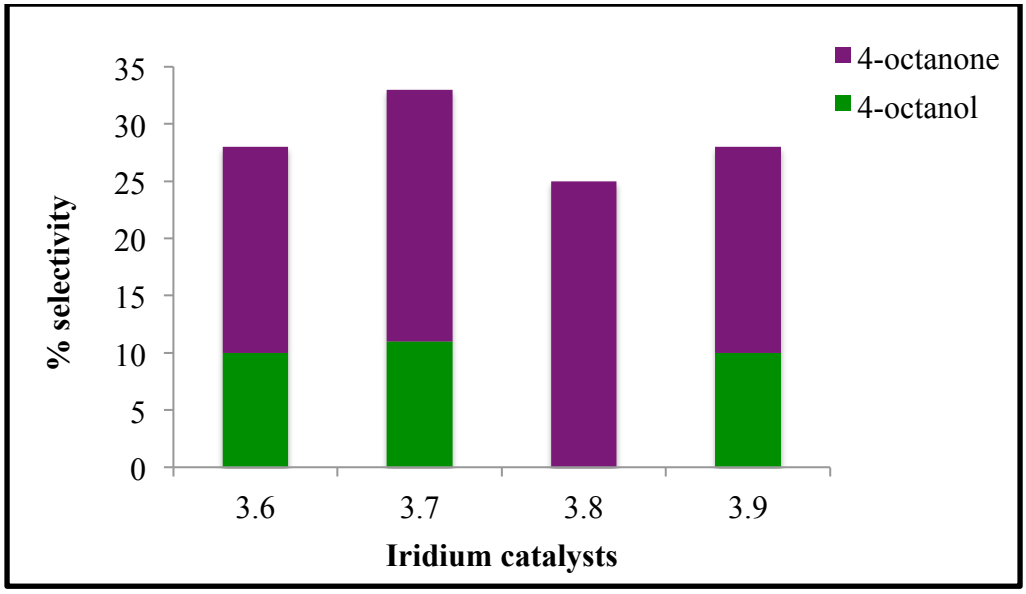

Fig. 5.7: Selectivity of the iridium catalysts (**3.6-3.9**) to C(4) products.

Table 5.3 : Selectivity parameters in the oxidation of *n*-octane by iridium catalyst (**3.6-3.9**).[a]

Catalyst	**Alcohol**[b] **C(1):C(2):C(3):C(4)**	**Ketone**[b] **C(2):C(3):C(4)**	**Total**[c] **C(1):C(2):C(3):C(4)**
[($^{Ph}PN_{cyclohexyl}P^{Ph}$)IrCOE][$BF_4$] (**3.6**)	1:7:0:5	1:1:1	1:2:1:2
[($^{Ph}PN_{pentyl}P^{Ph}$)IrCOE][BF_4] (**3.7**)	1:0:6:6	1:1:1	1:3:5:5
[($^{Ph}PN_{iso\text{-}propyl}P^{Ph}$)IrCOE][$BF_4$] (**3.8**)	1:0:5:0	1:1:1	1:3:5:3
[($^{Ph}PN_{benzyl}P^{Ph}$)IrCOE][BF_4] (**3.9**)	1:6:0:5	1:1:1	1:2:1:2

[a] Parameters C(1):C(2):C(3):C(4) are the relative reactivities of hydrogen atoms at carbon 1, 2, 3 and 4 of the *n*-octane chain.

[b] The calculated reactivities from the % selectivity are normalized, i.e. calculated taking into account the number of hydrogen atoms at each carbon. (Appendix 2B, Table B7)

[c] Includes the % selectivity of octanoic acid, octanal, alcohols and ketones and are normalized.

5.3.1.2 Cobalt catalysts (3.10-3.13)

The conversions observed for the cobalt catalysts **3.10-3.13** (Fig. 5.8) are much lower than for the iridium catalysts (Section 5.3.1.1, Fig. 5.2). This can be attributed to the ligand group bound to the metal. Iridium is bound to cyclooctene (COE), which is a good leaving group as noted by the thermal analysis of the complexes (**3.6-3.9**). In contrast, cobalt is bound to two chlorine atoms, which is a poor leaving group as observed in the proposed decomposition schemes (Chapter 4, Schemes 4.9 and 4.10). However, the catalyst containing ligand **3.1** (**3.10**) gives the highest conversion, which is also noted for the iridium catalyst **3.6** could possibly be attributed to the bite angle effect described in Section 5.3.1.1. Furthermore, the catalytic testing performed in DCM renders catalysts **3.11** and **3.12** inactive. As observed with the iridium catalysts, those that contain the pentyl and iso-propyl substituents on the nitrogen exhibit lower conversions. No conversion was observed for the cobalt catalysts using hydrogen peroxide as the oxidant.

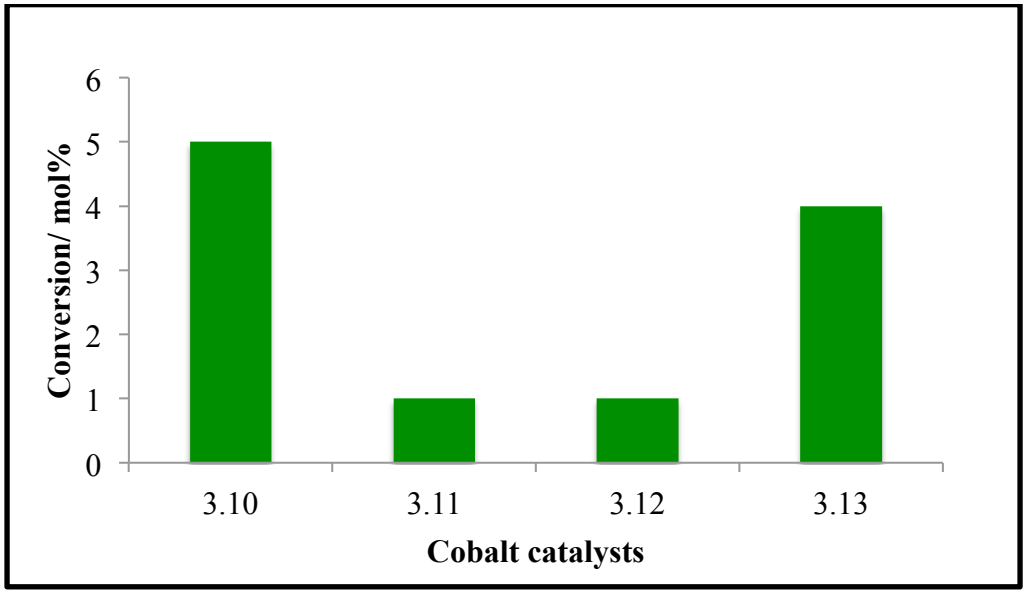

Fig. 5.8: Conversion observed for the cobalt catalysts (**3.10-3.13**) at substrate to oxidant ratio of 1:5.

Selectivity towards the products of oxidation (Fig. 5.9) shows that the catalysts are highly selective to the ketones (72%, catalyst **3.13**). A similar situation as observed with the iridium catalysts is noted for the cobalt catalysts. The catalyst that is most

selective to the alcohol (35%, catalyst **3.10**) is less selective to the ketone (56%) and more selective to the acid (9%). Furthermore, the cobalt catalysts are more selective to the alcohols (35%) than the iridium catalysts (27%).

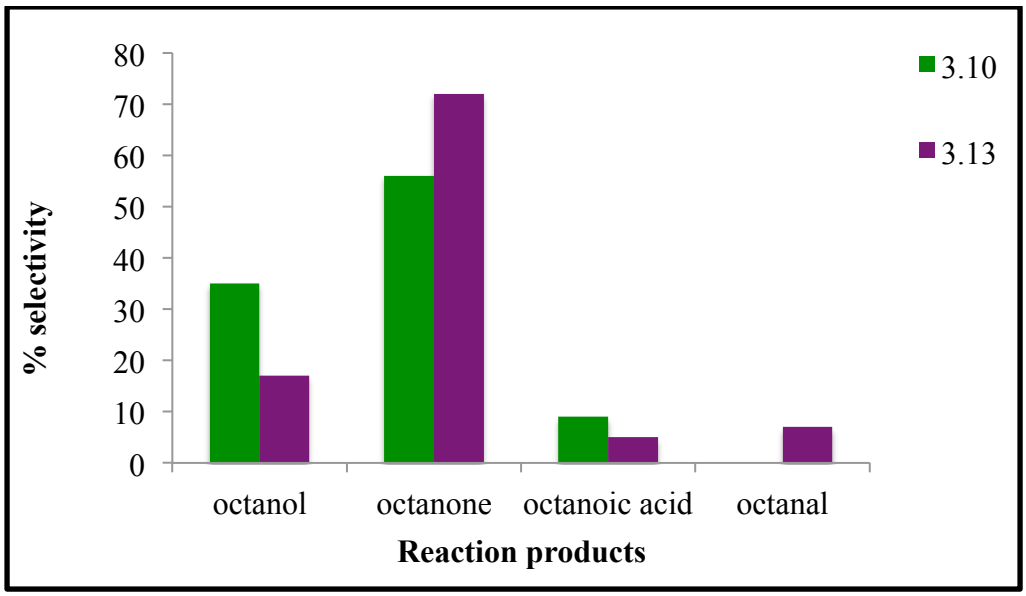

Fig. 5.9: Selectivity of the cobalt catalysts (**3.10** and **3.13**) to the products of oxidation.

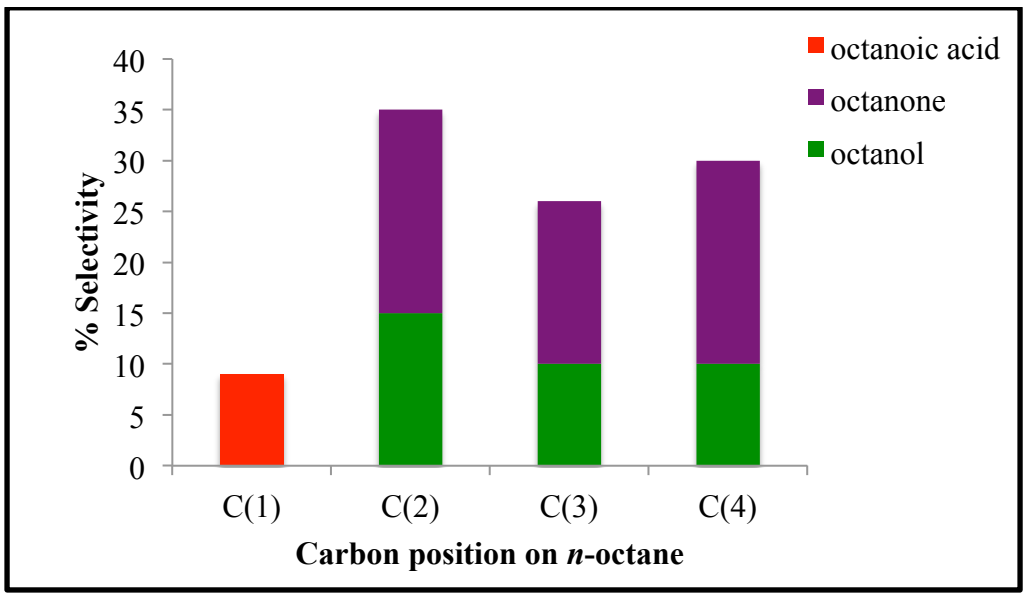

Fig. 5.10: Regioselectivity of the cobalt catalyst **3.10** to the products of oxidation.

Observing the regioselectivity of catalysts **3.10** and **3.13** (Figs. 5.10 and 5.11 and Table 5.4), carbon at position one of *n*-octane is least selective to the products of oxidation. Catalyst **3.13** is more susceptible to over oxidation, since the octanone

production dominates at all carbon positions, whilst for catalyst **3.10** there is a approximate 1:2 ratio of alcohol to ketone at positions (2)-(4). This indicates that catalyst **3.10** is more suitable for alcohol production. Selectivity of octanones is indiscriminate with respect to the carbon position.

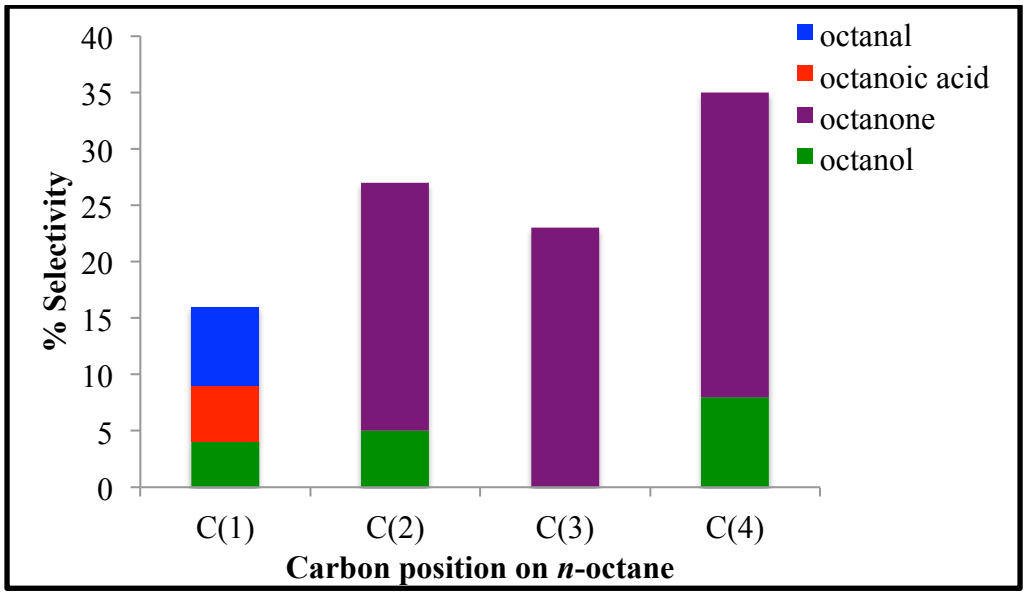

Fig. 5.11: Regioselectivity of the cobalt catalyst **3.13** to the products of oxidation.

Table 5.4: Selectivity parameters in the oxidation of *n*-octane by cobalt catalysts (**3.10-3.13**).[a]

Catalyst	**Alcohol**[b] **C(1):C(2):C(3):C(4)**	**Ketone**[b] **C(2):C(3):C(4)**	**Total**[c] **C(1):C(2):C(3):C(4)**
$[(^{Ph}PN_{cyclohexyl}P^{Ph})CoCl_2]$ **(3.10)**	0:2:1:1	1:1:1	1:6:4:5
$[(^{Ph}PN_{benzyl}P^{Ph})CoCl_2]$ **(3.13)**	1:2:0:3	1:1:1	1:3:2:3

[a] Parameters C(1):C(2):C(3):C(4) are the relative reactivities of hydrogen atoms at carbon 1, 2, 3 and 4 of the *n*-octane chain.

[b] The calculated reactivities from the % selectivity are normalized, i.e. calculated taking into account the number of hydrogen atoms at each carbon. (Appendix 2B, Table B7)

[c] Includes the % selectivity of octanoic acid, octanal, alcohols and ketones and are normalized.

5.3.2 Catalytic testing carried out in MeCN at 80 °C

5.3.2.1 Cobalt catalysts (3.10-3.13)

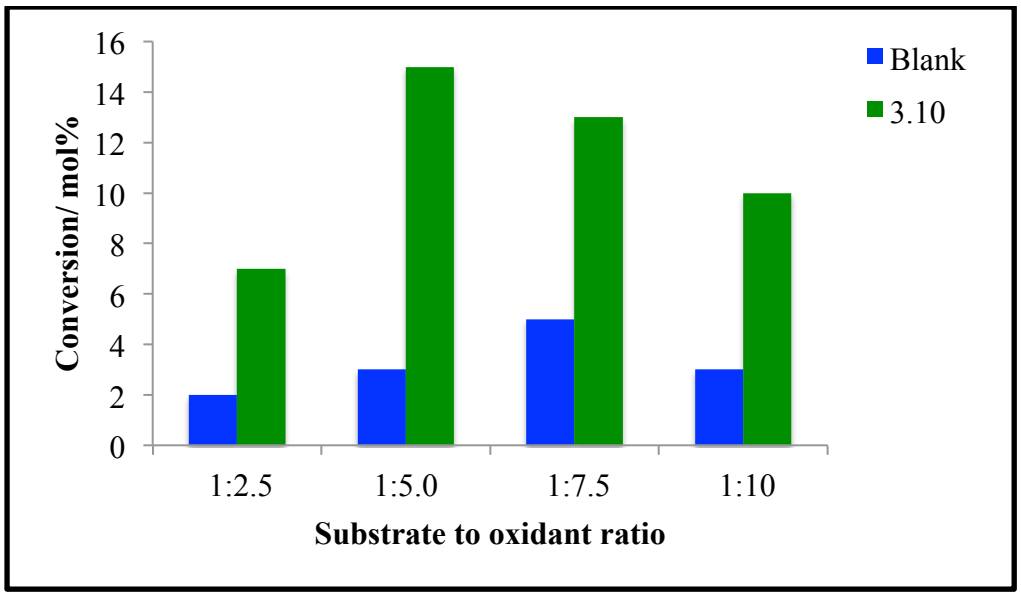

Fig. 5.12: Conversion observed for the optimization of substrate to oxidant ratio for both the catalyst ([(^{Ph}PN$_{cyclohexyl}$P^{Ph})CoCl$_2$] **(3.10)**) and the blank.

Conversions of 2-5% were obtained when only *t*-BuOOH was used as the oxidant in the blank run. (Fig. 5.12). The catalysts were completely soluble in MeCN and due to its high boiling point, it functioned as a suitable solvent as the catalytic testing could be undertaken at 80 °C (as compared to 40 °C in DCM), in the hope of increasing the conversion. [(^{Ph}PN$_{cyclohexyl}$P^{Ph})CoCl$_2$] **(3.10)** was used as the respective catalyst in determining the optimum ratio of substrate to oxidant. It is evident that the ratio of 1:5 was most suitable, since it gave the highest conversion (15%). Further increase in the substrate to oxidant ratio resulted in a decrease in the conversion and selectivity to the alcohols. Subsequent testing using catalysts **3.11-3.13** were carried out using this ratio (Fig. 5.13). The conversion observed was much higher than that observed in DCM, which is due to the higher temperature at which the testing is performed.[8] Higher activity in MeCN may also be attributed to the polarity of the solvent and solubility of the oxidant.[5,8] Catalysts **3.11** and **3.12**, which were inactive in the testing performed in DCM, exhibited conversions of 14% and 11%. As noted with the testing in DCM, the conversion is in accordance with the bulkiness of the ligand, with

catalyst **3.10** being most active. Interestingly, the iridium catalysts (**3.6-3.9**) were also tested in MeCN, but no conversion was observed. This could be attributed to the substitution of cyclooctene with MeCN, which binds strongly to iridium, impeding the radical formation.[26] Furthermore, the mass spectra of these catalysts showed molecular ion peaks corresponding to the MeCN complexes, i.e. cyclooctene substituted by MeCN.

Selectivities to the octanones were more pronounced (75%) than to the octanols (19%) (Fig. 5.14). Unlike the testing in DCM, where each catalyst displayed a distinct pattern in terms of selectivity to the alcohol and the ketone, in MeCN all catalysts exhibit similar selectivity. However, the high selectivity towards the ketones is an indication of over oxidation. This is more explicit upon observing the selectivity of the catalysts at each carbon atom C(1)-C(4) of octane (Figs. 5.15-5.18, Table 5.5).

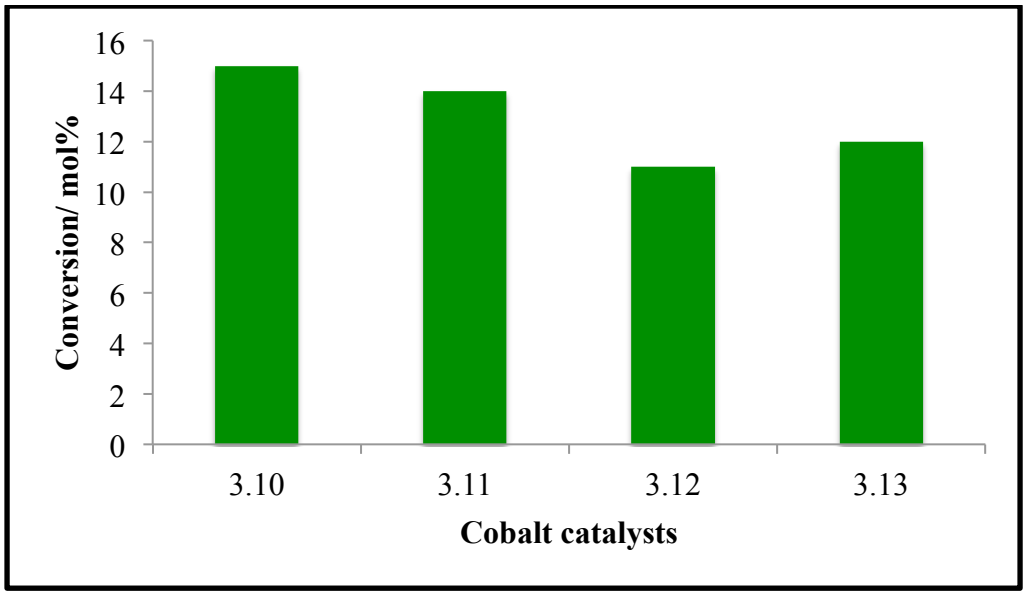

Fig. 5.13: Conversion observed for the cobalt catalysts (**3.10-3.13**) at substrate to oxidant ratio of 1:5.

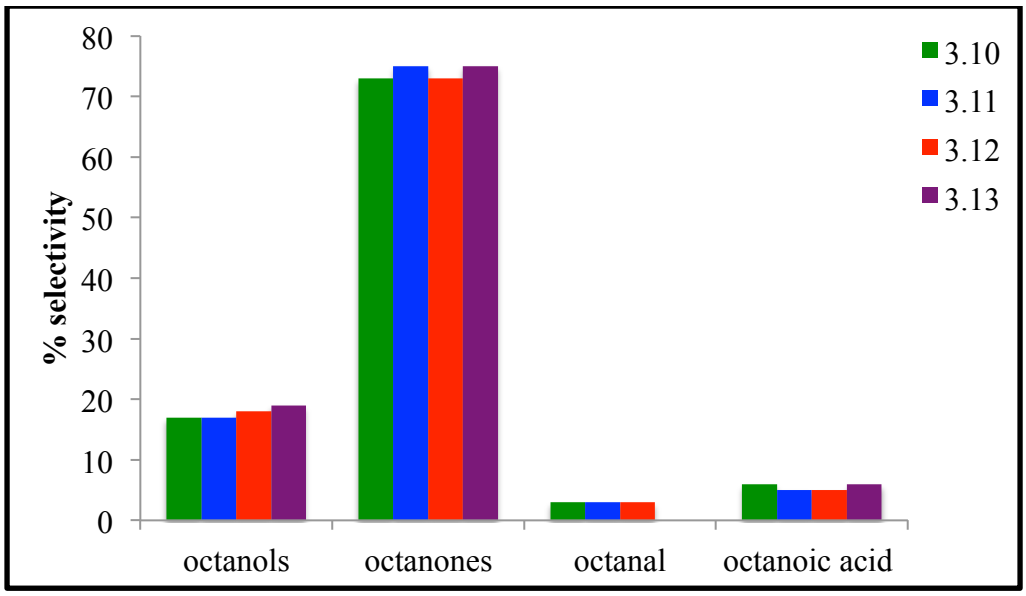

Fig. 5.14: Selectivity of the cobalt catalysts (**3.10-3.13**) to the products of oxidation.

Over oxidation is less pronounced at the C(1) carbon, since the alcohol production dominates over the acid and the aldehyde. However, it is only at the C(1) position that alcohol production is dominant. Figs. 5.16-5.18 clearly indicate over oxidation takes place, with high selectivity to the ketones and a selectivity of <4% to the alcohol (C(2) and C(4)). It can therefore be concluded, that higher conversions are observed at higher temperatures (40 °C versus 80 °C), but at the expense of reduced selectivity to the alcohols and over oxidation.

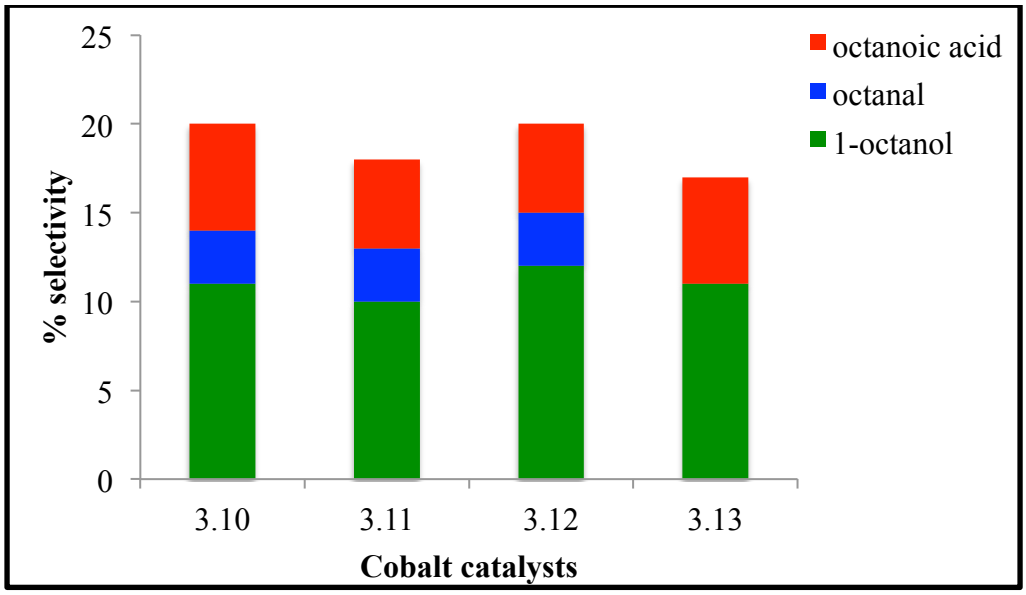

Fig. 5.15: Selectivity of the cobalt catalysts (**3.10-3.13**) to C(1) products.

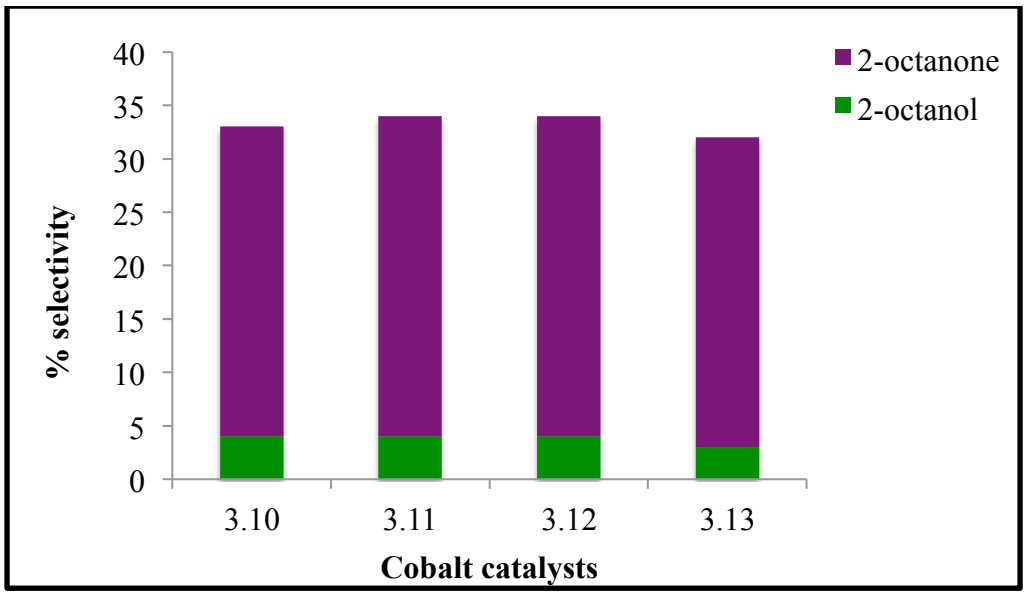

Fig. 5.16: Selectivity of the cobalt catalysts (**3.10-3.13**) to C(2) products.

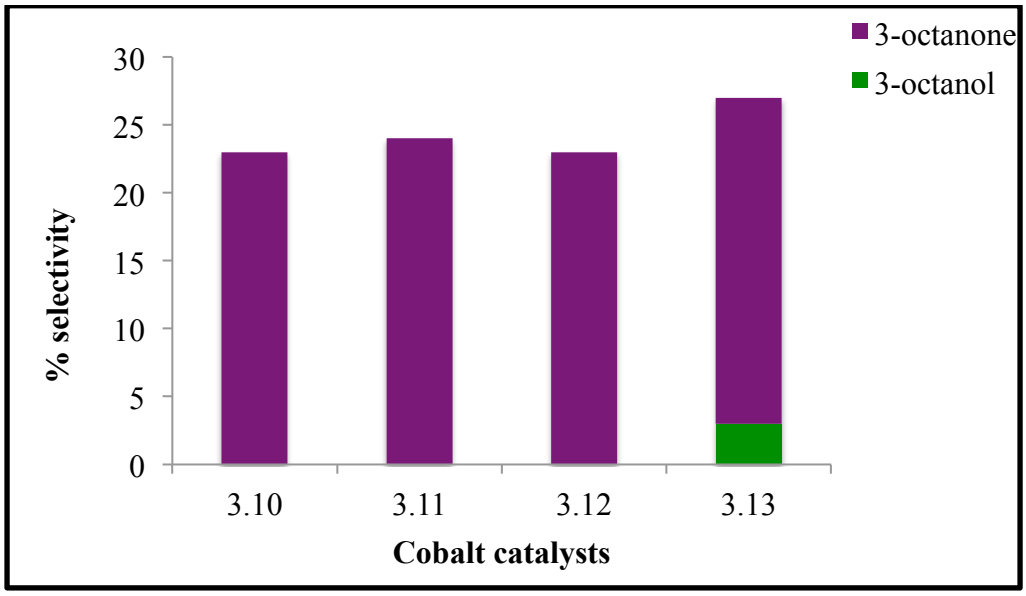

Fig. 5.17: Selectivity of the cobalt catalysts (**3.10-3.13**) to C(3) products.

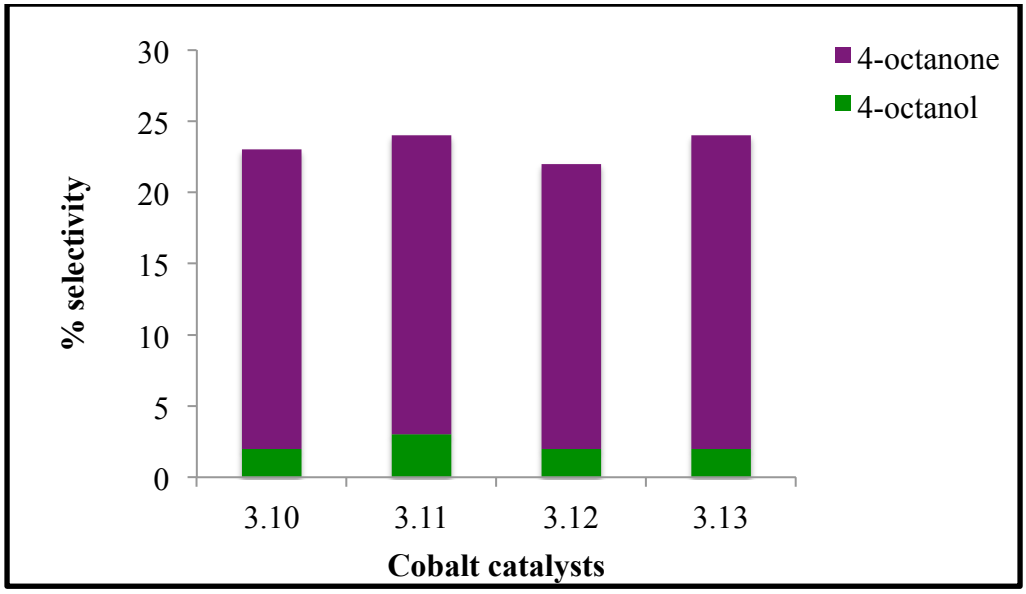

Fig. 5.18: Selectivity of the cobalt catalysts (**3.10-3.13**) to C(4) products.

Table 5.5: Selectivity parameters in the oxidation of *n*-octane by cobalt catalysts (**3.10-3.13**).[a]

Catalyst	**Alcohol**[b] **C(1):C(2):C(3):C(4)**	**Ketone**[b] **C(2):C(3):C(4)**	**Total**[c] **C(1):C(2):C(3):C(4)**
[($^{Ph}PN_{cyclohexyl}P^{Ph}$)$CoCl_2$] (**3.10**)	4:2:0:1	2:1:1	1:2:2:2
[($^{Ph}PN_{pentyl}P^{Ph}$)$CoCl_2$] (**3.11**)	2:1:0:1	1:1:1	1:3:2:2
[($^{Ph}PN_{iso\text{-}propyl}P^{Ph}$)$CoCl_2$] (**3.12**)	4:2:0:1	2:1:1	1:3:2:2
[($^{Ph}PN_{benzyl}P^{Ph}$)$CoCl_2$] (**3.13**)	4:2:2:1	1:1:1	1:3:2:2

[a] Parameters C(1):C(2):C(3):C(4) are the relative reactivities of hydrogen atoms at carbon 1, 2, 3 and 4 of the *n*-octane chain.

[b] The calculated reactivities from the % selectivity are normalized, i.e. calculated taking into account the number of hydrogen atoms at each carbon. (Appendix 2B, Table B7)

[c] Includes the % selectivity of octanoic acid, octanal, alcohols and ketones and are normalized.

5.3.3 *In situ* study with ruthenium precursor (3.14) and ligands 3.1-3.4

5.3.3.1 Catalytic evaluation in MeCN performed at 80 °C

A one-pot reaction was carried out using a ruthenium precursor (**3.14**), and ligands **3.1**-**3.4**, in MeCN and DCM, with *t*-BuOOH as the respective oxidant. The optimum substrate to oxidant ratio of 1:5 obtained using the cobalt catalyst where investigated in this study. As observed with the other catalysts, the highest conversions were noted with the complex containing the cyclohexyl ring substituent on the nitrogen atom of the ligand. This is also observed in this study (Fig. 5.19) where the ruthenium complex containing ligand **3.1** gave the highest conversion of 17%. The lowest conversion was for the complex containing ligand **3.4** (7%). No conversion was observed for catalysis performed in DCM.

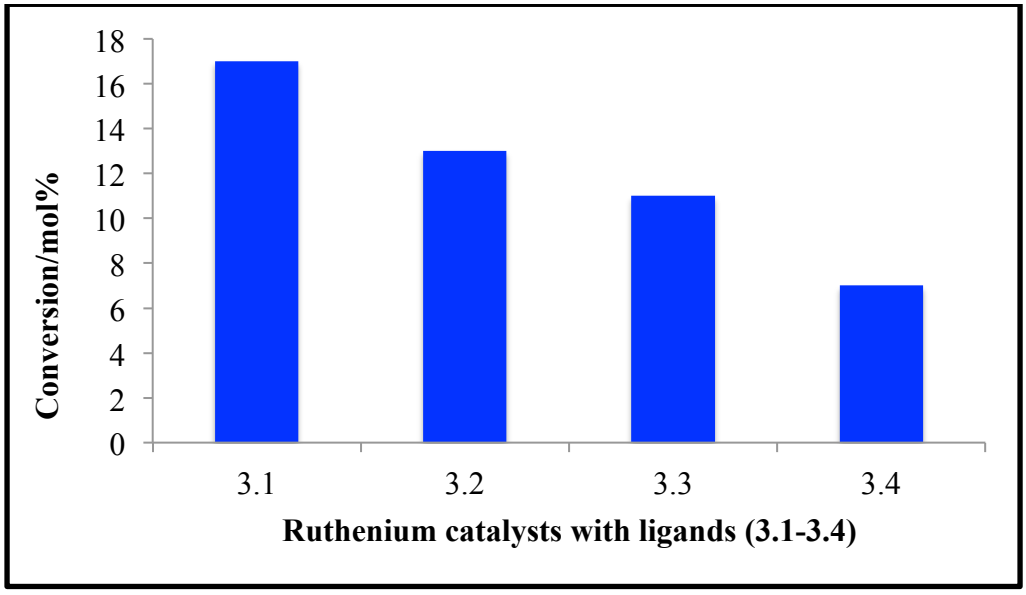

Fig. 5.19: Conversion observed using the ligands (**3.1-3.4**) at a substrate to oxidant ratio of 1:5.

Unlike the testing carried out in MeCN with the cobalt catalyst, in this study the ruthenium complexes display a distinct pattern in terms of selectivity (Fig. 5.20). For example, the catalyst (containing ligand **3.4**) least selective to the alcohol is most selective to the ketone and vice versa with catalyst containing ligand **3.2**. As with the other iridium and cobalt catalysts, elevated selectivity to the ketones is observed.

However, unlike the other catalysts, the ruthenium complexes display a much higher selectivity to the alcohols. This enhanced selectivity is pronounced when considering the selectivity to the products of oxidation at each carbon position (C(1)-C(4)) of octane (Figs. 21-23, Table 5.6). Interestingly, a very high selectivity to 1-octanol is observed at the C(1) position (Fig. 5.21), with very little or no signs of over oxidation. A similar situation is observed in Section 5.3.2.1 with the cobalt catalysts.. However, the selectivity is greatly enhanced with the ruthenium catalysts (23% versus 11%). All ruthenium complexes display a similar selectivity to the alcohols. Over oxidation is prevalent at carbon positions C(2)-C(4), where selectivity to the ketones dominate.

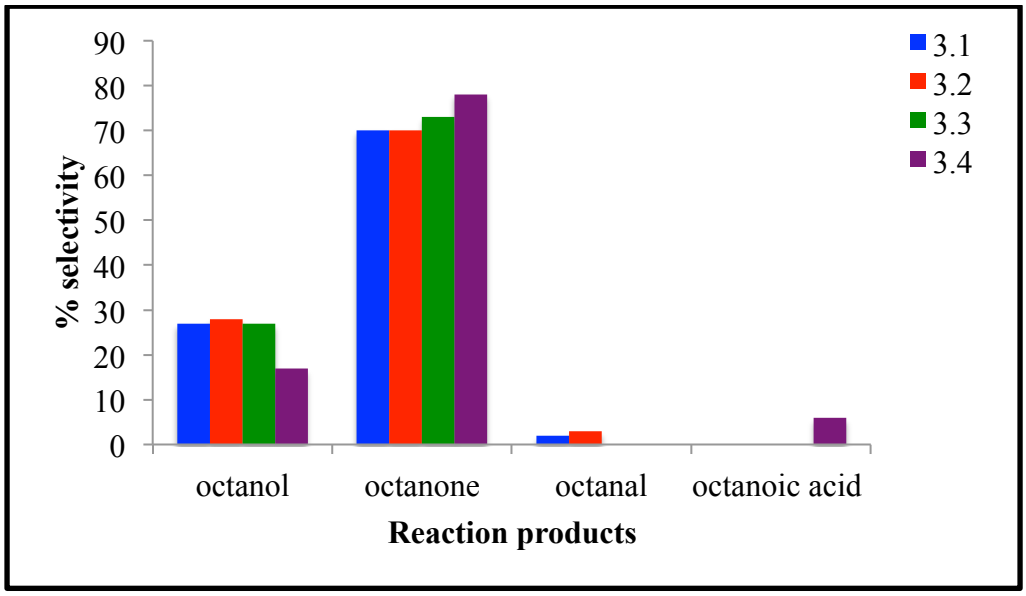

Fig. 5.20: Selectivity of the ruthenium precursor with ligands (**3.1-3.4**) to the products of oxidation.

Noteworthy, oxidation of *n*-octane by Mn(salen)- ,[salen = (R,R)-N,N-bis(3,5-di-tert-butylsalicylidenato)-1,2-cyclohexanediamine(2-)], complexes in MeCN with *t*-BuOOH, showed no products of oxygenation at the C(1) position of *n*-octane.[14] However, even when hydrogen peroxide is used as the oxidant, the selectivity to alcohols at the C(1) position is rather low.[13] Notably, oxidation of *n*-octane in the presence of an acid (HCl) gave high selectivities to alcohols at C(2)-C(4) (1:29:25:24), with the reaction at C(1) being least favoured.[27]

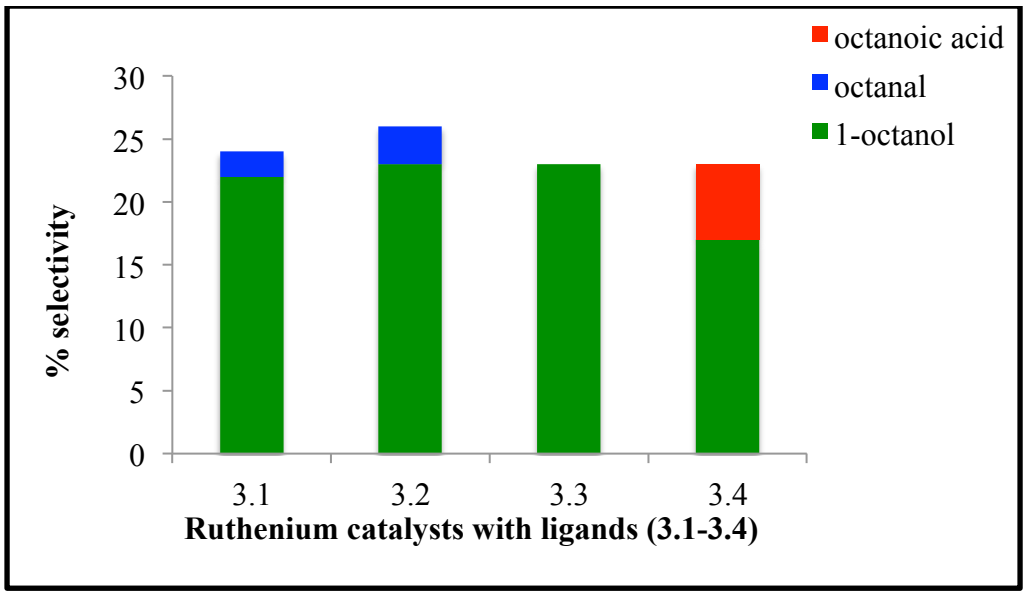

Fig. 5.21: Selectivity of the ruthenium catalyst with ligands (**3.1-3.4**) to C(1) products.

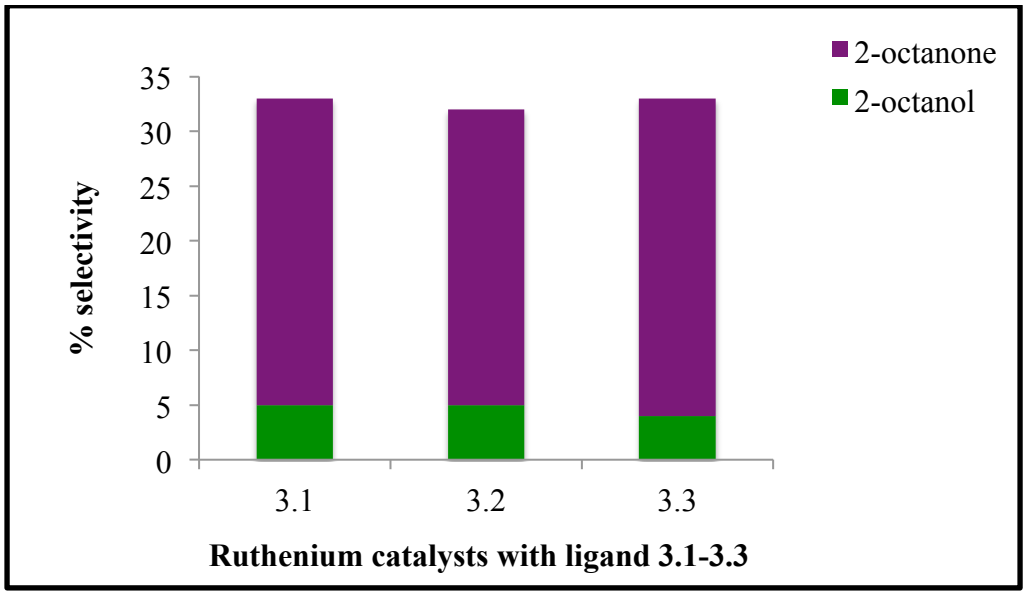

Fig. 5.22: Selectivity of the ruthenium precursor with ligands (**3.1-3.4**) to C(2) products.

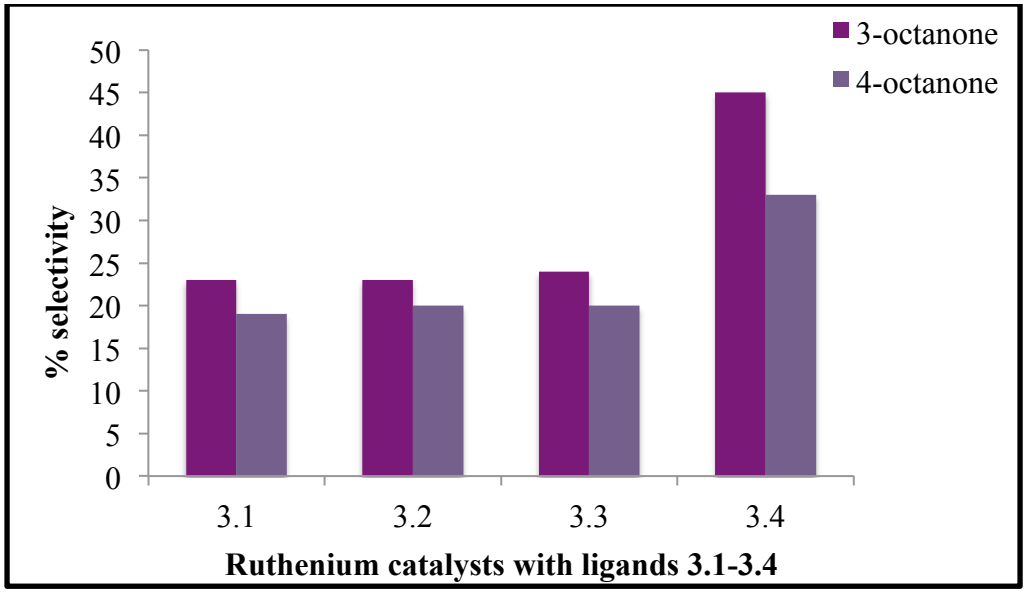

Fig. 5.23: Selectivity of the ruthenium precursor with ligands (**3.1-3.4**) to C(3) and C(4) products.

Table 5.6 : Selectivity parameters in the *in situ* oxidation of *n*-octane by ruthenium precursor with ligands (**3.1-3.4**). [a]

Ligand	**Alcohol[b] C(1):C(2)**	**Ketone[b] C(2):C(3):C(4)**	**Total[c] C(1):C(2):C(3):C(4)**
[$^{Ph}PN_{cyclohexyl}P^{Ph}$] (**3.1**)	3:1	1:1:1	1:2:1:1
[$^{Ph}PN_{pentyl}P^{Ph}$] (**3.2**)	3:1	1:1:1	1:2:1:1
[$^{Ph}PN_{iso\text{-}propyl}P^{Ph}$] (**3.3**)	4:1	1:1:1	1:2:2:1
[$^{Ph}PN_{benzyl}P^{Ph}$] (**3.4**)	3:1	1:2:1	1:2:3:2

[a] Parameters C(1):C(2):C(3):C(4) are the relative reactivities of hydrogen atoms at carbon 1, 2, 3 and 4 of the *n*-octane chain.

[b] The calculated reactivities from the % selectivity are normalized, i.e. calculated taking into account the number of hydrogen atoms at each carbon. (Appendix 2B, Table B7)

[c] Includes the % selectivity of octanoic acid, octanal, alcohols and ketones and are normalized.

5.4 Conclusion

For each solvent system, the optimum substrate to oxidant ratio of 1:5 was used in the testing of the catalyst for the oxidation of *n*-octane. No conversion was observed with hydrogen peroxide in both solvent systems. Therefore, catalytic evaluation was only carried out using *t*-BuOOH as the respective oxidant. The iridium catalysts were inactive in MeCN. In DCM, highest conversion observed with the iridium catalysts was 7% (**3.6**) and 5% with the cobalt catalyst (**3.10**), which is contributed to the bite angle effect. An increase in the steric bulk of the substituent on the nitrogen atom of the respective complexes decreases the bite angle, which was found to increase the reactivity of the catalyst. The iridium catalysts were highly selective to the ketones (75%) and selectivity to the alcohols was 27%. Catalysts **3.11** and **3.12** were inactive in DCM. The cobalt catalyst **3.10** was most suited for alcohol production; whilst with catalyst **3.13** over oxidation is highly prevalent. In MeCN, higher conversions are observed for the cobalt catalysts (15% for catalyst **3.10**). Unlike the catalytic testing in DCM, the C(1) position of *n*-octane was selective to 1-octanol. Over oxidation occurs at the other carbon positions (high production of ketones).

In the *in-situ* testing of the ruthenium precursor (**3.14**) with ligands **3.1**-**3.4** in MeCN, the complex containing ligand **3.1** gave the highest conversion of 17%. No conversion was observed in DCM. The selectivity pattern is generally similar to those of the cobalt catalysts in MeCN, with the C(1) position being most selective to the alcohols. However, the *in-situ* study with ruthenium the selectivity to 1-octanol is double that of the cobalt catalysts (24% versus 11%). Over oxidation is prevalent at the other carbon positions.

5.5 References

(1) Klei, S. R.; Tan, K, L.; Golden, J. T.; Yung, C, M.; Thalji, R. K.; Ahrendt, K. A.; Ellman, J. A.; Tilley, T. D.; Bergman, R. G. *In Activation and Functionalization of C-H Bonds*; American Chemical Society: **2004**; Vol. 885, p 46.

(2) Shul'pin, G. B. *Comptes Rendus Chimie* **2003**, *6*, 163.

(3) Yiu, S.; Man, W.; Lau, T. *Journal of the American Chemical Society.* **2008**, *130*, 10821.

(4) Nizova, G. V.; Krebs, B.; Süss-Fink, G.; Schindler, S.; Westerheide, L.; Cuervo, G. L.; Shul'pin, G. B. *Tetrahedron* **2002**, *58*, 9231.

(5) Bahramian, B.; Mirkhani, V.; Mogahadam, M.; Tangestaninejad, S. *Catalysis Communications* **2006**, *7*, 289.

(6) Parshall, G. W. *Homogenous catalysis*; Wiley-Interscience Publications, New York **1980**.

(7) Centi, G.; Trifiro, F.; Ebner, J. R.; Franchetti, V. M. *Chemical Reviews* **1988**, *88*, 55.

(8) Mirkhani, V.; Moghadam, M.; Tangestaninejad, S.; Mohammadpoor-Baltork, I.; Rasouli, N. *Catalysis Communications* **2008**, *9*, 2411.

(9) Shul'pin, G. B. *Mini-reviews in Organic Chemistry* **2009**, *6*, 95.

(10) Fokin, A. A.; Schreiner, P. R. *Chemical Reviews* **2002**, *102*, 1551.

(11) Shul'pin, G. B.; Golfeto, C. C.; Süss-Fink, G.; Shul'pina, L. S.; Mandelli, D. *Tetrahedron Letters* **2005**, *46*, 4563.

(12) Shul'pin, G. B.; Kozlov, Y.; Shul'pina, L. S.; Kudinov, A. R.; Mandelli, D. *Inorganic Chemistry Communication* **2009**, *48*, 10480.

(13) Shul'pin, G. B.; Süss-Fink, G.; Shul'pina, L.S. *Journal of Molecular Catalysis A: Chemical* **2001**, *170*, 17.

(14) Mac Leod, T. C. O.; Kirillova, M., V.; Pombeiro, A. J. L.; Schiavon, M. A.; Assis, M. D. *Applied Catalysis A: General* **2010**, *372*, 191.

(15) Anisia, K. S.; Kumar, A. *Applied Catalysis A: General* **2004**, *273*.

(16) van Leeuwen, P. W. N. M.; Kamer, P. C. J.; Reek, J. N. H. *Pure Applied Chemistry* **1999**, *71*, 1443.

(17) Teo, S.; Weng, Z.; Hor, T. S. A. *Organometallics* **2008**, *27*, 4188.

(18) Engelbrecht, I.; Visser, H. G.; Roodt, A. *Acta Crystallographica Section E* **2010**, *E66*, m922.

(19) Bollmann, A.; Blann, K.; Dixon, J. T.; Hess, F. M.; Killian, E.; Maumela, H.; McGuiness, D. S.; Morgan, D. H.; Neveling, A.; Otton, S.; Overette, M.; Slawin, A. M. Z.; Wasserchеid, P.; Kihlmann, S. *Journal of the American Chemical Society* **2004**, *126*, 14712.

(20) Miller, S. F., *Synthesis, characterisation and application of functionalised phosphine ligands* MSc Thesis, University of Johannesburg, **2010**, p 86.

(21) Tolman, C. A. *Chemical Reviews* **1977**, *77*, 313.

(22) van Zeist, W.-J.; Visser, R.; Bickelhaupt, F. M. *Chemistry: A European Journal* **2009**, *15*, 6112.

(23) Shul'pin, G. B.; Kudinov, A. R.; Shul'pina, L. S.; Petrovskaya, E. A. *Journal of Organometallic Chemistry* **2006**, *691*, 837.

(24) Blann, K.; Bollmann, A.; de Bod, H.; Dixon, J. T.; Killian, E.; Nongodlwana, P.; Maumela, M. C.; Maumela, H.; McConnel, A. E.; Morgan, D. H.; Overette, M. J.; Pŕetorius, M.; Kuhlmann, S.; Wasserscheid, P. *Journal of Catalysis* **2007**, *249*, 244.

(25) Shul'pina, L. S.; Kirillova, M. V.; Pombeiro, A., J.L.; Shul'pin, G. B. *Tetrahedron* **2009**, *65*, 2424.

(26) Dorta, R.; Goikhman, R.; Milstein, D. *Organometallics* **2003**, *22*, 2806.

(27) Kirillova, M. V.; Kozlov, Y. N.; Shul'pina, L. C.; Lyakin, O. Y.; Kirillov, A. M.; Talsi, E. P.; Pombeiro, A. J. L.; Shul'pin, G., B. *Journal of Catalysis* **2009**, *268*, 26.

Chapter Six

Summary

The pincer ligands with a PNP framework were successfully synthesized and characterized by NMR, IR spectroscopy and HRMS. The success of the synthesis was determined by the shifts in the ^{31}P NMR spectra from free phosphine to the nitrogen bound phosphine. The peak shifts depended on the nature of the substituent on the nitrogen atom. The branched substituents (**3.1** and **3.3**) are shifted upfield in comparison to the straight chain and aromatic substituents (**3.2** and **3.4**). The IR data reflect the crystallinity of the ligands.

The ligands were successfully complexed to the transition metals iridium and cobalt. The complexes were characterized by elemental analyses, IR spectroscopy and HRMS. A novel approach in the synthesis of the iridium complex was carried out, so as to increase its solubility. Due to rapid decomposition, the NMR spectra of the iridium complexes were not elucidated. The cobalt complexes are paramagnetic in nature.
Therefore, the elemental analyses, the shifts of the bands in the IR spectra, HRMS and TGA were used to confirm complexation. The IR band shifts were also an informative tool in determining the coordination of the metal to the ligand.

Thermal analyses of the ligands and complexes were performed. Decomposition schemes for all ligands and complexes were proposed based on their weight loss at the respective temperatures. A similar decomposition pattern is noted for those ligands which have unsaturated C–H substituents (cyclohexyl, pentyl and *iso*-propyl) on the nitrogen atom. Also, the iridium and cobalt complexes containing the ligands with the cyclohexyl ring and the *iso*-propyl substituent on the nitrogen atom displayed similar decomposition schemes. The major weight loss was attributed to the fragmentation of the PNP backbone.

The oxidation of *n*-octane was undertaken with an optimum ratio of substrate to oxidant of 1:5. In DCM and MeCN, with hydrogen peroxide as the respective oxidant, no conversion was observed. In DCM, with *t*-BuOOH as the respective oxidant, for the cobalt complexes a much lower conversion was obtained in comparison to the testing carried out MeCN. No conversion was observed for the iridium catalysts in MeCN. All catalysts were highly selective to the ketones. The C(1) position of the octane chain was selective to the alcohols, whilst at the other positions (C(2)-C(4)) over oxidation was prevalent. The iridium and cobalt complexes containing the ligand with the cyclohexyl substituent on the nitrogen atom gave the highest conversion. This is attributed to the bite angle effect, where an increase in the size of the substituent on the nitrogen atom, decreases the bite angle and increases the reactivity of the catalyst.

The *in situ* testing using a ruthenium precursor and ligands **3.1**-**3.4**, was carried in DCM and MeCN with *t*-BuOOH, with a substrate to oxidant ratio of 1:5. No conversion was observed in DCM. In MeCN, the complex with ligand **3.1** gave the highest conversion. The C(1) carbon position was most selective to the alcohols, whilst at the other carbon positions over oxidation took place. In MeCN, the C(1) selectivity to the alcohols, of the ruthenium catalyst, was double that of the cobalt catalysts.

Appendix A

Appendix A

List of figures

Fig. 1A: ^{1}H NMR of ligand **3.1**. 117

Fig. 2A: ^{13}C NMR of ligand **3.1.** 117

Fig. 3A: ^{31}P NMR of ligand **3.1**. 118

Fig. 4A: ^{1}H NMR of ligand **3.2**. 118

Fig. 5A: ^{13}C NMR of ligand **3.2.** 119

Fig. 6A: ^{31}P NMR of ligand **3.2.** 119

Fig.7A: ^{1}H NMR of ligand **3.3.** 120

Fig. 8A: ^{13}C NMR of ligand **3.3.** 120

Fig. 9A: ^{31}P NMR of ligand **3.3.** 121

Fig. 10A: ^{1}H NMR of ligand **3.4.** 121

Fig. 11A: ^{31}P NMR of ligand **3.4.** 121

Fig. 12A: ^{31}P NMR of chlorodiphenylphosphine. 122

Fig. 13A: ^{1}H NMR of ruthenium precursor **3.14.** 122

Fig. 14A: ^{31}P NMR of ligand **3.14.** 122

Fig. 15A TG curve of diphosphinocyclohexylamine ($^{Ph}PN_{cyclohexyl}P^{Ph}$) (**3.1**). 123

Fig. 16A: TG curve of diphosphinopentylamine ($^{Ph}PN_{pentyl}P^{Ph}$) (**3.2**). 123

Fig. 17A: TG curve of diphosphinopentylamine ($^{Ph}PN_{\textit{iso}\text{-propyl}}P^{Ph}$) (**3.3**). 124

Fig. 18A: TG curve of diphosphinobenzylamine ($^{Ph}PN_{benzyl}P^{Ph}$) (**3.4**). 124

Fig. 19A: DSC curve of diphosphinocyclohexylamine ($^{Ph}PN_{cyclohexyl}P^{Ph}$) (**3.1**). 125

Fig. 20A: DSC curve of diphosphinopentylamine ($^{Ph}PN_{pentyl}P^{Ph}$) (**3.2**). 125

Fig. 21A: DSC curve of diphosphino*iso*-propylamine ($^{Ph}PN_{\textit{iso}\text{-propyl}}P^{Ph}$) (**3.3**). 126

Fig. 22A: DSC curve of diphosphinobenzylamine ($^{Ph}PN_{benzyl}P^{Ph}$) (**3.4**). 126

Fig. 23A: TG curve of [($^{Ph}PN_{cyclohexyl}P^{Ph}$)Ir COE][$BF_4$] **(3.6)**. 127

Fig. 24A: TG curve of [($^{Ph}PN_{pentyl}P^{Ph}$)Ir COE][BF_4] **(3.7)**. 127

Fig. 25A: TG curve of [($^{Ph}PN_{\textit{iso}\text{-propyl}}P^{Ph}$)Ir COE][$BF_4$] **(3.8)**. 128

Fig. 26A: TG curve of [($^{Ph}PN_{benzyl}P^{Ph}$)Ir COE][BF_4] **(3.9)**. 128

Fig. 27A: DSC curve of [($^{Ph}PN_{cyclohexyl}P^{Ph}$)Ir COE][$BF_4$] **(3.6)**. 129

Fig. 28A: DSC curve of [($^{Ph}PN_{pentyl}P^{Ph}$)Ir COE][BF_4] **(3.7)**. 129

Fig. 29A: DSC curve of [($^{Ph}PN_{\textit{iso}\text{-propyl}}P^{Ph}$)Ir COE][$BF_4$] **(3.8)**. 130

Fig .30A: DSC curve of [($^{Ph}PN_{benzyl}P^{Ph}$)Ir COE][BF_4] **(3.9)**. 130
Fig. 31A: TG curve of [($^{Ph}PN_{cyclohexyl}P^{Ph}$)$CoCl_2$] **(3.10)**. 131
Fig. 32A: TG curve of [($^{Ph}PN_{pentyl}P^{Ph}$)$CoCl_2$] **(3.11)**. 131
Fig. 33A: TG curve of [($^{Ph}PN_{iso\text{-}propyl}P^{Ph}$)$CoCl_2$] **(3.12)**. 132
Fig. 34A: DSC curve of [($^{Ph}PN_{cyclohexyl}P^{Ph}$)$CoCl_2$] **(3.10)**. 132
Fig. 35A: DSC curve of [($^{Ph}PN_{pentyl}P^{Ph}$)$CoCl_2$] **(3.11)**. 133
Fig. 36A: DSC curve of [($^{Ph}PN_{iso\text{-}propyl}P^{Ph}$)$CoCl_2$] **(3.12)**. 133

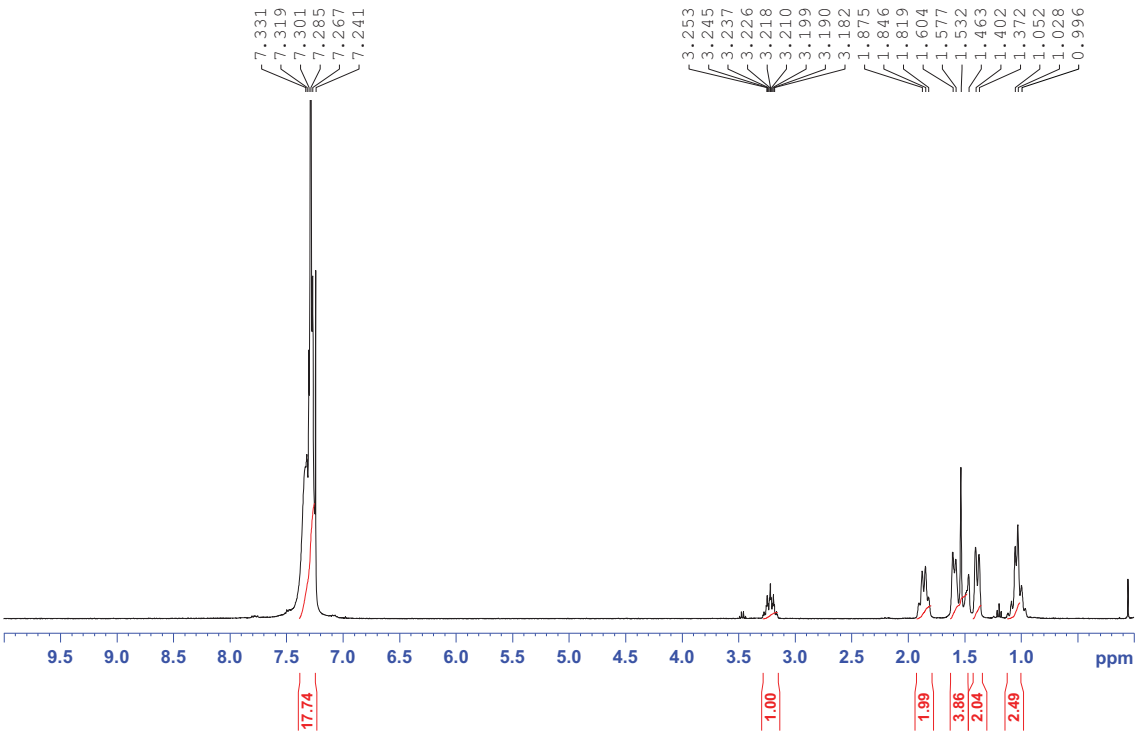

Fig. 1A: ^{1}H NMR spectrum of ligand **3.1.**

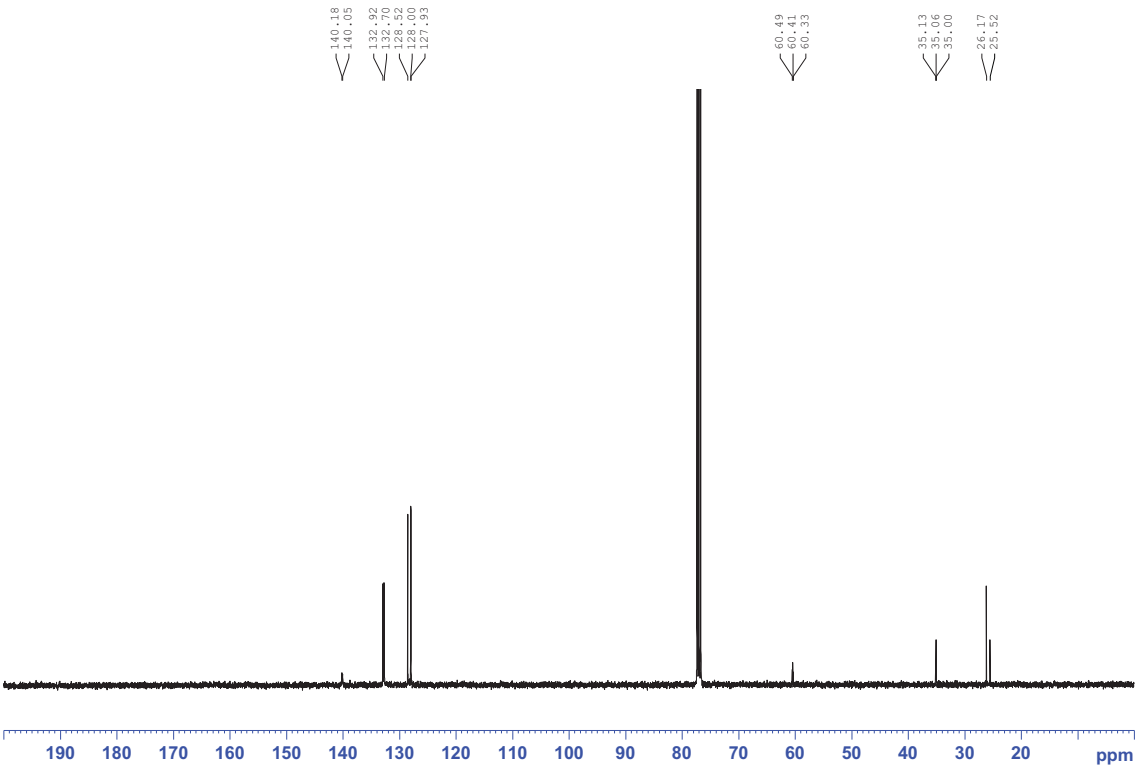

Fig. 2A: ^{13}C NMR spectrum of ligand **3.1**.

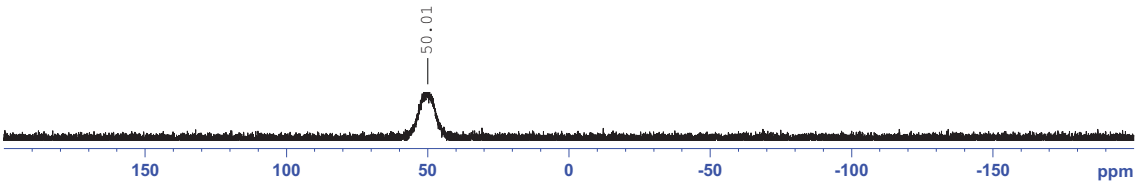

Fig. 3A: ^{31}P NMR spectrum of ligand **3.1**.

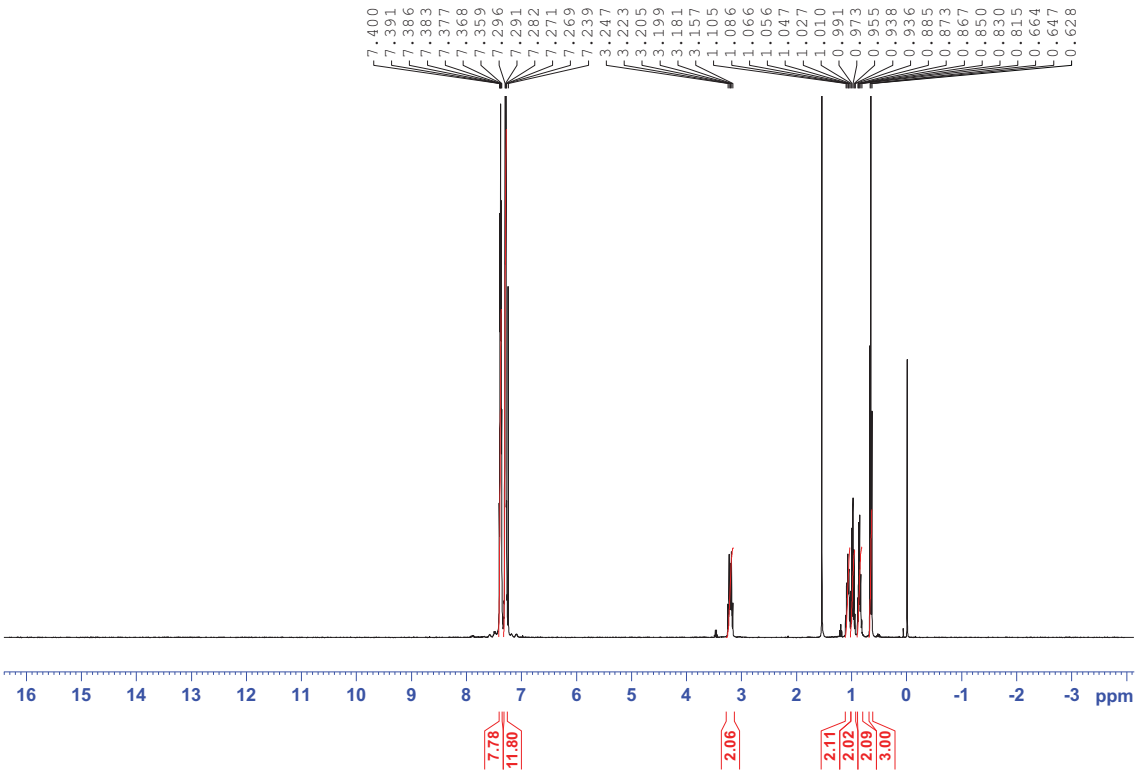

Fig. 4A: ^{1}H NMR spectrum of ligand **3.2**.

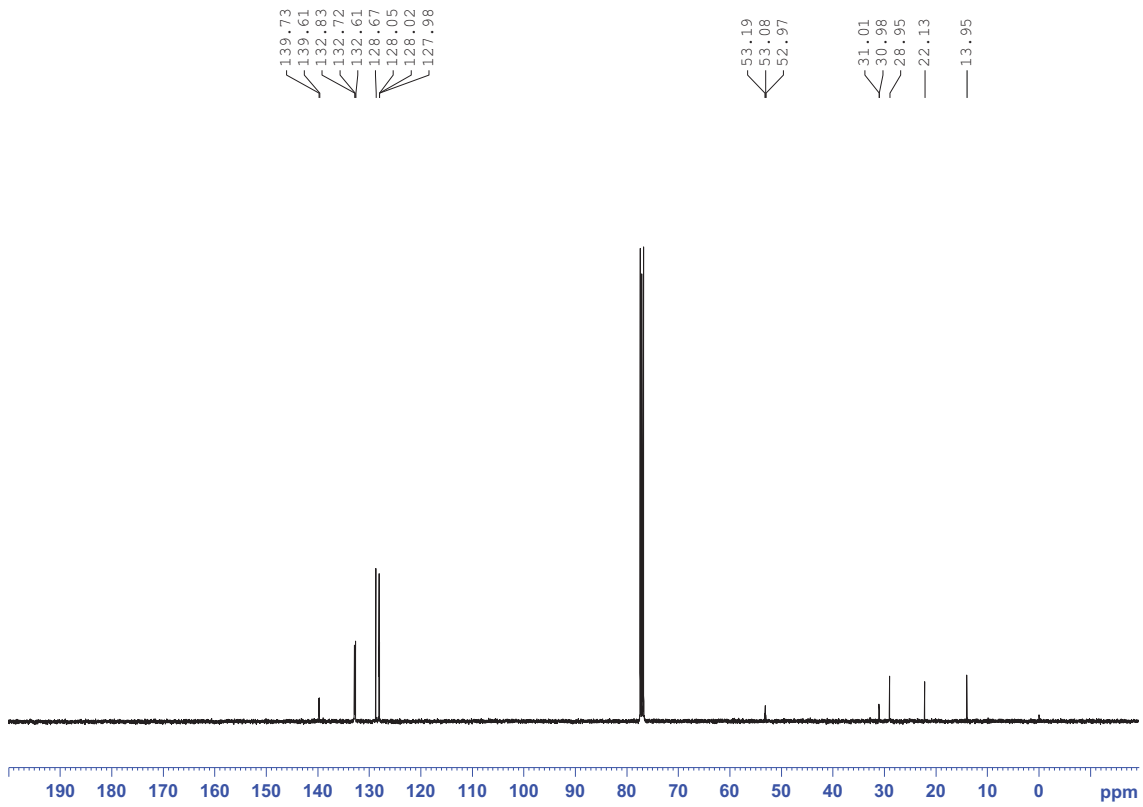

Fig. 5A: ^{13}C NMR spectrum of ligand **3.2.**

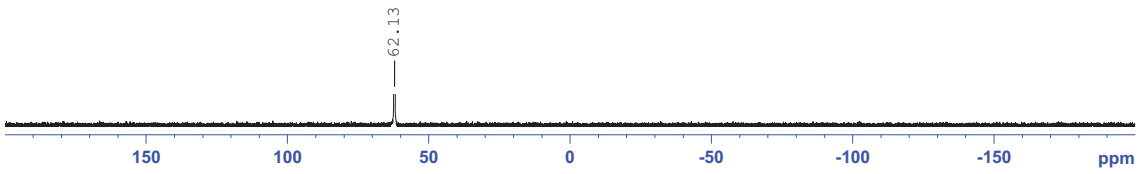

Fig. 6A: ^{31}P NMR spectrum of ligand **3.2.**

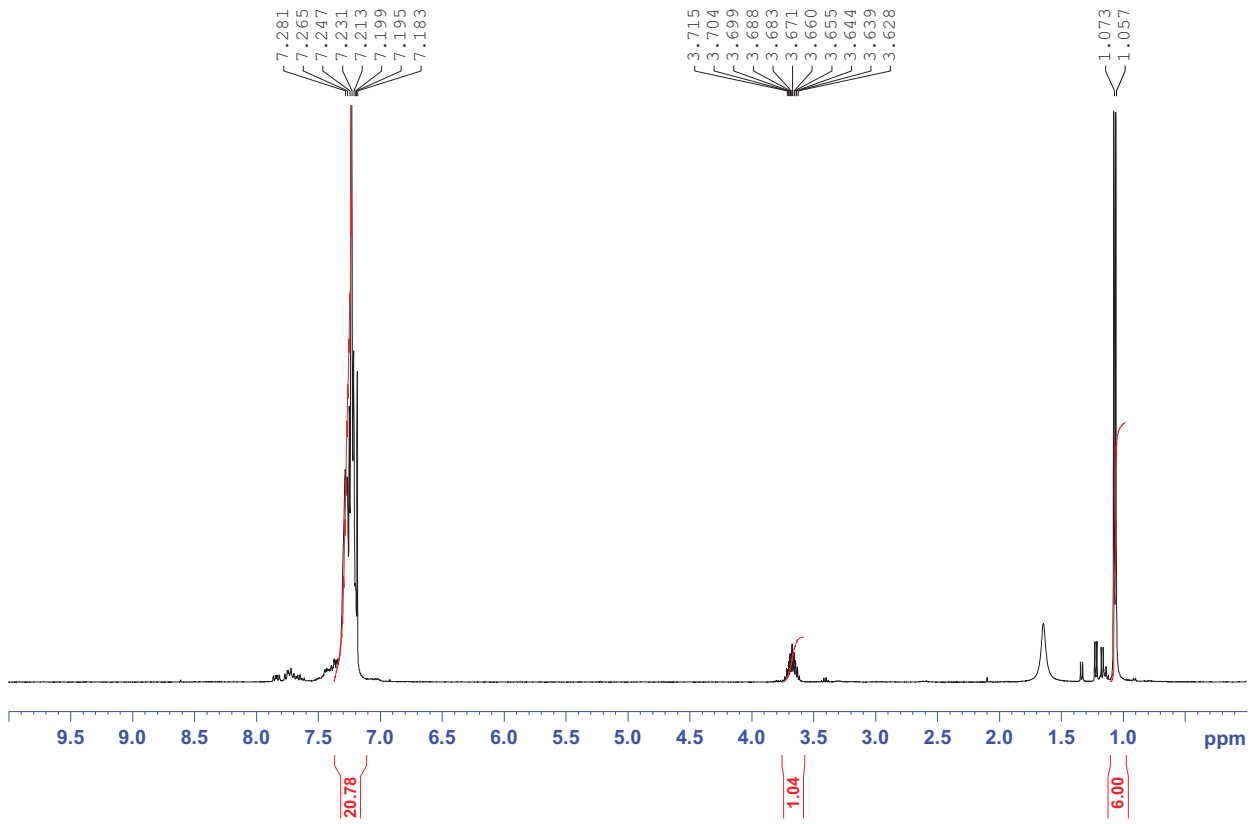

Fig. 7A: ^{1}H NMR spectrum of ligand **3.3.**

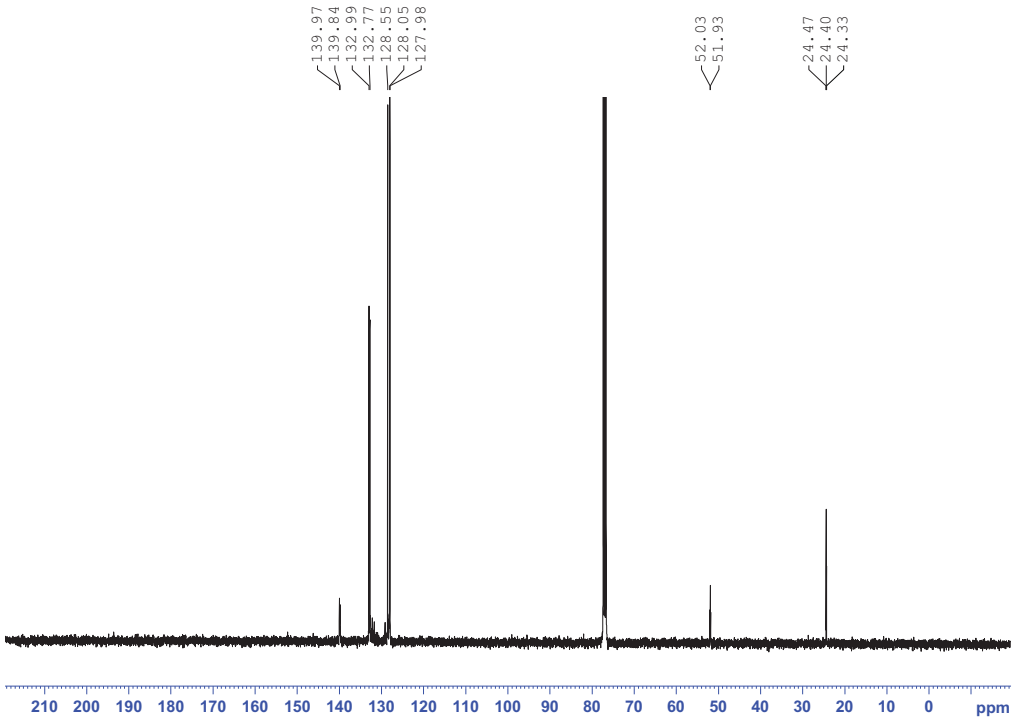

Fig. 8A: ^{13}C NMR spectrum of ligand **3.3.**

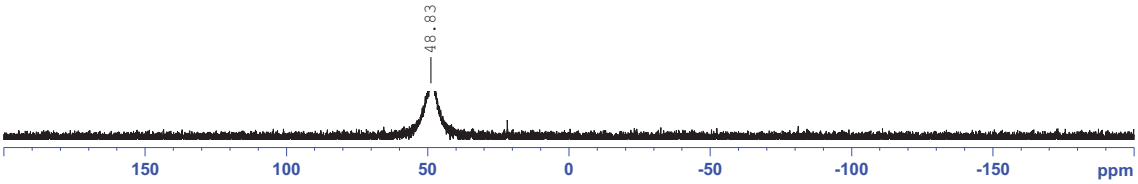

Fig. 9A: ^{31}P NMR spectrum of ligand **3.3**

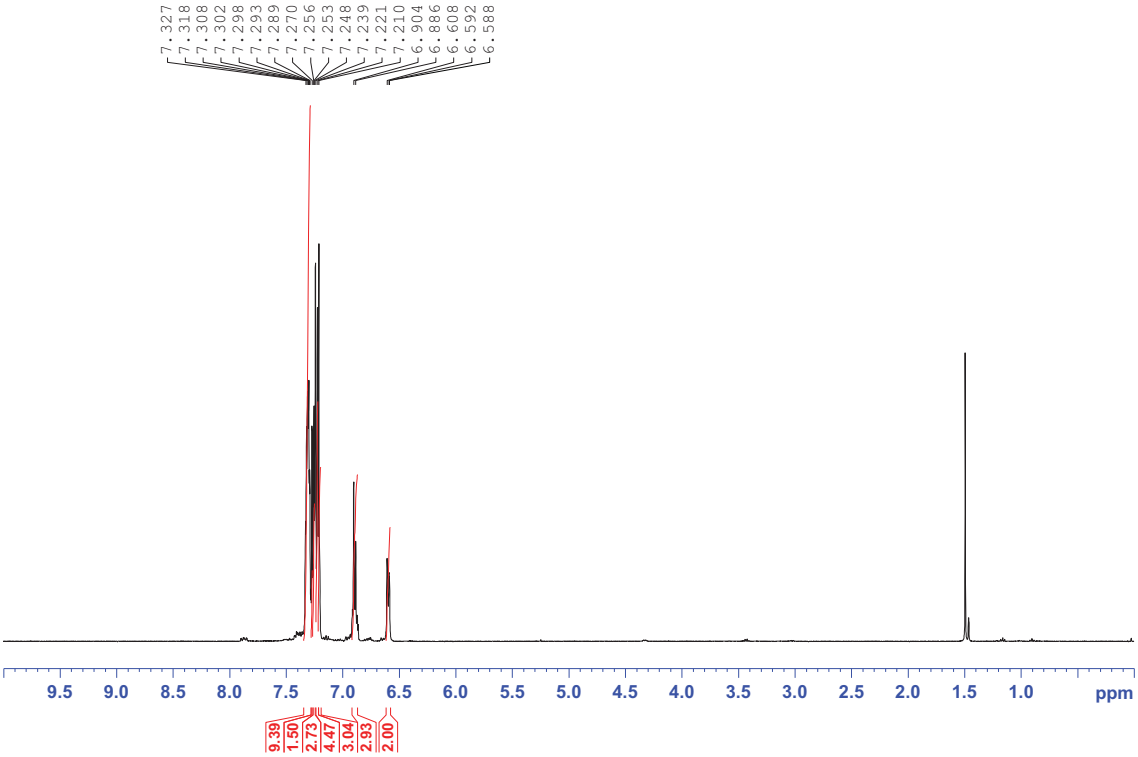

Fig.10A: ^{1}H NMR spectrum of ligand **3.4.**

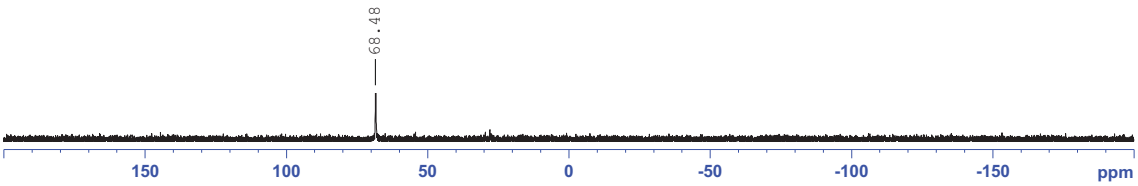

Fig. 11A: ^{31}P NMR spectrum of ligand **3.4.**

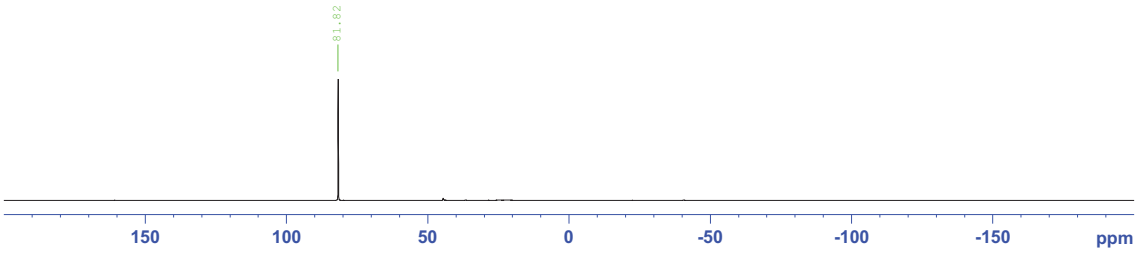

Fig. 12A: ^{31}P NMR spectrum of chlorodiphenylphosphine.

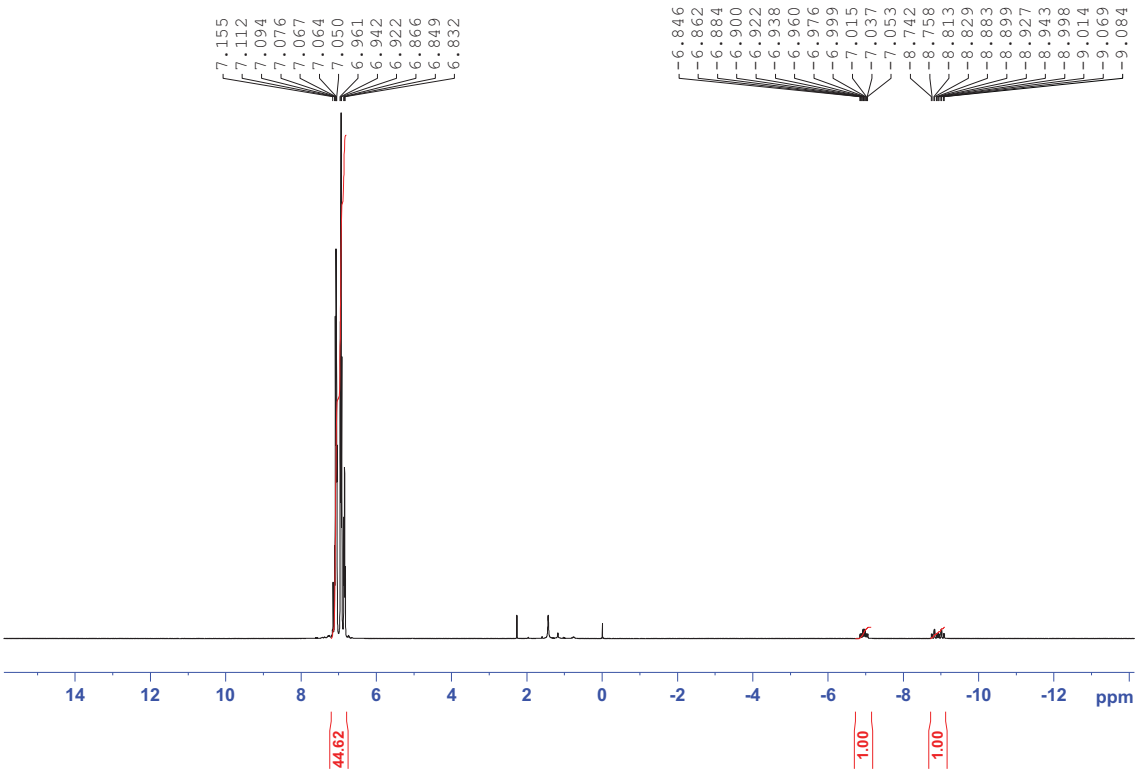

Fig. 13A: ^{1}H NMR spectrum of ruthenium precursor **3.14.**

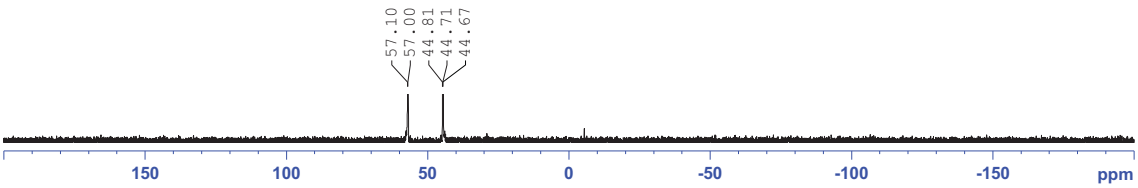

Fig. 14A: ^{31}P NMR spectrum of ruthenium precursor **3.14.**

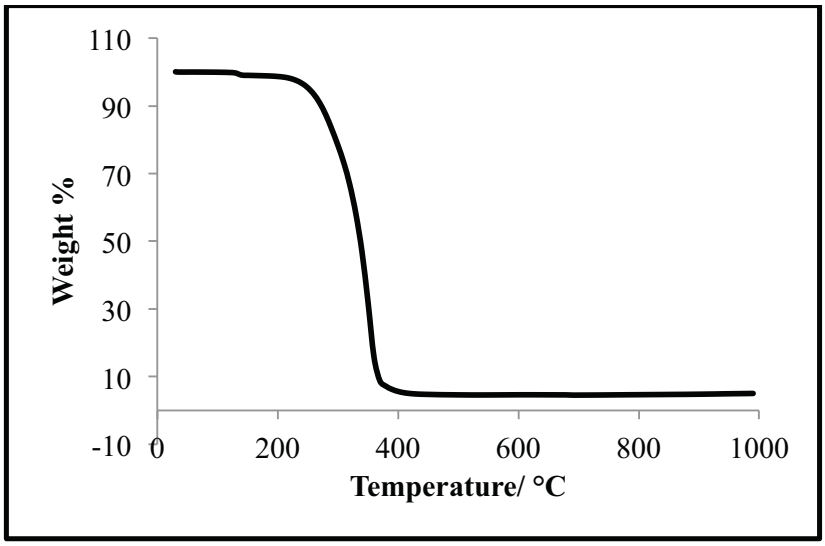

Fig. 15A TG curve of diphosphinocyclohexylamine ($^{Ph}PN_{cyclohexyl}P^{Ph}$) (**3.1**).

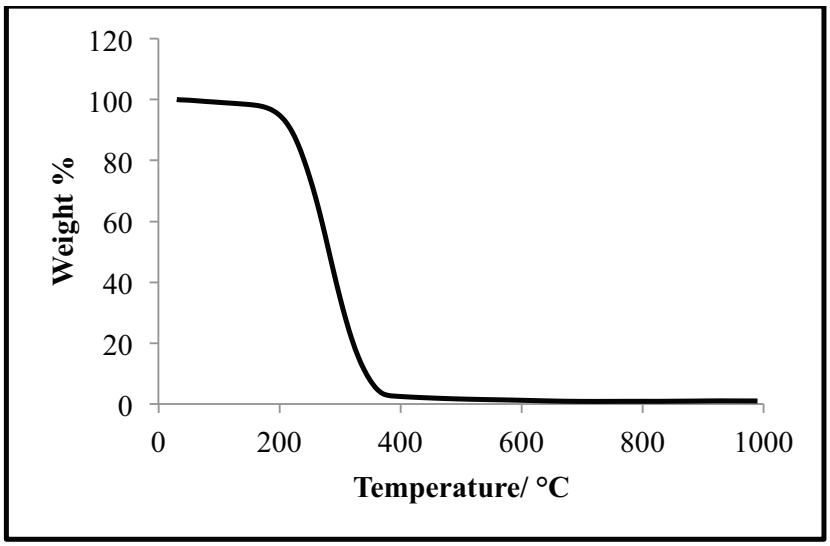

Fig. 16A: TG curve of diphosphinopentylamine ($^{Ph}PN_{pentyl}P^{Ph}$) (**3.2**).

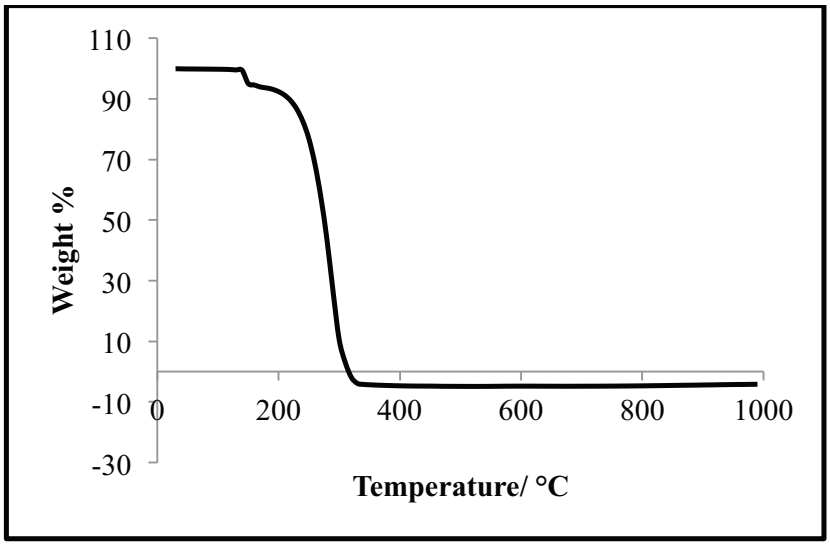

Fig. 17A: TG curve of diphosphinopentylamine ($^{Ph}PN_{\textit{iso}\text{-propyl}}P^{Ph}$) (**3.3**).

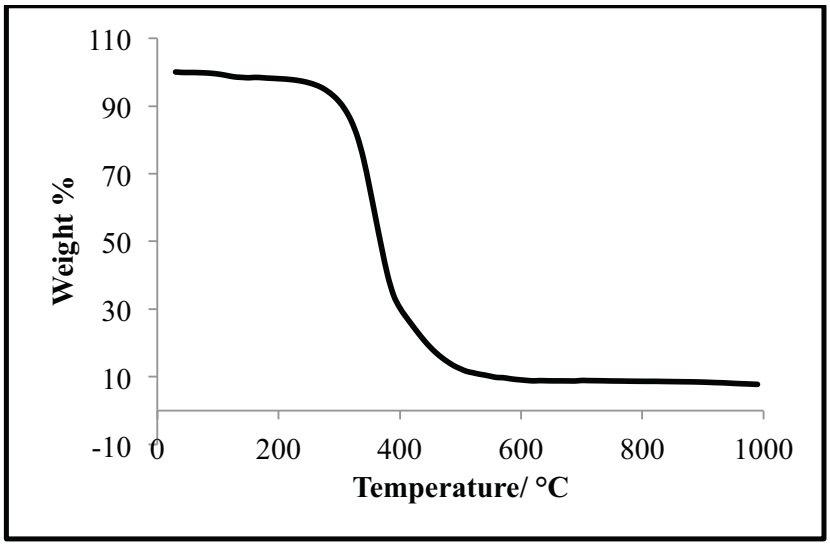

Fig. 18A: TG curve of diphosphinobenzylamine ($^{Ph}PN_{benzyl}P^{Ph}$) (**3.4**).

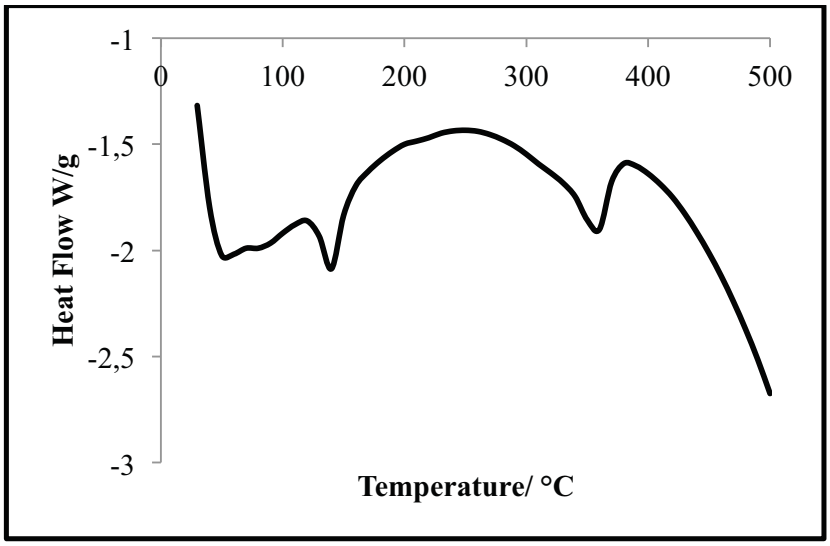

Fig. 19A: DSC curve of diphosphinocyclohexylamine ($^{Ph}PN_{cyclohexyl}P^{Ph}$) (**3.1**).

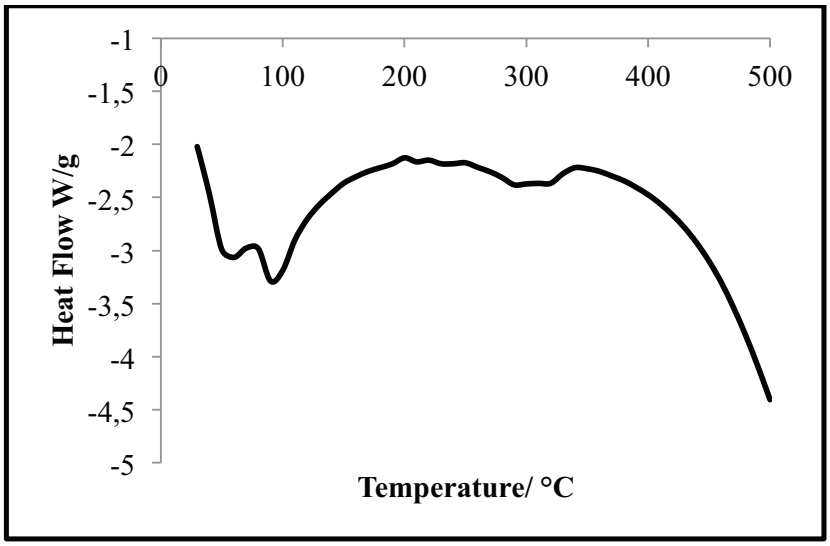

Fig. 20A: DSC curve of diphosphinopentylamine ($^{Ph}PN_{pentyl}P^{Ph}$) (**3.2**).

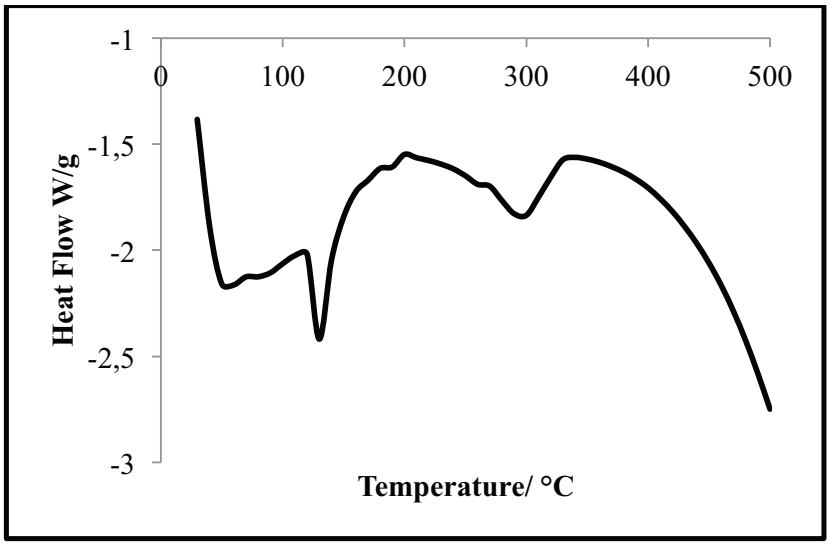

Fig. 21A: DSC curve of diphosphino*iso*-propylamine ($^{Ph}PN_{iso\text{-}propyl}P^{Ph}$) (**3.3**).

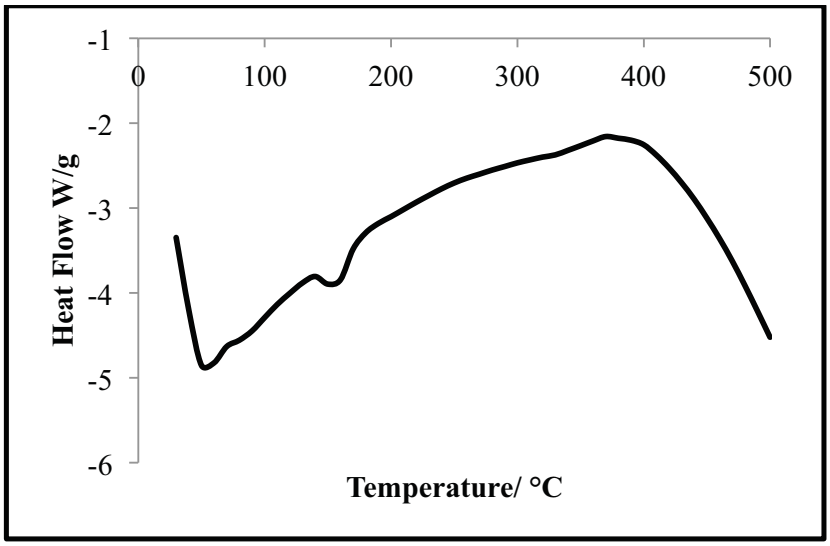

Fig. 22A: DSC curve of diphosphinobenzylamine ($^{Ph}PN_{benzyl}P^{Ph}$) (**3.4**).

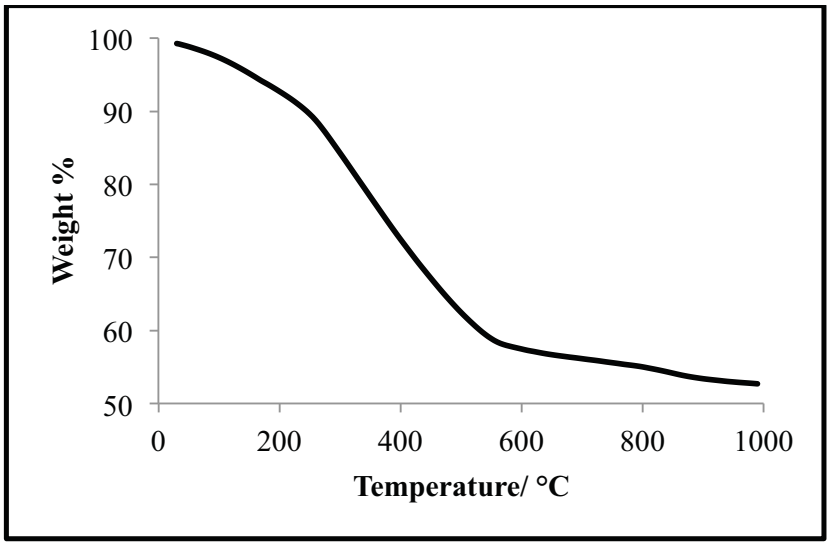

Fig. 23A: TG curve of [($^{Ph}PN_{cyclohexyl}P^{Ph}$)Ir COE][$BF_4$]**(3.6)**.

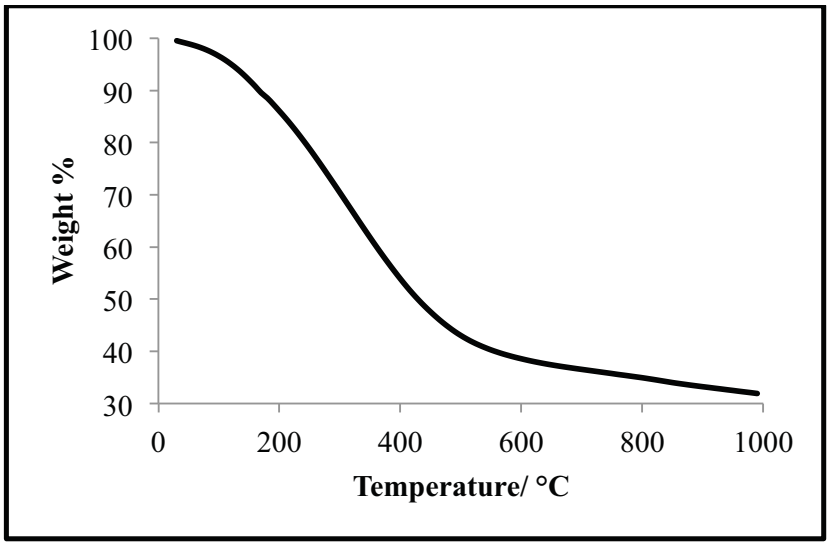

Fig. 24A: TG curve of [($^{Ph}PN_{pentyl}P^{Ph}$)Ir COE][BF_4]**(3.7)**.

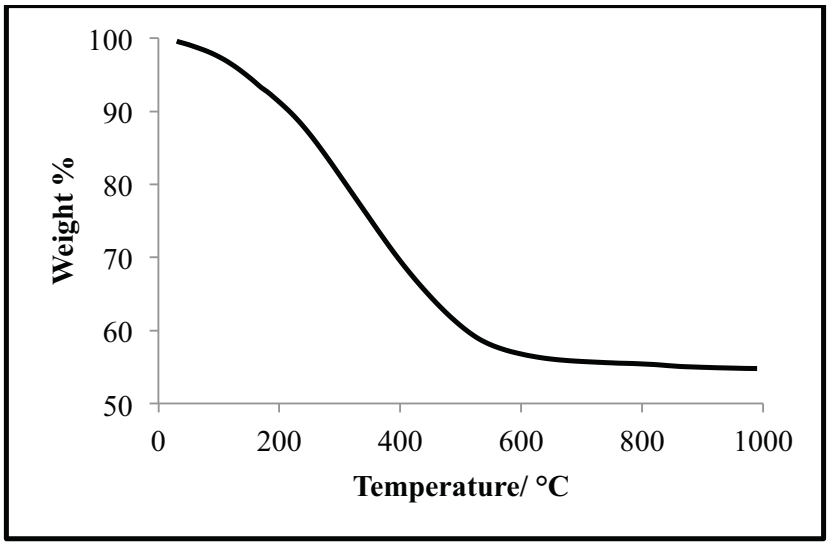

Fig. 25A: TG curve of [(^{Ph}PN$_{iso\text{-propyl}}$P^{Ph})Ir COE][BF_4]**(3.8)**.

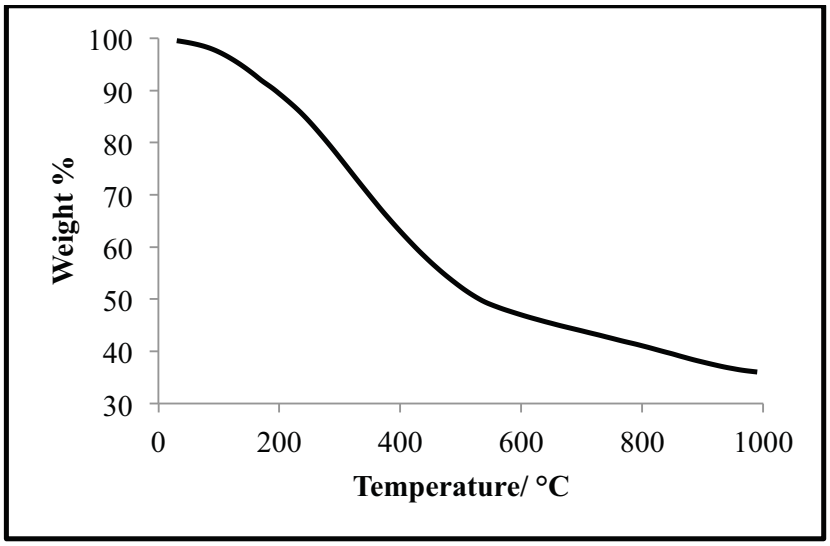

Fig. 26A: TG curve of [(^{Ph}PN$_{benzyl}$P^{Ph})Ir COE][BF_4]**(3.9)**.

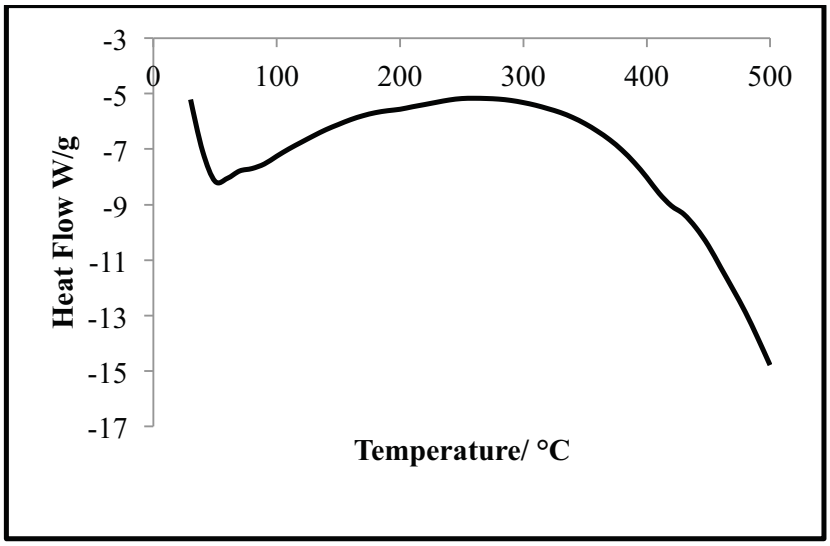

Fig. 27A: DSC curve of [($^{Ph}PN_{cyclohexyl}P^{Ph}$)Ir COE][$BF_4$]**(3.6)**.

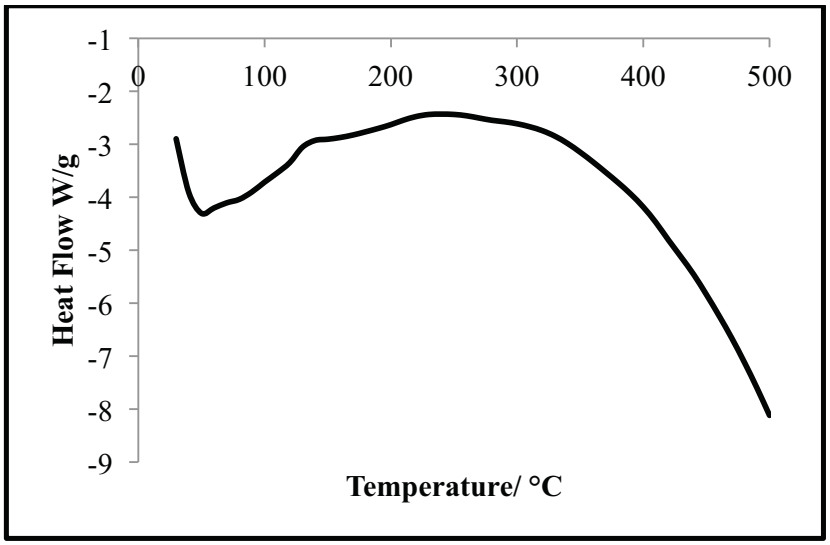

Fig. 28A: DSC curve of [($^{Ph}PN_{pentyl}P^{Ph}$)Ir COE][BF_4]**(3.7)**.

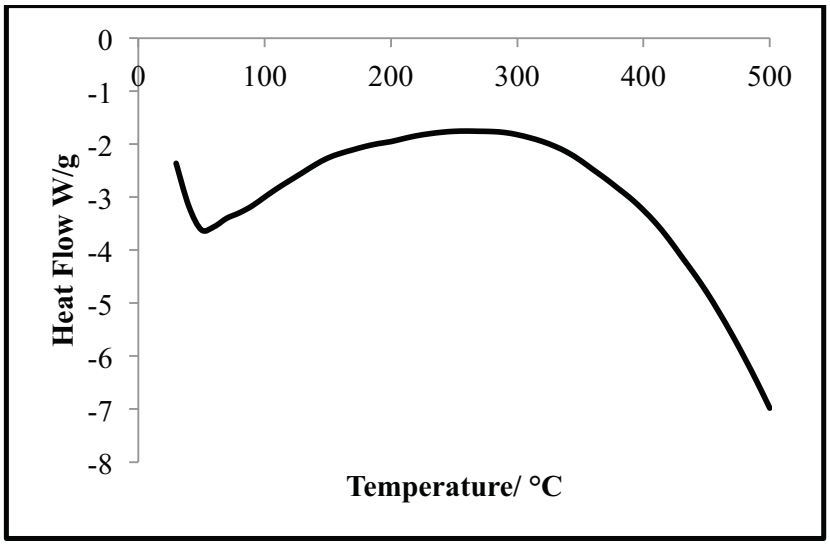

Fig. 29A: DSC curve of [($^{Ph}PN_{iso\text{-}propyl}P^{Ph}$)Ir COE][$BF_4$]**(3.8)**.

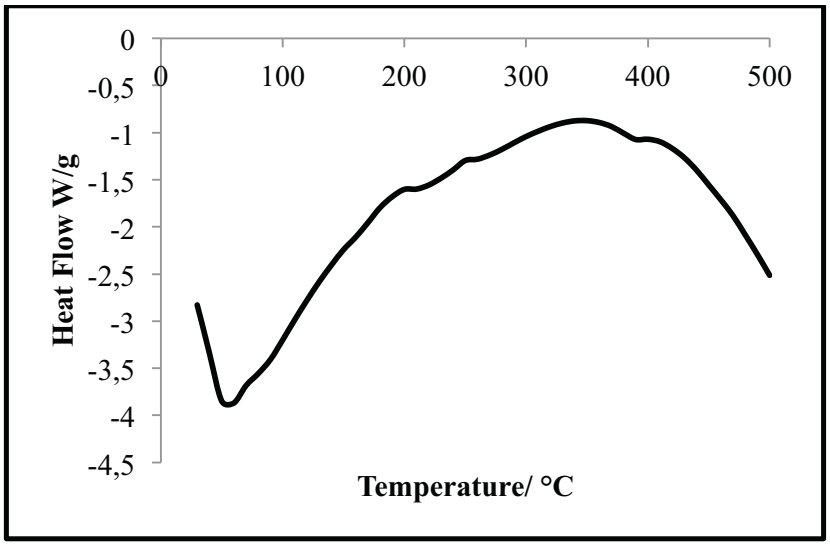

Fig. 30A: DSC curve of [($^{Ph}PN_{benzyl}P^{Ph}$)Ir COE][BF_4]**(3.9)**.

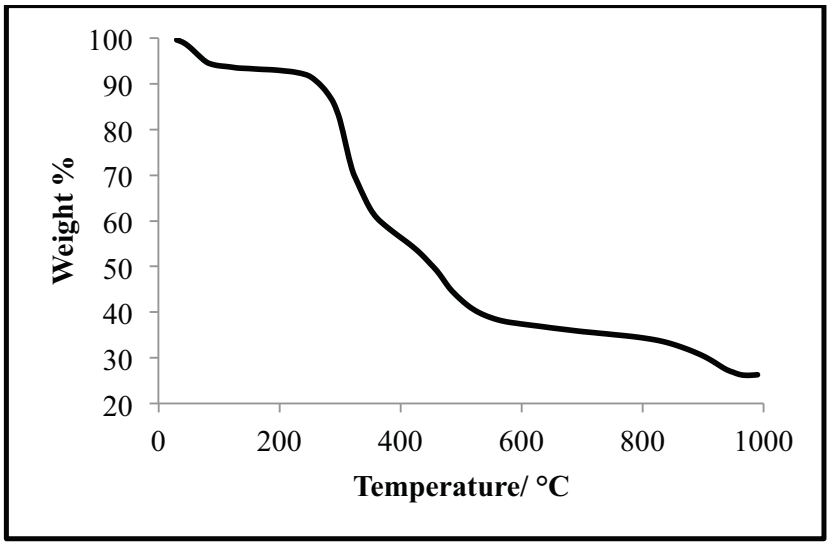

Fig. 31A: TG curve of [($^{Ph}PN_{cyclohexyl}P^{Ph}$)$CoCl_2$]**(3.10)**.

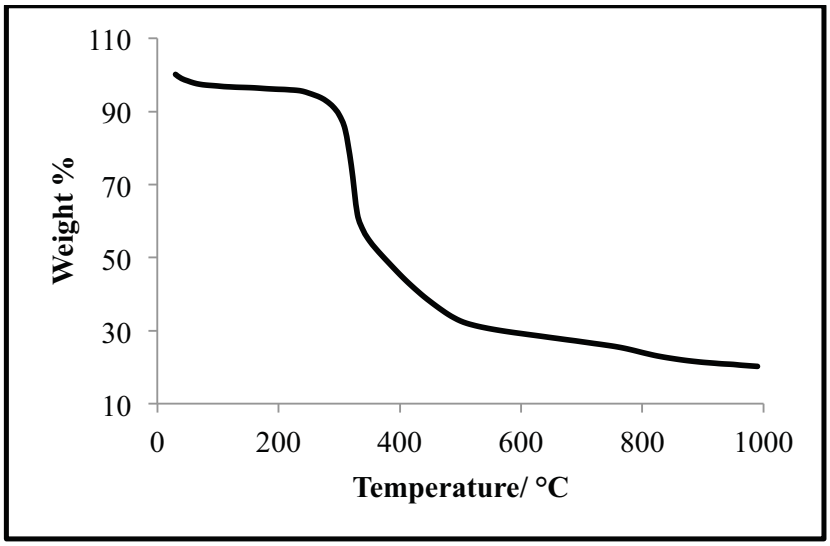

Fig. 32A: TG curve of [($^{Ph}PN_{pentyl}P^{Ph}$)$CoCl_2$]**(3.11)**.

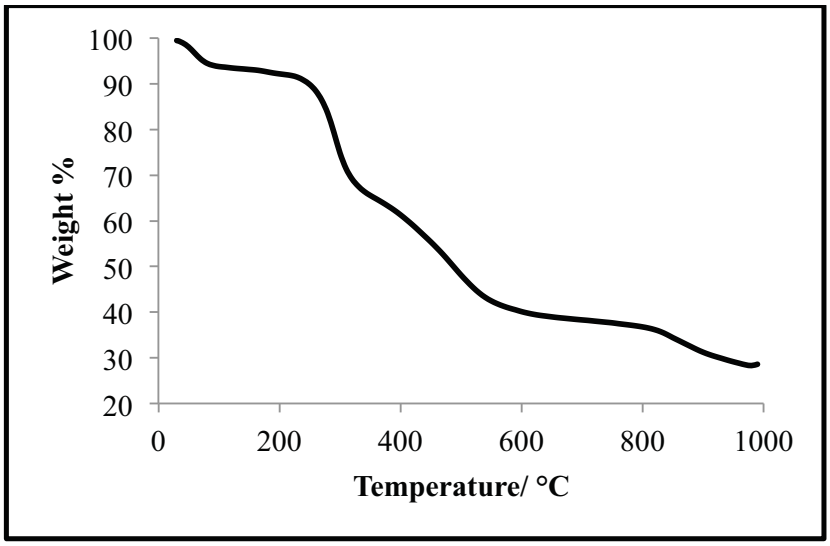

Fig. 33A: TG curve of [($^{Ph}PN_{iso\text{-}propyl}P^{Ph}$)$CoCl_2$]**(3.12)**.

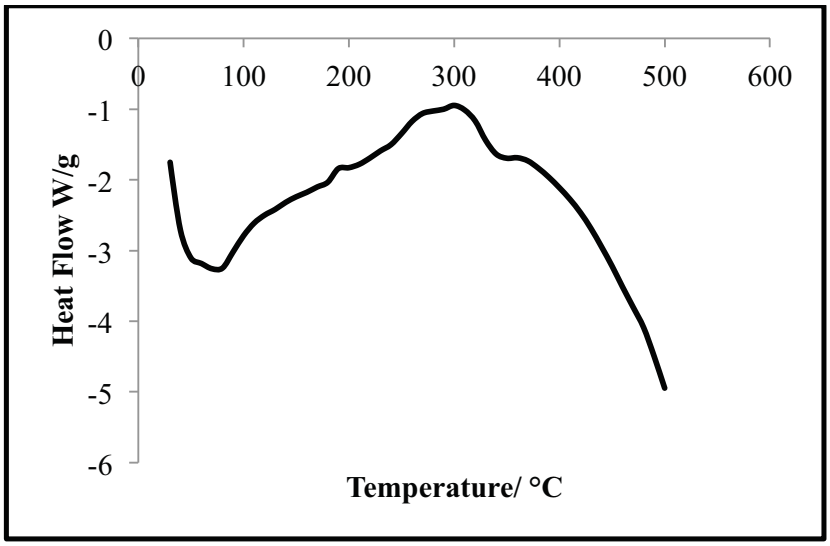

Fig. 34A: DSC curve of [($^{Ph}PN_{cyclohexyl}P^{Ph}$)$CoCl_2$]**(3.10)**.

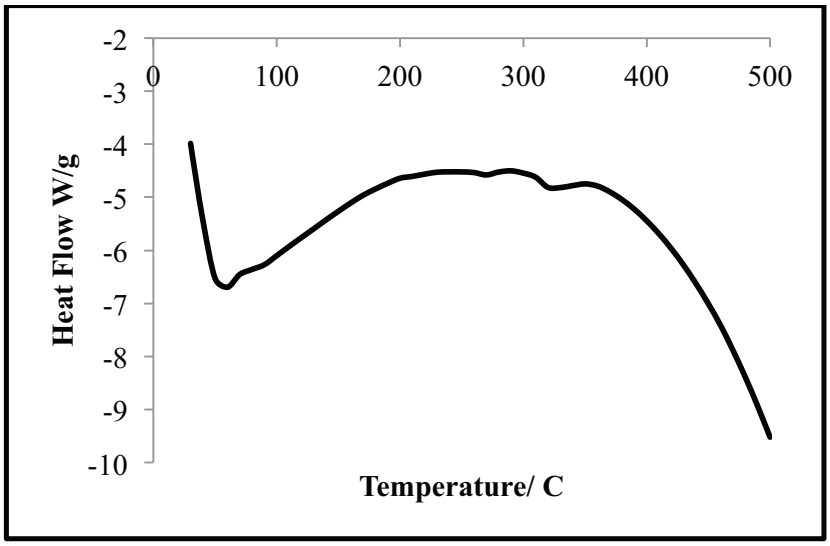

Fig. 35A: DSC curve of [($^{Ph}PN_{pentyl}P^{Ph}$)$CoCl_2$]**(3.11)**.

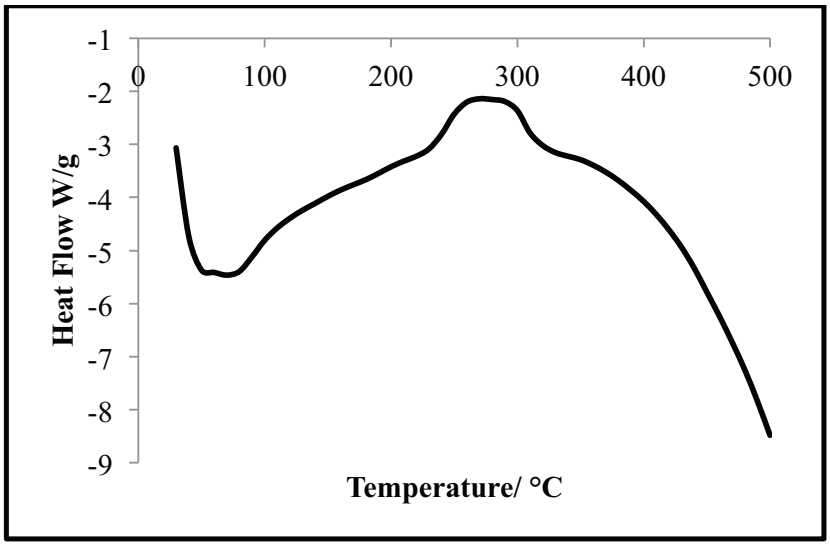

Fig. 36A: DSC curve of [($^{Ph}PN_{iso\text{-}propyl}P^{Ph}$)$CoCl_2$]**(3.12)**.

Appendix B

Appendix 1B 134

List of Tables

Table B1: Mass of standards used in the dichloromethane and acetonitrile solutions and the respective RF values 136

Appendix 2B 137

List of Tables

Table B2: Quantities used in the optimization of the substrate to oxidant ratio using catalyst 3.6. 137
Table B3: Quantities used in the blank runs for the optimization of the substrate to oxidant ratio. 137
Table B4: Quantities used in the optimization of the substrate to oxidant ratio using catalyst **3.10.** 138
Table B5: Quantities used in the blank runs for the optimization of the substrate to oxidant ratio. 138
Table B6: Masses and molar quantities used in the catalytic testing in dichloromethane with *tert*-butyl hydroperoxide (*t*-BuOOH) as the respective oxidant. 139
Table B7: Calculated reactivities from the % selectivity of the alcohols for complex **3.6.** 139
Table B8: Masses and molar quantities used in the catalytic testing in acetonitrile with *tert*-butyl hydroperoxide (*t*-BuOOH) as the respective oxidant 140

Appendix 3B 141

List of Tables

Table B9: Masses and molar quantities used in the catalytic testing in dichloromethane with *tert*-butyl hydroperoxide (*t*-BuOOH) as the respective oxidant. 141

Table B10: Masses and molar quantities used in the catalytic testing in acetonitrile with *tert*-butyl hydroperoxide (*t*-BuOOH) as the respective oxidant. 142

Appendix 1B

Multicomponent standard used in the calibration of the GC

Reagents used in the standards:

octane (C_8H_{18}) Fluka

1-octanol ($C_8H_{17}O$), Sigma Aldrich

2-octanol ($C_8H_{17}O$), Sigma Aldrich

3-octanol ($C_8H_{17}O$), Merck

4-octanol ($C_8H_{17}O$), Fluka

2-octanone ($C_8H_{16}O$), Fluka

3-octanone ($C_8H_{17}O$), Fluka

4-octanone ($C_8H_{17}O$), Sigma Aldrich

octanal ($C_8H_{17}O$), Sigma Aldrich

octanoic acid ($C_8H_{17}O_2$), Sigma Aldrich

The standard solution was made in a 25 ml volumetric flask and made to the mark using dichloromethane or acetonitrile (depending on the solvent system utilized).
RF values were calculated based on the following equation:

RF= ((area internal standard)(mol analyte)) / ((area analyte) (mol internal standard))

Table B1: Mass of standards used in the dichloromethane and acetonitrile solutions and the respective RF values.

Standard	Dichloromethane		Acetonitrile	
	Mass/ g	**RF**	**Mass/ g**	**RF**
octane	0.0386	0.447	0.0329	0.478
1-octanol	0.0336	0.461	0.0245	0.485
2-octanol	0.0300	0.517	0.0259	0.455
3-octanol	0.0293	0.562	0.0254	0.564
4-octanol	0.0083	0.525	0.0216	0.550
2-octanone	0.0271	0.485	0.0282	0.465
3-octanone	0.0360	0.490	0.0271	0.483
4-octanone	0.0316	0.491	0.0316	0.491
octanal	0.0311	0.658	0.0262	0.652
octanoic acid	0.0315	0.591	0.0268	0.881
pentanoic acid	0.0311		0.0271	

Appendix 2B

Optimization of the substrate to oxidant ratio in dichloromethane using complex 3.6

Table B2: Quantities used in the optimization of the substrate to oxidant ratio using catalyst **3.6**.

Ratio	Catalyst		Octane		*t*-BuOOH		Pentanoic acid	
	Mass /g	mol/ $x10^{-5}$	Mass /g	mol $x10^{-3}$	Mass /g	mol $x10^{-3}$	Mass/g	mol $x10^{-4}$
1:2.5	0.010	1.17	0.14	1.19	0.36	0.41	0.02	1.77
1:5	0.0104	1.21	0.13	1.18	0.77	8.51	0.02	2.36
1:7.5	0.0101	1.18	0.13	1.18	1.13	0.13	0.02	1.75
1:10	0.010	1.17	0.14	1.20	1.51	16.7	0.01	1.41

Table B3: Quantities used in the blank runs for the optimization of the substrate to oxidant ratio.

Ratio	Octane		*t*-BuOOH		Pentanoic acid	
	Mass /g	mol $x10^{-3}$	Mass /g	mol $x10^{-2}$	Mass/g	mol $x10^{-4}$
1:2.5	0.13	1.16	0.37	0.41	0.02	1.78
1:5	0.13	1.18	0.75	0.83	0.02	1.94
1:7.5	0.13	1.16	1.23	1.25	0.02	1.98
1:10	0.13	1.17	1.51	1.68	0.02	1.90

Optimization of the substrate to oxidant ratio in acetonitrile using complex 3.10

Table B4: Quantities used in the optimization of the substrate to oxidant ratio using catalyst **3.10.**

Ratio	Catalyst		Octane		*t*-BuOOH		Pentanoic acid	
	Mass /g	mol/ $x10^{-5}$	Mass /g	mol $x10^{-3}$	Mass /g	mol $x10^{-2}$	Mass/g	mol $x10^{-4}$
1:2.5	0.0104	1.74	0.19	1.68	0.54	0.60	0.01	1.39
1:5	0.0103	1.72	0.19	1.70	1.07	1.19	0.01	1.21
1:7.5	0.0105	1.76	0.19	1.67	1.61	1.79	0.02	1.88
1:10	0.0107	1.79	0.20	1.73	2.15	2.39	0.01	1.25

Table B5: Quantities used in the blank runs for the optimization of the substrate to oxidant ratio.

Ratio	Octane		*t*-BuOOH		Pentanoic acid	
	Mass /g	mol $x10^{-3}$	Mass /g	mol $x10^{-2}$	Mass/g	mol $x10^{-4}$
1:2.5	0.13	1.17	0.36	0.40	0.01	1.14
1:5	0.13	1.17	0.77	0.85	0.01	0.89
1:7.5	0.13	1.17	1.13	1.26	0.02	2.07
1:10	0.13	1.17	1.54	1.71	0.01	1.06

Catalytic testing carried out in dichloromethane with *tert*-butyl hydroperoxide (*t*-BuOOH) as the respective oxidant, Table B6, (Substrate: oxidant (1:5)).

Table B6: Masses and molar quantities used in the catalytic testing in dichloromethane with *tert*-butyl hydroperoxide (*t*-BuOOH) as the respective oxidant.

Catalyst			**Octane**		***t*-BuOOH**		**Pentanoic acid**	
	Mass /g	**mol/ x10^{-5}**	**Mass /g**	**mol x10^{-3}**	**Mass /g**	**mol x10^{-2}**	**Mass/g**	**mol x10^{-4}**
3.6	0.0104	1.21	0.13	1.18	0.77	8.51	0.02	2.36
3.7	0.0114	1.35	0.14	1.19	0.80	8.90	0.02	1.17
3.8	0.0104	1.27	0.14	1.22	0.79	8.82	0.02	1.53
3.9	0.0104	1.27	0.13	1.18	0.76	8.39	0.02	1.55
3.10	0.0105	1.76	0.19	1.69	1.09	1.21	0.02	1.84
3.11	0.0101	1.69	0.20	1.74	1.11	1.23	0.01	1.34
3.12	0.0102	1.71	0.21	1.82	1.16	1.29	0.02	1.78
3.13	0.0101	1.71	0.20	1.71	1.11	1.23	0.01	1.34

Calculation of selectivity parameters

Table B7: Calculated reactivities from the % selectivity of the alcohols for complex **3.6.**

Alcohol	**% Selectivity**	**Number of hydrogens per carbon**	**Normalized**
1-octanol	3	3	1
2-octanol	14	2	7
3-octanol	0	2	0
4-octanol	10	2	5

Therefore ratio = 1:7:0:5

Catalytic testing carried out in acetonitrile with *tert*-butyl hydroperoxide (*t*-BuOOH) as the respective oxidant, Table B7, (Substrate: oxidant (1:5)).

Table B8: Masses and molar quantities used in the catalytic testing in acetonitrile with *tert*-butyl hydroperoxide (*t*-BuOOH) as the respective oxidant.

Catalyst			**Octane**		***t*-BuOOH**		**Pentanoic acid**	
	Mass /g	**mol/ x10^{-5}**	**Mass /g**	**mol x10^{-3}**	**Mass /g**	**mol x10^{-2}**	**Mass/g**	**mol x10^{-4}**
3.10	0.0103	1.72	0.19	1.70	1.07	1.19	0.01	1.21
3.11	0.0110	1.88	0.20	1.72	1.10	1.22	0.01	1.19
3.12	0.0108	1.94	0.30	2.66	1.16	1.28	0.01	1.11
3.13	0.0108	1.83	0.19	1.69	1.09	1.21	0.01	1.18

Appendix 3B

In situ study with the ruthenium precursor (3.14, Chapter 3, Section 3.5) and ligands (3.1-3.4, Chapter 3, Section 3.2).

Catalytic testing carried out in dichloromethane with *tert*-butyl hydroperoxide (*t*-BuOOH) as the respective oxidant, Table B8, (Substrate: oxidant (1:5)).

Table B9: Masses and molar quantities used in the catalytic testing in dichloromethane with *tert*-butyl hydroperoxide (*t*-BuOOH) as the respective oxidant.

Ligand			**Ruthenium Precursor (3.14)**		**Octane**		***t*-BuOOH**		**Pentanoic acid**	
	Mass/g	**mol x10^{-5}**	**Mass/g**	**mol/ x10^{-5}**	**Mass/g**	**mol x10^{-3}**	**Mass/g**	**mol x10^{-2}**	**Mass/g**	**mol x10^{-4}**
3.1	0.0078	1.69	0.016	1.71	0.19	1.67	1.10	1.22	0.03	2.76
3.2	0.0082	1.80	0.016	1.71	0.19	1.67	1.10	1.21	0.01	1.31
3.3	0.0078	1.82	0.016	1.71	0.19	1.69	1.09	1.21	0.02	1.54
3.4	0.0082	1.72	0.016	1.71	0.19	1.69	1.10	1.22	0.01	1.07

Catalytic testing carried out in acetonitrile with *tert*-butyl hydroperoxide (*t*-BuOOH) as the respective oxidant, Table B9, (Substrate: oxidant (1:5))

Table B10: Masses and molar quantities used in the catalytic testing in acetonitrile with *tert*-butyl hydroperoxide (*t*-BuOOH) as the respective oxidant.

Ligand			**Ruthenium Precursor (3.14)**		**Octane**		***t*-BuOOH**		**Pentanoic acid**	
	Mass/g	**mol x10^{-5}**	**Mass /g**	**mol/ x10^{-5}**	**Mass /g**	**mol x10^{-3}**	**Mass /g**	**mol x10^{-2}**	**Mass/g**	**mol x10^{-4}**
3.1	0.0079	1.71	0.016	1.71	0.19	1.69	1.09	1.21	0.01	1.22
3.2	0.0083	1.70	0.016	1.71	0.19	1.69	1.03	1.22	0.02	1.47
3.3	0.0081	1.89	0.016	1.71	0.19	1.69	1.09	1.21	0.01	0.96
3.4	0.0082	1.72	0.016	1.71	0.19	1.69	1.10	1.22	0.01	1.26